THE UNIVERSITY OF CALGARY

Minimum Reinforcement for High-Performance Concrete Slabs

by

Robert G. McLeod

A THESIS

SUBMITTED TO THE FACULTY OF GRADUATE STUDIES

IN PARTIAL FULFILLMENT OF THE REQUIREMENTS FOR THE

DEGREE OF MASTER OF SCIENCE

DEPARTMENT OF CIVIL ENGINEERING

CALGARY, ALBERTA

MARCH, 1998

ABSTRACT

The thesis objective was to establish minimum reinforcement required to prevent unacceptable cracking in fully-restrained high-performance concrete (HPC) slabs. Large-scale specimens were tested with compressive strength of 30 MPa (normal strength) and 85 MPa (high-performance). Shrinkage and thermal (hydration) strains acted on the specimens. Reinforcement ratio was varied from 0.2% to 0.8%. Slabs were cured under conditions of extremely low humidity (minimum of 10%).

For normal strength slabs, 0.4% reinforcement adequately controlled cracking: maximum crack width was 0.6 mm. For HPC slabs, 0.8% was inadequate: maximum crack width was 2.1 mm. Use of a curing compound was ineffective in controlling drying shrinkage in HPC.

Extensive shrinkage measurements were analyzed. Comparison is made to ACI (American Concrete Institute), CEB (Comite Euro-International Du Beton), and Dilger/Wang/Niitani (1997) prediction models.

Time-step analysis, including the effects of creep, was performed to estimate tensile stresses due to shrinkage and thermal strains.

ACKNOWLEDGMENTS

I would like to thank Dr. Walter Dilger, my supervisor, for his thoughtful guidance throughout the period of my research. His wisdom, flexibility, and patience were essential to the success of this work.

Thank you to Bruce Sidorsky for his practical "know how" in the lab. His service as the central technician for all aspects of the testing program is greatly appreciated. Harry Pollard is recognized for his work in producing concrete of consistent, and excellent, quality. Because of the long duration of testing, the lab work was also assisted at various times by all of the Civil Engineering technicians and many fellow graduate students.

Scholarships were provided to me by the Natural Sciences and Engineering Research Council of Canada and the Association of Professional Engineers, Geologists, and Geophysicists of Alberta. Additional financial support was given by the Department of Civil Engineering. I am grateful that these resources were available as they made it possible for me to return to university studies between periods of employment as a professional engineer.

I am very thankful for the support of my family and friends during my periods of study and research. It was a lonely and self-absorbed pursuit at times. Their love and understanding (and sometimes gentle prodding) always helped. To my parents, and especially to my wife, Lynda, my dearest thanks for this opportunity.

TABLE OF CONTENTS

CHAPTER 4 EXPERIMENTAL RESULTS

LIST OF TABLES

LIST OF FIGURES

LIST OF SYMBOLS & NOTATIONS

(Note: Symbols are defined in the same manner as they are presented in the literature.)

A	=	concrete area in tension
A_c	=	concrete cross-sectional area
A_g or A_{gross}	=	gross area of section
A_i	=	area of concrete member including reinforcement (transformed)
A_s	=	area of steel tension reinforcement
$A_{s,critical}$	=	critical area of tension reinforcement to prevent wide isolated cracks
A_{smin}	=	minimum area of tension reinforcement (not a standard notation used by CSA A23.3 or ACI 318)
$A_{s,rec}$	=	minimum reinforcement to produce distributed cracking
A_{st}	=	cross-sectional area of tension reinforcement
ACI	=	American Concrete Institute
AS	=	Australian Standard
b	=	width of a cross-section
b_t	=	beam width, in tension
c	=	distance from extreme compression fibre to neutral axis
C_{ca}	=	empirical aggregate coefficient (to calculate elastic modulus)
CEB	=	Comite Euro-International du Beton
d	=	effective depth of a cross-section
D	=	overall depth of a cross-section in the plane of bending
DG	=	dial gauge
d_b	=	nominal diameter of steel reinforcing bar
E_c	=	modulus of elasticity of concrete
E_{cj}	=	modulus of elasticity of concrete at j days
$E_c(t_i)$	=	elastic modulus of concrete at the middle of the ith time interval

E_s	=	modulus of elasticity of reinforcement
f_{cc}	=	compressive cylinder strength of concrete
f_{cj}	=	compressive strength of concrete at j days
f_{ck}	=	characteristic compressive strength of concrete
$f_{cm}(t)$	=	median compressive strength at age of t days
f_{cm}	=	median compressive strength at age of 28 days
F_{crack}	=	tensile load producing first crack
f_{ct}	=	tensile strength of concrete, determined from split cylinder tests
f_{ctm}	=	mean concrete tensile strength
f_r	=	modulus of rupture of concrete
$f_{ct,sp}$	=	mean splitting tensile strength
f_{sp} or f'_{sp}	=	splitting tensile strength of concrete
f_{sy}	=	yield strength of reinforcing steel
f_t	=	tensile strength of concrete
f_{tj}	=	tensile strength of concrete at j days
f_{tk}	=	characteristic direct tensile strength of concrete
f_y	=	specified yield strength of nonprestressed reinforcement
f'_c	=	specified compressive strength of concrete
f'_{cf}	=	characteristic flexural tensile strength of concrete
f'_{ct}	=	characteristic principal tensile strength.
f'_t	=	direct tensile strength
FIP	=	Federation Internationale de la Precontrainte
G	=	shear modulus
h	=	overall depth of cross-section
	=	notional size of member
HPC	=	high-performance concrete (for thesis: slabs 100-2, 100-4, 100-8)
HSC	=	high-strength concrete
I_g	=	moment of inertia of gross concrete section
k	=	coefficient relating tensile to compressive strength

K	=	adjustment factor to determine minimum reinforcement ratio
k_1	=	shrinkage strain coefficient
k_2	=	environment factor, for humidity and thickness
k_3	=	maturity coefficient
$k_{s,t}$	=	time factor
L	=	full length of restrained member
M_{cr}	=	cracking moment of concrete section
M_n	=	nominal resisting moment of concrete section
n	=	modular ratio (E_s / E_c)
N_{cr}	=	tensile force in member after cracking
NSC	=	normal strength concrete (for thesis: slabs 30-2, 30-4)
r	=	reinforcement ratio
r_{min}	=	minimum reinforcement ratio
RH	=	ambient relative humidity
s	=	coefficient to account for cement type (0.25 for normal cement)
s_o	=	development length on either side of crack
t	=	age of concrete
t_i	=	age of concrete at the middle of the ith interval
t_{i+1} or $t_{i+1/2}$	=	age of concrete at the end of the ith interval
t_{i-1} or $t_{i-1/2}$	=	age of concrete at the beginning of the ith interval
t_0	=	age of concrete at beginning of drying
	=	age of concrete at loading
t_1	=	1 day
T	=	tension force in concrete member
	=	temperature
$T_{concrete}$	=	tension force in concrete slab at time of cracking
T_{reinf}	=	tension force in reinforcement at yield
T_i	=	temperature at time t_i
$(\Delta T)_j$	=	temperature increment in the jth time interval.
u	=	exposed surface area of concrete

V/S	=	volume to surface ratio of concrete member
w or W	=	water content, by mass
w/b	=	water-cement or water-cementitious binder ratio
w_{max}	=	maximum crack width
z	=	parameter limiting distribution of flexural reinforcement
α	=	coefficient for type of cement
	=	E_s / E_c , modular ratio
α_1	=	ratio of average stress in rectangular compression block to the specified concrete strength
α_T	=	coefficient of thermal expansion
β	=	coefficient for type of curing
β_1	=	ratio of depths of rectangular compression block to neutral axis
$\beta(f_{cm})$	=	coefficient for compressive strength
$\beta(t_0)$	=	coefficient for age at loading
$\beta_c(t-t_0)$	=	coefficient for development of creep from time of loading, t_0 , to time t
$\beta_{cc}(t)$	=	coefficient which depends on the age of concrete at time t
Δ	=	change
Δ_v	=	shear deflection
ε_c	=	strain in concrete
ε_{cs}	=	total concrete shrinkage strain
$\varepsilon_{cs,b}$	=	basic concrete shrinkage strain
ε_{end}	=	strain in slab due to end block deflection
ε_s	=	strain in reinforcement
ε_{sh}	=	shrinkage strain in concrete
$\varepsilon_{sh}(t,t_0)$	=	shrinkage strain occurring between t and t_0
$\varepsilon_{sh\infty}$	=	ultimate long term shrinkage
ε_t	=	thermal strain in concrete

ϕ = material resistance factor (value varies, refer to specific equation)

$\phi(t, t_0)$ = creep coefficient at time t for loading at time t_0

$\phi(t_{i+1/2}, t_i)$ = creep coefficient for load applied at t_i, and sustained to $t_{i+1/2}$

ϕ_0 = notional creep coefficient

ϕ_{cc} = concrete creep

$\phi_{cc.b}$ = basic creep factor

$\phi_{CEB}(t, t_0)$ = creep coefficient at time t for loading at time t_0, calculated in accordance with CEB MC90

$\phi_{DNW}(t, t_0)$ = creep coefficient at time t for loading at time t_0, calculated in accordance with Dilger, Niitani, and Wang (1997)

ϕ_{RH} = creep coefficient dependent on RH and h

γ = curvature

γ_c = density of concrete

γ_{xy} = shear strain

λ_{Reinf} = factor inherent stress caused by reinforcement and chemical (basic) shrinkage

μ = reinforcement ratio

ν = Poisson's ratio

ρ = reinforcement ratio

$\rho_{critical}$ = critical reinforcement ratio to prevent wide isolated cracks

ρ_{min} = minimum flexural reinforcement ratio

σ_B = bond strength

σ_{cp} = average intensity of effective prestress in concrete

$(\Delta\sigma_{res})_i$ = restrained stress increment in the ith time interval

$\sigma_{s,sul}$ = steel stress

σ_T = stress in slab due to thermal strain

σ_{total} = total stress in slab due to thermal and shrinkage strain

τ_{xy} = shear stress

CHAPTER 1

INTRODUCTION

1.1 General

The development of cracks in nonprestressed concrete structures is unavoidable due to the relatively low tensile strength of concrete. Tensile strains develop in restrained concrete from several different sources of contraction such as temperature drop, drying shrinkage, and flexural loading. If the induced tensile stress is greater than the tensile strength of the concrete, cracking occurs.

One of the objectives of good structural design is to limit the cracks which form in concrete members to an acceptable width. The definition of what is acceptable depends on the intended use of the structure, the anticipated loading, and the environment to which it is exposed. For a water-retaining concrete vessel or a foundation wall protecting a dry basement space, 0.5 mm cracks that allow water to seep through are not acceptable. But the same cracks in a non-exposed beam within a building envelope may be permissible. Engineering judgment and experience should lead to a decision on the level of crack control that is necessary. Some guidelines are also given by codes of practice.

Providing a minimum amount of nonprestressed steel reinforcement is the conventional method of crack control. The idea is to use enough reinforcement to prevent a single, wide crack from forming. Instead, it is preferable that cracking is distributed so that many cracks of small widths form. Distributed, small cracks provide much better resistance to the flow of water through the concrete. They are also much less visible, if this is a concern. Increased deflection due to the closing of cracks under loading, is also greatly reduced if crack width is limited.

Three classifications of minimum reinforcement are generally considered important in design. In areas of slabs where bending stresses are low, reinforcement which controls cracks due to temperature and shrinkage is used. For beams in regions of significant flexure, reinforcement to limit flexural cracks is provided. As well, for beams where the depth of section is controlled by requirements other than strength, a minimum amount of reinforcement is still needed. Sufficient reinforcement must be used so that the member does not fail suddenly at the first flexural crack. Because of the less ductile behavior of unreinforced high-performance concrete, as compared to normal strength concrete, the provision of enough steel to avoid brittle failure is essential.

The amount of reinforcement that is enough for crack control is not easily determined. Since the formation of cracks is a complex behavior, simple rules are not readily available in national codes of practice. As will be discussed in greater detail in Chapter 2, the present guidelines for minimum reinforcement for temperature and shrinkage are empirical in nature, and do not normally consider the effect of concrete strength.

1.2 Objective

The objective of the research presented here was to determine the minimum reinforcement required to control cracking in high-performance concrete (HPC) [1]. Specifically, highly-restrained slabs subjected to the effects of temperature, due to concrete heat of hydration, and shrinkage were tested. Drying under conditions of very low humidity was to be included.

1.3 Organization

Chapter 2 presents a broad literature review on many topics underlying the study of minimum reinforcement in high-performance concrete (HPC). The properties of HPC are discussed in detail. As well, various prediction models for strength development, creep, and shrinkage are reported. Recognized recommendations for crack control, including minimum reinforcement, are identified. Although a limited amount of the information from the literature review is referenced in the remainder of the thesis, it is presented as a comprehensive basis for further study.

The procedures followed in the testing program are outlined in Chapter 3. Chapter 4 includes the observations made during the testing program and the interpretation of these results. Conclusions and recommendations form Chapter 5.

1. The term "high-performance concrete" is used to describe the concrete tested in presenting this thesis. However, the only variation in material performance which was considered was strength. Thus, it would be more exact to use the term "high-strength concrete". The decision to use "high-performance concrete" was made to be consistent with current terminology. (Refer also to Section 2.2)

CHAPTER 2

LITERATURE REVIEW

2.1 General

To properly investigate the basis for minimum reinforcement in high-performance concrete slabs, several topics of research must be reviewed. As a starting point, the material itself, high-performance concrete, must be identified and described. Its basic mechanical properties as well as its creep and shrinkage behavior need to be understood.

If minimum reinforcement is adequate, concrete members have satisfactory ductility and cracking is controlled. Research in these areas is also important to the topic of this thesis.

2.2 Definition and use of high-performance concrete

Aïtcin (1996) describes high-performance concrete (HPC) as a concrete with a low water-cement or water-cementitious binder (w/b) ratio. Generally, HPC has a w/b ratio of 0.30 to 0.35. Concrete with a w/b ratio greater than 0.45 is considered normal-strength concrete (NSC). The American Concrete Institute (ACI) chose 41 MPa (6000 psi) as the lower limit for HSC, high-strength concrete (ACI 363R-84). As well, so-called exotic concrete, such as polymer-impregnated or epoxy-based, was excluded from general specifications by ACI.

Some research has further classified concrete above 105 MPa (15,000 psi) as VHSC, very high-strength concrete (Bertero, 1979). Another classification, VHPC, very high-performance concrete, has been suggested by some researchers (de Larrard, Malier

1992). These special categories overlap with the upper bounds for HPC and are probably unnecessary.

The FIP-CEB Working Group on HSC (1990) has established a range of strength to consider. (FIP is the Federation Internationale de la Precontrainte; CEB is the Comite Euro-International du Beton.) This range, from 60 to 130 MPa, is intended to account for concrete that is beyond the scope of current national building codes.

A more detailed definition of HPC has been given by the Strategic Highway Research Program (Shah 1994) as concrete which meets one of three different strength development criteria:

1. 4 hour strength exceeding 2500 psi (18 MPa)
2. 24 hour strength exceeding 5000 psi (35 MPa)

or 3. 28 day strength exceeding 10000 psi (70 MPa).

As the name suggests, high-performance concrete is not valued for its high strength only. (The term "high-strength concrete" is now considered too limiting, and is no longer in common use.) Indeed, as Aïtcin suggests, HPC may become more widely used because of its improved durability. This is especially true in the consideration of structural slabs. The reason for this is that higher strength can only be taken advantage of to a certain point. Slab deflection will become critical as thickness is decreased (Nilson 1994). There is an important counterpoint to the argument that thin HPC slabs will be governed by deflection limits. As summarized in the FIP-CEB 1990, experiments have indicated that long-term deflections of slabs can be considerably reduced by using HPC. This benefit is achieved through a reduction in creep and an increase in elastic modulus and tensile strength.

Currently HPC is about 25 to 50% more costly than normal-strength concrete. For this reason it is unlikely that a structural slab design would be less expensive using HPC. However, the long term benefits of improved durability and reduced deflections, may justify the higher initial investment.

2.3 Composition and microstructure of HPC

Several important factors need to be considered in the production of a good HPC mix, as described by Aïtcin (1996). Superplasticizer must be used to achieve acceptable workability with the low water cement ratio needed to produce HPC. The strength of aggregate becomes the limiting factor for compressive strength. By using common river gravel, a 28-day strength of 85 MPa was reached for the current research. Other researchers, using the same mix but with crushed limestone, have obtained up to 120 MPa strength (Hanevy, 1996). The reason for crushed stone giving higher strengths is that paste-aggregate bond is greatly improved (Mindess, 1994).

In order to improve the microstructure of the cement paste a very fine pozzolanic material, such as silica fume or fly ash, is commonly used to replace a portion of the portland cement in HPC. Silica fume, or microsilica, is up to one hundred times finer than ordinary cement (PCI, 1994). The ability of the fine material to fill voids in the paste improves strength and reduces permeability (ACI 363R-84). Also, cement content, which can range from 400 to 550 kg/m^3, can be reduced. Common practice is to substitute 5 to 15 % of the portland cement with silica fume (de Larrard, Malier, 1992).

An undesirable side effect of using silica fume is that autogenous shrinkage is increased. (Autogenous shrinkage is defined in Section 2.5.1.) Acker (1995) notes that in going from a water cement ratio greater than 0.45 to less than 0.40, a three-fold increase in autogenous shrinkage may occur. During hydration, the movement of free water out of the very fine pore structure creates a high tensile force due to capillary

action. The resulting contraction is observed as shrinkage that is greater than for non-silica fume concrete. If restrained, slabs may crack at an early age from autogenous shrinkage alone.

Another difficulty with concrete containing silica fume is the tendency for the mix to be sticky. (Russell 1994). Consequently, a smooth finish for HPC slabs can be difficult to obtain.

The decreased ductility of plain HPC is explained by its microstructure. (Wittmann 1979). In normal concrete, where the aggregate is stronger than the cement paste, cracks propagate around the aggregate. These longer crack paths consume more energy. For concrete of a higher strength, the aggregate becomes the weaker part of the matrix. Shorter cracks form through the aggregate using less energy. Propagation of cracks is more sudden and brittle.

Although plain HPC exhibits brittle failure, a number of researchers have shown that the ductility of under-reinforced HPC members is satisfactory. For example, Shin et al. (1989) tested beams with compressive strength ranging from 25 to 100 MPa. In general, they found that ductility increased with concrete strength for reinforcement in the range of 0.3 to 1.0%. This increase in ductility was confirmed by Pendyala et al. (1996) for testing of beams with concrete strengths from 55 to 80 MPa. Earlier tests, such as Leslie et al. (1973), have shown that for higher reinforcement ratios, ductility is significantly reduced.

2.4 Mechanical properties of HPC

2.4.1 *Compressive strength development*

The most explicit prediction of compressive strength development is given in the CEB MC90:

$$f_{cm}(t) = \beta_{cc}(t) f_{cm} \tag{2.1}$$

Where,

$$\beta_{cc}(t) = \exp\left\{s\left[1 - \left(\frac{28}{t/t_1}\right)^{1/2}\right]\right\} \tag{2.2}$$

$f_{cm}(t)$ = median compressive strength at age of t days

f_{cm} = median compressive strength at age of 28 days

$t_1 = 1$ day

$s = 0.25$ for normal cement.

It is noted that all CEB MC90 expressions should be used with caution for strengths over 50 MPa due to limited testing.

The expression for the strength development of NSC as given by ACI Committee 209 (1982) is:

$$f_c'(t) = f_c' \cdot \frac{t}{\alpha + \beta \cdot t} \tag{2.3}$$

where α and β allow for the type of cement and curing, and $f'_c(t)$ is the compressive strength of concrete at time t.

Both the ACI (1984) and the FIP-CEB (1990) State-of-the-Art Reports on HSC recognize that concrete with a lower water-cement ratio gains strength more rapidly. However, no qualification to the CEB MC90 equation has been made which would allow its use for strengths above 50 MPa. As an approximate comparison, ACI (1984) reports that HSC may reach 80% of its strength within 7 days while NSC reaches about 70%.

2.4.2 *Tensile strength*

Several different expressions for the tensile strength of HPC have been proposed. From the FIP-CEB 1990:

$f_{sp} = 0.54\sqrt{f_{cc}}$ = splitting tensile strength, in terms of compressive strength, f_{cc} (2.4)

$f_{tk} = 0.3 f_{ck}^{0.6}$ = characteristic direct tensile strength, for characteristic compressive strength at 28 days, f_{ck} (2.5)

$f_r = k \cdot f_{cm}^{0.6}$ = tensile strength under flexure (modulus of rupture), for mean value of concrete compressive strength, f_{cm}; k ranging from 0.76 to 0.86 (2.6)

ACI 363R-84 proposes:

$$f'_{sp} = 0.59\sqrt{f'_c} \qquad = \qquad \text{splitting tensile strength} \tag{2.7}$$

A more recent proposal for the split tensile strength of HPC at early ages is given by Imam et al. (1993) for concrete compressive strength, f'_c, from 70 to 115 MPa:

$$f'_{sp} = 0.85\left(f'_c\right)^{0.44} \tag{2.8}$$

The concrete code in France (de Larrard, Malier 1992) gives a tensile strength at an age of j days, f_{ij}, in relation to compressive strength, f_{cj}, as

$$f_{ij} = 0.6 + 0.06 f_{cj} \tag{2.9}$$

The Australian Standard AS 3600 gives expressions for the tensile strength of NSC only:

$$f'_{cf} = 0.6\sqrt{f'_c} \tag{2.10}$$

where f'_{cf} = characteristic flexural tensile strength

f'_c = characteristic compressive strength from 20 to 50 MPa.

$$f'_{ct} = 0.4\sqrt{f'_c} \tag{2.11}$$

where f'_{ct} = characteristic principal tensile strength.

2.4.3 *Modulus of elasticity*

An estimate of the modulus of elasticity for concrete, E_c, in MPa, derived from Carrasquillo et al. (1981) is given in both CSA A23.3-94 and ACI 363R-84:

$$E_c = \left(3300\sqrt{f'_c} + 6900\right)\left(\gamma_c \ / \ 2300\right)^{1.5} \tag{2.12}$$

for f'_c = compressive strength at 28 days (from 20 to 80 MPa)

γ_c = density of concrete in kg/m^3.

An alternative expression for very high-performance concrete, with compressive strength at j days of f_{cj} greater than 80 MPa, is given by de Larrard, Malier (1992) as:

$$E_{cj} = 11{,}000\left(f_{cj}\right)^{1/3} \tag{2.13}$$

FIP-CEB 1990 also recommends a slightly lower value given by the Norwegian Standard, for compressive strength, f_{cc}, less than 85 MPa :

$$E_c = 9{,}500\left(f_{cc}\right)^{0.3} \tag{2.14}$$

Most researchers agree that the elastic modulus of high-performance concrete is very sensitive to the stiffness of the aggregate (Acker, 1995) An expression which attempts to account directly for the influence of aggregate has been proposed by Iravani (1996):

$$E_c = 4{,}700C_{ca}\sqrt{f'_c} \tag{2.15}$$

The term C_{ca} is an empirical aggregate coefficient ranging from 0.61 for sandstone to 0.97 for quartzite. The stated limit of validity for this expression is 55 MPa $< f'_c <$ 125 MPa.

Because of aggregate variability, the common recommendation is that if the elastic modulus needs to be known accurately, specific tests for the HPC mix in question should be done. Other research has also shown that the elastic modulus is sensitive to curing conditions. Sealed specimens were tested and found to have a 25% higher E_c value than companion unsealed specimens.

The development of elastic modulus with time is given by CEB MC90 as:

$$E_c(t) = E_c\left(\beta_{cc}(t)\right)^{1/2} \tag{2.16}$$

where, E_c = elastic modulus at 28 days

$\beta_{cc}(t)$ = coefficient as given by Equation 2.2

2.4.4 *Bond strength to reinforcement*

The bond strength that develops between reinforcement and concrete has an effect on the width of cracks which form. Research done on the bond strength of high-performance concrete has shown an increase proportional to $(f'_c)^{1/2}$ (FIP-CEB 1990). Due to the limited test data available, it is recommended that the same bond properties be used for HPC as for normal concrete.

For concrete with silica fume, a different suggestion has been made by Hwang et al. (1994). From tests on concrete with 10% silica fume, they found that bond strength was reduced by 15% with respect to $\sqrt{f'_c}$. The reason for the reduction in bond is attributed to reduced adhesion between silica fume concrete and steel.

2.5 Creep and shrinkage of HPC

2.5.1 *Terminology*

There has been a recent suggestion to simplify the terminology for the components of shrinkage (Dilger, Wang, and Niitani 1996). "Self-desiccation," "chemical shrinkage," or "autogenous shrinkage" are terms that have been used to describe the shrinkage which occurs internally within the concrete as a result of hydration and without moisture exchange with the surrounding environment. The suggestion is to refer to this as "basic shrinkage", which is entirely analogous to basic creep, the preferred term for creep of concrete at a constant moisture content. The other component of shrinkage that occurs only as a result of water loss from the concrete to the environment is termed "drying shrinkage". For this thesis, the two terms basic shrinkage and drying shrinkage will be used exclusively, with the term total shrinkage equaling their sum.

2.5.2 *Prediction and analysis methods*

The estimate of creep and shrinkage is at best an inexact science. Because of the many variable factors involved, prediction methods generally appear to be quite complex. For example, Committee 209 of the American Concrete Institute (ACI) presented a draft for a new method Model B3 (1995) based on statistical analysis of a large database of creep and shrinkage tests for concrete strengths up to 70 MPa. Although the method is elaborate and is meant to reflect physical processes, it can not be more precise than the test results on which it was developed. For reference, it is mentioned that shrinkage strain data used had a coefficient of variation of 34%. (Coefficient of variation is equal to the mean value divided by the standard deviation.) The accuracy of predictions should not be overstated. A calculated shrinkage estimate of 785×10^{-6}, for example, is more reasonably reported as 800×10^{-6}. To recognize a limitation of Model B3, the high basic

shrinkage exhibited by HPC is not accounted for directly. A modifying formula is given separately.

The importance of measuring shrinkage at very early ages is emphasized for Model B3. If initial measurements are unavailable, a method of extrapolation is presented to help establish the base line.

A more simplified method, which is commonly used, has also been presented earlier by ACI Committee 209 (1982). Factors are used to account for curing conditions, humidity, member thickness, cement content, slump, fine / total aggregate ratio, and air content. From these factors an ultimate shrinkage value is determined. Then, using a simple time function, shrinkage at any time is calculated.

Another common method for predicting shrinkage development is contained within the CEB MC90. Here, the input factors are cement type, characteristic member thickness, humidity, and concrete compressive strength.

A commentary on the prediction models presented in the CEB MC90 code is given by Muller (1992). He points out that the models have fairly high coefficients of variation with respect to the test data that they are based on: 33% for shrinkage prediction and 20% for creep. Of interest to the study of young concrete, the FIP-CEB model for creep is noted as giving poor accuracy for loading at early ages. It is suggested that rate of flow or the improved Dischinger method will give a better estimation of creep. The prediction for shrinkage is described as being based on unloaded and unreinforced concrete sections. An improvement of the model is expected if water content is directly accounted for instead of indirectly through concrete strength. For HPC, with very low water cement ratios this refinement might be especially helpful in improving accuracy.

Sakata (1995) presented shrinkage prediction equations that have been incorporated into the Japanese Building Code:

$$\varepsilon_{sh}(t,t_0) = \varepsilon_{sh\infty}\left[1-\exp\left\{-0.108(t-t_0)^{0.56}\right\}\right] \tag{2.17}$$

$$\varepsilon_{sh\infty} = -50 + 78\{1-\exp(RH/100)\} + 38\ln W - 5\{\ln(V/S)\}^2 \tag{2.18}$$

where $\varepsilon_{sh\infty}$ = ultimate long term shrinkage (x 10^{-5})

$\varepsilon_{sh}(t,t_0)$ = predicted shrinkage occurring between t and t_0 (x 10^{-5})

t = age of concrete (days)

t_0 = age of concrete at beginning of drying

RH = ambient relative humidity (%)

V/S = volume to surface ratio of concrete member (cm)

W = water content (kg/m^3)

The predicted value for shrinkage, as given by the Australian Standard AS 3600 is:

$$\varepsilon_{cs} = k_1 \varepsilon_{cs,b} \tag{2.19}$$

The value of the shrinkage strain coefficient k_1 is determined from AS 3600 Figure 6.1.7.2. It accounts for the humidity of the drying environment and the thickness of the concrete member. Rather than specify a value of relative humidity, a map of Australia showing different climatic zones is given. Of course, this makes it more difficult to use the standard for international comparison. The value of "basic" shrinkage strain, $\varepsilon_{cs,b}$, is given as 700 x 10^{-6}. (This "basic" value is not meant to represent autogenous shrinkage but rather a baseline value.) The standard recognizes the difficulty in predicting shrinkage and suggests a ±30% range in accuracy.

Creep is estimated in AS 3600 as a function of the basic creep factor $\phi_{cc.b}$, an environment factor, k_2, for humidity and thickness, and a maturity coefficient, k_3:

$$\phi_{cc} = k_2 k_3 \phi_{cc.b} \tag{2.20}$$

Values for basic creep are given in terms of compressive strength. And, figures are given to determine k_2, and k_3.

A prediction model for estimating creep and shrinkage in HPC has been recently proposed by Dilger, Niitani, and Wang (1997). This model is based on their own testing and on comparison with existing data. Since one of the concrete mixes used in their tests (H80) is the same as the HPC for this thesis, the accuracy of predictions is excellent (refer to Section 4.7.3). The proposed model separates both shrinkage and creep into their components: basic and drying. The parameters which are considered to influence shrinkage are water-binder ratio, compressive strength, volume to surface ratio, relative humidity, and time at which drying starts. The model is especially useful for very low humidity, since it included data from testing under extreme conditions. Creep is estimated by the model based on the same parameters as for shrinkage (except for compressive strength) and also accounts for age at loading.

Thorough methods of analysis involving creep and shrinkage have been published. Two references which were used in preparing this thesis are Neville, Dilger, and Brooks (1983) and Rüsch, Jungwirth, and Hilsdorf (1983). Details are presented later as required.

2.5.3 *Creep and shrinkage tests on HPC*

To measure basic shrinkage alone, sealed specimens must be used. For this thesis, only the combination of basic plus drying shrinkage was measured. Other tests on the same HPC mix have been done to determine basic shrinkage. Dilger, Wang, and Niitani (1996) have reported that up to -200 x 10^{-6} basic shrinkage strain can occur in the first 24 hours after casting. They also observed long-term shrinkage up to four times as high as other researchers who did not measure basic shrinkage in their experiments. These findings emphasize how large early shrinkage strains can be, and identify the potential for cracking in young HPC, even if water loss is prevented.

Ravindrarajah et al. (1994) tested concrete with a water binder ratio of 0.35, silica fume content of 8%, and compressive strength of 87 MPa. They found total shrinkage to be 520 x 10^{-6} at 28 days, 685 x 10^{-6} at 100 days, and 775 x 10^{-6} at 460 days. Specimens were water-cured for 3 days and then put in a 65% humidity environment. By increasing the silica fume content to 15%, they found that long-term shrinkage could be reduced by 25%. No mention was made of when strain measurements began. Therefore it is difficult to estimate how much shrinkage at very early ages was missed.

Other tests were made on silica fume concrete with a water / binder ratio of 0.33 and a 100 MPa compressive strength. The internal tensile stress was 2 MPa from basic shrinkage in the restrained slab specimens (Bloom, Bentur 1993,1995). Silica fume was also found to increase plastic shrinkage and to produce cracking at an earlier age than for the same concrete without silica fume.

Bloom and Bentur (1995) tested high-strength concrete, with and without silica fume, under conditions of free and restrained shrinkage. Water-cement ratios of the mixes used ranged from 0.33 for the HSC to 0.50 for the NSC control mix (compressive strengths were not reported). They used small scale specimens (40 mm x 40 mm x 1000

mm) and a specially-designed frame with end jaws to grip the specimens and provide restraint. With this set-up they were able to directly measure the tensile force which develops under full restraint. They found that significant stresses developed due to basic shrinkage for concrete exposed to a temperature of 40 °C and 45 % relative humidity: 0.1 MPa within 3 hours and up to 1.9 MPa after 3 days. The addition of silica fume increased the tensile stress due to higher basic shrinkage. Free shrinkage specimens experienced strains of 400 to 500 x 10^{-6} within 6 hours. Even in sealed specimens, substantial internal tensile stresses developed for concrete with a low water-cement ratio due to high basic shrinkage.

The development of shrinkage cracks was also studied by Bloom and Bentur (1995). They observed both plastic cracking, which occurs in fresh concrete prior to setting, and early-age cracking within the first week after casting. Concrete with silica fume set quicker: at about 3.8 hours versus 5.0 hours for the same concrete without silica fume. Consequently, the restrained silica fume concrete specimens cracked 4 hours after casting as compared to 7 hours without silica fume.

The FIP-CEB 1990 summarizes testing which has shown that high-strength concrete will experience a high rate of early shrinkage. However, shrinkage is expected to slow down such that after 100 days or more, normal and high-strength would have similar values.

It is commonly agreed that creep is reduced with an increase in concrete strength. For example, FIP-CEB 1990 observes that the creep coefficient is about 25% lower for 80 MPa HPC than for concrete with a strength below 50 MPa. Ngab et al. (1981) observed a similar reduction in creep. The main reason for this reduction is that HPC exhibits less drying creep because of its low rate of moisture exchange with the environment. Tests have been done which support this conclusion. Sealed specimens of both HPC and NSC were compared. The measured creep coefficients varied by only 10%

showing that differences in creep values for unsealed specimens can be attributed to drying creep alone (FIP-CEB 1990).

An earlier series of tests by Nagataki and Yonekura (1982) reported a much different result. They observed that drying creep is insignificant for concrete with a water-cement ratio less than 0.27. They also found that creep for the 95 MPa concrete tested was only 20 - 25% that of 35 MPa concrete. In comparing the different components of creep in HPC, Dilger et al.(1996) found that drying creep was between 25 to 35% of the basic creep.

Han and Walraven (1995) performed testing on high-strength concrete to determine properties of creep and shrinkage at early ages. The mixes tested used rapid hardening portland cement (class C), 5% silica fume, and a water to cement + silica fume ratio of 0.30. The reported compressive strengths varied from 80 to 100 MPa. The relative humidity during testing was 50%. They found that both the ACI 209 and the CEB MC90 expressions underestimated both compressive strength and elastic modulus at early ages. Other observations included high basic shrinkage at early ages, and a higher rate of creep for young versus mature high-strength concrete. In comparing test measurements with prediction models, it was noted that the ACI 209 model is better than the CEB MC90 model in predicting the shrinkage of HSC for drying starting at 28 days. For early shrinkage, with drying from an age of 16 hours, they found that the CEB MC90 model is more accurate, although strains are underestimated up to 15 days. After about 15 days the actual rate of shrinkage drops much lower than predicted. Creep for HSC loaded at 16 hours had an initial rate far higher than predicted. This trend was seen to reverse at an age of about 10 days. Tests from 16 hours to 90 days gave shrinkage of about 400×10^{-6} with a creep coefficient of about 1.7 for 50% stress/strength loading. Up to 50% of the shrinkage and 75% of the creep occurred within the first four days.

The effect of hydration temperature rise on creep at early ages has been studied by Guenot et al. (1996). They tested an HPC with a water to cement + silica fume ratio of 0.3. The temperature in the 300 mm diameter cylindrical specimens reached a peak of 36 °C at 20 hours. The specimens were subjected to a varying stress history beginning with 4 MPa at 20 hours and reaching 18 MPa at 8 days. Creep measurements were compared to the predictions of three different methods including the CEB MC90, which gave good results. This observation contradicts that made by Muller (1992).

Very little tensile creep research has been conducted. Bissonette and Pigeon (1994) tested high-performance silica fume concrete made with a compressive strength of 70 MPa. Their conclusion was that creep due to tension can be expected to significantly reduce the stresses which develop due to restrained shrinkage. They found that a reduction in water cement ratio reduced tensile creep, but that the use of silica fume had no noticeable effect.

The effect of cycles in ambient humidity on drying shrinkage is discussed by Acker (1995) and in Model B3 by Bazant (1995). Because drying is a very slow process, short term variations in relative humidity are not significant to shrinkage. Only mean humidity over long periods of time are important to consider. Seasonal variations, for instance, have a noticeable effect.

2.6 Cracking and crack control

2.6.1 *Code guidelines*

National codes give some guidance about the control of cracking. In 1971, the American standard ACI 318 first introduced an expression for flexural crack control in beams. An explanation is given by Nawy (1972). The more recent code, ACI 318-89,

sets a limit on the parameter z, which is calculated from the steel stress, f_s, cover thickness, d_c, and concrete area in tension, A:

$$z = f_s \sqrt[3]{d_c A} \tag{2.21}$$

Canadian Standard A23.3-94 uses the same parameter. Expected crack widths are not calculated for ordinary design by ACI 318. Other methods such as those suggested by ACI Committee 446 may be consulted if the level of design requires the extra effort. Crack control in nonprestressed beams is addressed by Australian Standard AS 3600 through limitations on bar spacing. No calculation of concrete tensile stress is required.

Flexural crack control for slabs is addressed in AS 3600 by limiting bar spacing to 500 mm or 2.5 times the slab depth. For the control of cracks due to temperature and shrinkage, a distinction is made between the primary and secondary direction of reinforcement. In the primary direction, the requirement for strength governs. For the secondary direction, in restrained slabs the designer must first consider the exposure of the structure. As exposure becomes more severe, and/or desired crack control increases, a greater amount of minimum reinforcement is stipulated. The range given is:

$A_{st} = 0.7bD / f_{sy}$ for minor crack control in a moderate environment, to (2.22)

$A_{st} = 2.5bD / f_{sy}$ for strong crack control in a severe environment. (2.23)

Recommended maximum crack width for normal structures, as given by FIP-CEB 1990 is about 0.3 mm. This requirement applies to either HPC or normal concrete. For the same intended service the concrete strength makes no difference to the allowable width of cracks. Since cracks are obviously void of concrete, stronger or weaker concrete has no effect on the penetration of corrosive elements through open cracks.

Methods to achieve flexural crack control are also discussed in the FIP-CEB 1990. A simplified approach is presented in which expected crack width is not calculated. Instead, maximum bar diameter and spacing is suggested based on the calculated stress in the reinforcing steel. For concrete with tensile strength, f_{ctm}, greater than 2.5 MPa, the bar diameter values may be conservatively multiplied by $f_{ctm} / 2.5$. If an estimate of crack width is desired, a more detailed method of analysis is described.

2.6.2 *Research efforts*

Based on long-term tests of 160 mm thick slabs with a span of 3100 mm, Jaccoud et al. (1993) reported that minimum reinforcement for crack control is only slightly increased for an increase in concrete compressive strength from 30 to 85 MPa. Their explanation was that although higher strength concrete exerts greater tensile forces, bond to reinforcement is improved. The result is a balance which tends to keep crack width fairly constant over a range of compressive strength.

One suggestion for calculating maximum crack width w_{max} caused by shrinkage and thermal strain, ε_{sh} and ε_{t}, is given by Rangan (1992). The estimate is based on the ratio of direct tensile strength to bond strength f'_t / σ_b. It is noted that this ratio is independent of concrete strength and can be taken as 0.5. Also in the equation are bar diameter, d_b, and reinforcement ratio, r:

$$w_{\max} = \frac{f'_t d_b (\varepsilon_{sh} + \varepsilon_t)}{2\sigma_b r} \tag{2.24}$$

The amount of reinforcement, $\rho_{critical}$, required to prevent wide isolated cracks from forming due to the yielding of steel, has been given by Elbadry and Ghali (1995):

$$\rho_{critical} = \frac{A_{s,critical}}{A_{gross}} = \frac{f_{ct} / f_y}{1-(\alpha - 1)(f_{ct} / f_y)} \tag{2.25}$$

where $\alpha = E_s/E_c$, f_{ct} = tensile strength of concrete determined from split cylinder tests, f_y = yield strength of steel, A_{gross} = gross cross sectional area. For typical values of f_{ct} and f_y, this expression gives a steel ratio which is much higher than normally used values such as 0.2%

A series of tests was conducted by Yokoyama et al. (1994) to assess early-age cracking in high-strength concrete. They tested several different concrete mixes exposed to an air flow of 8 m/s after four hours. One of the mixes had a water-cement ratio of 0.30 and a cement content of 567 kg/m^3. No silica fume was used in any of the mixes and strengths were not reported. Their tests used a steel frame which effectively restrained shrinkage and caused cracks to form at an age as early as 2 hours. Crack widths up to 2 mm were observed in the unreinforced specimens.

Although Yokoyama's tests primarily identified the potential for plastic shrinkage in low water/cement ratio concrete, they also underlined the risk of early-age cracking in high-performance concrete. A secondary effect was discovered that the use of different forms of superplasticizer influences free shrinkage. Specifically, concrete with a polycarbonic acid admixture experienced much less shrinkage than concrete with a napthalene type admixture.

Wiegrink et al. (1996) also performed tests to study shrinkage cracking of restrained HSC cured in 50% humidity. Using ring specimens they found that crack widths increased and age of cracking decreased with an increase in silica fume content. They observed cracks up to 0.90 mm in width for concrete with a silica fume content equal to 15% by weight of cement. Complementary tests showed that specific creep was

lower and free shrinkage was much higher for the concrete with more silica fume. Earlier demolding increased shrinkage even further. Specifically, specimens with 15% silica fume demolded after six hours and then cured in 50% humidity had free shrinkage strains of $400\text{x}10^{-6}$ in 5 days, $700\text{x}10^{-6}$ in 20 days, and $800\text{x}10^{-6}$ in 90 days.

The explanation given by Wiegrink for earlier cracking in HSC is complex but reasonable. Although tensile strength develops quickly, it is exceeded at an early age by tensile stress. The compound effect of rapid shrinkage, higher elastic modulus, and lower creep (less relaxation) creates very high tensile stress at young ages.

Lambotte and Taerwe (1990) tested 35 MPa and 80 MPa slabs with reinforcement ratios of 0.48% and 0.95%. From CEB prediction models, they showed that the concrete strength does not have a large effect on crack widths and spacing. This prediction was confirmed by their experiments. The conclusion of their research was that deflections of uncracked slabs can be greatly reduced by using higher strength concrete. However, for cracked sections concrete strength is of minor influence. Further confirmation of these results was presented through testing by Battista (1992).

A theoretical analysis of the development of shrinkage cracks in restrained members is presented by Gilbert (1992). He determines a formula of predicting the tensile force in the member immediately after cracking, N_{cr}, in terms of reinforcement ratio
$\rho = A_s/A_c$, modular ratio $n = E_s/E_c$, and tensile strength f_t,

$$N_{cr} = \frac{n\rho f_t A_c}{C_1 + n\rho(1+C_1)} \qquad \text{with} \quad C_1 = \frac{2s_o}{3L - 2s_o} \tag{2.26}$$

L is the full length of the restrained member, and the term s_o represents the distance on either side of a crack over which steel stress develops. A suggestion for estimating s_o from the bar diameter d_b is,

$$s_o = d_b / 10\rho \tag{2.27}$$

Gilbert (1992) also gives a procedure and formulas to predict crack spacing and final crack width. Although numerical examples are included to illustrate the method, no comparison is given to measured cracking of test specimens.

2.7 Minimum reinforcement

2.7.1 *For crack control*

The minimum reinforcement for slabs, to control cracking due to shrinkage and temperature, is specified in CSA Standard A23.3-94, Clause 7.8.1 as:

$$A_{s\min} = 0.002 A_g \tag{2.28}$$

where A_g is the gross area of the cross-section. A similar provision is made in ACI 318-89 Clause 7.12 with the additional dependence on the yield strength of steel reinforcement:

$$A_{s\min} = 0.002 A_g \qquad \text{for Grade 40 or 50 reinforcement} \qquad (f_y = 40 \text{ or } 50 \text{ ksi, } 275 \text{ or } 345 \text{ MPa}) \tag{2.29}$$

$A_{s\min} = 0.018 A_g$ for Grade 60 reinforcement (2.30)

(f_y = 60 ksi, 415 MPa, most common grade used)

$A_{s\min} = 0.018 A_g \times 60{,}000 / f_y$ for f_y > 60,000 psi (415 MPa). (2.31)

Rangan (1992) gives a recommended minimum reinforcement ratio for slabs, r_{min} :

$$r_{\min} = K f_t' / f_{sy} \tag{2.32}$$

where K is an adjustment factor (1.2 suggested) and f_{sy} is steel yield strength. The desired result is to prevent yielding of the reinforcement due to shrinkage cracks.

2.7.2 *Minimum flexural reinforcement*

The ratio of minimum flexural reinforcement recommended by the ACI 318-89 (American Concrete Institute) is given in Clause 10.5.1 as:

$$\rho_{\min} = \frac{200}{f_y} = \left(\frac{1.4}{f_y}\right) \tag{2.33}$$

with f_y = steel yield stress in psi (MPa). In lieu of this amount, the designer may alternatively provide reinforcement which is "one-third greater than required by analysis." The intent of this alternative is to provide sufficient ductility for beams which are so large that 1.4 / f_y would be impractical.

Naaman (1992) suggested a revision to the ACI 318-89 provisions for the minimum flexural reinforcement in beams, ρ_{min} :

$$\phi \cdot M_n \geq 1.2 M_{cr} \quad \text{and} \tag{2.34}$$
$$\rho \geq \rho_{min} = 0.03 f_c' / f_y$$

where ϕ, with a value of 0.9, is the material resistance factor for concrete, M_n is the nominal resisting moment, and M_{cr} is the cracking moment for the concrete section. The suggested limits were intended to account for higher strength concrete.

Specific to concrete in the higher strength range, 20 to 80 MPa, ACI 363R-84 recommends the minimum reinforcement ratio for beams, ρ_{min} of

$$\rho_{min} = 2.7\sqrt{f_c'} / f_y \geq 200 / f_y \qquad (\text{for } f'_c \text{ and } f_y \text{ in psi}) \tag{2.35}$$

$$\rho_{min} = 0.22\sqrt{f_c'} / f_y \geq 1.38 / f_y \qquad (\text{for } f'_c \text{ and } f_y \text{ in MPa}). \tag{2.36}$$

This expression is derived from the specification of having a resisting moment that is at least equal to the cracking moment. To account for the difference between beams of varying cross-section, Nilson (1994) recommends (for f'_c and f_y in MPa):

$$\rho_{min} = 0.149\sqrt{f_c'} / f_y \qquad \text{for rectangular cross-sections} \tag{2.37}$$

$$\rho_{min} = 0.224\sqrt{f_c'} / f_y \qquad \text{for T beams of normal proportions.} \tag{2.38}$$

The latest Canadian code A23.3-94 also considers strength in stipulating minimum reinforcement, A_{smin}, for beams with a width in tension, b_t, and an overall depth, h:

$$\frac{A_{s\min}}{b_t h}(=\rho_{\min}) = 0.2\sqrt{f'_c}/f_y \qquad (\text{for } f'_c \text{ and } f_y \text{ in MPa}). \qquad (2.39)$$

The limit of validity is given as 20 MPa $< f'_c <$ 80 MPa. This expression is practically the same as given for ACI 363R-84.

Minimum flexural reinforcement for beams is stipulated in AS 3600 in relation to the yield strength of reinforcement, f_{sy}, as:

$$A_{st}/bd = 1.4/f_{sy} \qquad (2.40)$$

Alternatively, the designer is given the option of ensuring that the ultimate moment is 1.2 times the cracking moment.

As stipulated by AS 3600 for slabs, the amount of minimum flexural reinforcement for strength is dependent on support conditions. Slabs on columns require:

$$A_{st}/bd = 1.0/f_{sy} \qquad (2.41)$$

while slabs supported by beams or walls need less reinforcement:

$$A_{st}/bd = 0.8/f_{sy}. \qquad (2.42)$$

In the secondary direction, reinforcement for crack control in slabs is specified as:

$$(0.7-\sigma_{cp})bD/f_{sy}, \quad \text{for a minor degree of crack control, and up to} \qquad (2.43)$$

$$(2.5-\sigma_{cp})bD/f_{sy}, \quad \text{for strong crack control, and for more severe exposure.}$$

2.7.3 *Research on minimum reinforcement for HPC*

The specific research for minimum reinforcement in high-performance concrete has been limited. Bosco et al. (1990) have proposed values of steel percentage which produce first cracking at the same load as ultimate flexural capacity. They tested beams of 90 MPa compressive strength with a width of 150 mm and depths of 100 to 400 mm. The minimum reinforcement which they determined took into account beam size effects. This was done by using the concepts of fracture mechanics. With this approach, confirmed by their testing, they have shown that current ACI reinforcement ratios are conservative for greater beam depths, but are inadequate for shallower beams. A similar conclusion was reached by Ouyang and Shah (1994) also using a fracture energy approach to predict cracking.

In studying the cracking in restrained HSC members due to temperature and shrinkage strains, Bergner (1994) presents an equation predicting the tensile load at first cracking:

$$F_{crack} = A_i f_{ctm} k_{z,t} \lambda_{Reinf} \tag{2.44}$$

where F_{crack} = tensile load producing first crack

A_i = area of concrete member including reinforcement (transformed)

A_s = area of reinforcement

f_{ctm} = mean tensile strength of concrete at 28 days

$k_{z,t}$ = time factor (suggested values given by Bergner)

λ_{Reinf} = factor of inherent stress caused by reinforcement and chemical (basic) shrinkage

$= 0.85$ for $0 \le \mu \le 1.0\%$

$= 0.90 - 0.05\,\mu$ for $\mu \ge 1.0\ \%$

μ = reinforcement ratio (%)

Also given by Bergner is an estimate of the minimum reinforcement that will produce distributed cracking without yielding of the reinforcement:

$$A_{s,rec} = F_{crack} / \sigma_{s,zul} \tag{2.45}$$

where $A_{s,rec}$ = minimum reinforcement

$\sigma_{s,zul}$ = steel stress

In an earlier report on the same subject, Bergner (1993) identified, through testing, the critical phase for cracking at an early age. He found that at a time about three hours after the peak temperature had been reached in the member, cracking potential was critical. This was found to be the point in time when the combined effect of early basic shrinkage and contraction due to cooling was the greatest. If the member was going to form a single wide crack this is when it would most likely occur.

Tests to determine the amount of reinforcement required to prevent brittle failure in high-strength concrete slabs have been conducted by Battista (1992). He found that the code requirement of CSA A23.3-84 Clause 7.8.1, which requires $A_{smin} = 0.002\, A_g$, to be sufficient in producing a ductile failure for slabs with strengths up to 85 MPa. The suitability of this same percentage of steel in preventing unacceptable cracking due to thermal and shrinkage strains is the subject of this thesis.

A related topic is the effect which low amounts of reinforcement have on the shear strength of high-performance concrete beams. Ahmad et al. (1986) have shown that shear capacity can be much less than expected if the amount of flexural reinforcement used is low. The design of HPC beams with only minimum reinforcement should recognize this possibility, and shear strength should be conservatively estimated.

CHAPTER 3

EXPERIMENTAL PROCEDURES

3.1 Description of test specimens

3.1.1 *General*

Five large-scale slabs were cast in the test program carried out for this thesis in an effort to determine the amount of reinforcement necessary to control shrinkage cracking. The slabs were constructed with a high degree of restraint and were subject to the drying effect of very low laboratory humidity and to thermal effects caused by their own heat of hydration. No external loads were applied to the specimens.

The restrained concrete slab specimens tested are shown in Figure 3.1. The large-scale slabs were 4300 mm in length overall and 800 mm in width. The "test section" of the slab was 2550 mm long, 800 mm wide and 125 mm in thickness. End blocks 800 x 800 x 375 mm were cast monolithically with the slab section. The end blocks were tapered up to the underside of the slab to aid in the release of the formwork. The exposed edges of the slab were covered with a waterproof membrane, trade name Bituthene, to prevent moisture loss. The black membrane can be seen on the slab edge pictured in Figure 3.5. (The apparent discoloration of the top surface of the slab in this photo is actually caused by the partial drying of the curing compound.)

The slabs were identified by their nominal 28 day compressive strength and percentage of reinforcement. The high-performance concrete slabs were expected to reach a strength close to 100 MPa based on earlier trial mixes performed by others at the University of Calgary. However, a lesser strength of about 85 MPa was achieved. The mix proportions for the concrete used are given in Appendix A, and the petrographic analysis of the aggregate is given in Appendix B. The HPC used for the tests described

here had a *w/b* ratio of 0.30. The control mix of NSC had a *w/b* ratio of 0.64. More details on the material components can be found in Dilger et al. (1996) under the H80 mix description.

SLAB IDENTIFIER	COMPRESSIVE STRENGTH (MPa)	REINFORCEMENT (%)
30-2	30 (NSC)	0.2
30-4	30	0.4
100-2	85 (HPC)	0.2
100-4 *	85	0.4
100-8	85	0.8

Table 3.1 Test slab identification and composition

* The first attempt for slab 100-4 was removed shortly after casting. An incorrectly labeled admixture (later identified as an accelerator) had been added to the mix instead of the superplasticizer Rheobuild 1000. An accelerator has the opposite effect of the recommended retarding admixture for high-performance concrete (ACI 363R-84, Ryell and Bickley, 1987). Expectedly, slump loss was very quick and the concrete could not be properly consolidated. Voids were abundant upon removal of formwork. As a result concrete strength was very low within slab, as confirmed using Schmidt hammer testing. A replacement slab was cast with the correct admixture and subsequent strength.

3.1.2 *Reinforcement*

The reinforcement placed in the slabs was based on Clause 7.8.1 of CSA Standard A23.3. (No account of concrete compressive strength is made in this clause.) For the test slabs the minimum reinforcement specified is:

$$A_{smin} = 0.002\,A_g = (0.002)(125)(800) = 200\ \text{mm}^2 = \quad 2 - 10\text{M bars}$$
$$(0.2\%\,A_g) \qquad\qquad\qquad\qquad\qquad\qquad\qquad\qquad (10\text{M @ 400 o/c.})$$

Slabs 30-2 and 100-2 were accordingly reinforced with 2 - 10M bottom bars in the longitudinal direction and 10M @ 400 on center transverse. To model the reinforcing used in a continuous slab, and to prevent cracks from occurring at the edge of the end blocks, top reinforcement was also placed at the slab ends. For the first slab, 2 - 10M bars were used and extended out a distance of 650 mm (0.25 times the clear span of 2550 mm). The extension used was equal to the curtailment length specified in Clause 13.12.5 of CSA A23.3.

Since wide cracks formed in both slabs with 0.2% reinforcement, subsequent slabs had 4 - 10M bottom (30-4 and 100-4), and 4 - 15M bottom bars (100-8). The reinforcement used is detailed in Figures 3.2 and 3.3, and pictured in Figure 3.4.

3.1.3 *Free shrinkage specimens*

With each large slab, two companion specimens were cast to measure free shrinkage. The free specimens for slab 30-2 are pictured in Figure 3.7. The specimens were of the same thickness as the main slab, 125 mm, and were 300 mm wide by 800 mm long. The edges were sealed with the same membrane as the main slab. One of the

specimens was also sealed on the bottom surface. This was done to assess differential shrinkage without moisture loss from the bottom.

3.1.4 *Casting procedure*

Both of the NSC slabs were cast in four batches of approximately 0.25 m^3 each. The batches were similar in consistency and were easily consolidated using internal vibrators. The entire casting was completed to first trowel finish within four hours. Following the evaporation of bleed water, eight hours after casting, the final slab finish was done.

The HPC slabs were cast in a similar manner. It was necessary to work more quickly with the HPC mixes because of rapid slump loss: final finish was completed within four hours. (Methods to control the slump loss in HPC are discussed by Punkki et al. (1996).) The slab surface was difficult to finish because almost no bleed water could be brought up during trowelling. A fine mist of water was applied during the final finish, but the resulting surface was still much rougher than that of the NSC slabs.

Although some sources have reported the tendency for high-performance concrete slabs to form extensive plastic shrinkage cracks (Russell 1994), this was not the case with the test slabs.

3.1.5 *Curing protection*

The same means of protecting the slabs from moisture loss was used for all of the test specimens. Immediately after completing the final finishing of the slab and free specimens, a curing compound was applied to the top surface. A hydrocarbon resin-based compound produced by Conchem under the trade name LR-151 was used. The amount recommended by the manufacturer was applied: about 0.25 L / m^2 of surface area. No

additional water was applied to the top surface of the slab during curing. Neither were the slabs covered with plastic or wet burlap. This dry method of curing was chosen to follow typical industry practice today (Mather, 1987). Formwork for the main slabs and free specimens was removed 24 hours after casting.

3.1.6 *Curing environment*

All of the slabs and the free shrinkage specimens were located in an indoor temperature controlled laboratory for the duration of testing. The relative humidity in the lab is typically very low for six months of the year, as shown in Figure 3.8. The outside relative humidity is fairly constant in Calgary, between 60 and 80% over the year (Smith, 1998). However, due to the colder temperatures in the winter months, outside air is substantially heated for use indoors, and thus its relative humidity is greatly reduced. The volume of moisture in the air is not reduced, but the amount of moisture which can be absorbed by the air before it is saturated is increased when the air is heated. Hence, relative humidity, which is a measurement of the degree of saturation of the air, is reduced.

The temperature in the lab is maintained in the range of 19 to 22° C. Temperature and humidity measurements were taken with a digital thermo-hygrometer with a reported accuracy of 0.1° C and 2% relative humidity.

Periodically, in very dry conditions, the humidity readings from the meter dropped to less than 5% and did not rise even when the meter was placed in a water-saturated fog room. Subsequently, the meter was repaired. But the same low readings occurred in the next dry season. When measurements were repeated later with a more sophisticated device a minimum value of 10% was recorded. This is the lower bound humidity value which is deemed most accurate, and is referred to in later discussions.

The test slabs were cast at different times of the year. Thus, the humidity during the critical period after casting varied for each slab. Figure 3.9 plots the curing humidity profile for each slab in its first 28 days after casting.

The concrete cylinders used for strength tests were demolded after 24 hours and placed in a fog room with temperature and humidity controlled as specified by ASTM C 192-88.

3.1.7 *Slab restraint*

Restraint was applied by prestressing 25 mm diameter Dywidag bars to clamp the end blocks to the 750 mm thick load floor slab. The location of the prestressing bars can be seen on Figures 3.2 and 3.3. Prestress force was applied such that the developed frictional force between the end block and the load floor exceeded the tensile strength of the 125 x 800 mm slab cross section. Thus, the slab would fail in tension and crack prior to the end blocks slipping. This was deemed to be a near fully restrained condition.

To follow the development of strength in the NSC slabs, the prestressing was applied in several stages. For slabs 30-2 and 30-4 a prestressing force of 140 kN was first applied at an age of about 36 hours, for a concrete compressive strength of 9 MPa. The prestressing force was later increased to 250, 300, and 400 kN at 2, 3, and 7 days of age as strength developed to 13, 16, and 22 MPa.

Because of the rapid development of compressive strength for the HPC, a single application of prestressing was sufficient. For slabs 100-2, 100-4, and 100-8 the full force of 500 kN was applied within 30 hours as concrete strength had already reached 30 MPa.

3.1.8 *Deflection measurements*

During the measurement of shrinkage for the first slab tested, it was found that over its full 4300 mm length, the slab was shortening. Dial gauges #1 and #2 were then installed at 50 mm from the top and 50 mm from the bottom of the end block, respectively, to monitor the deformation at the end block (Figure 3.6 and 3.10). Shear deformations were observed with the top of the end block was deflecting laterally. This shear deformation was a partial loss of restraint and is discussed in Section 4.8.2.

Dial gauge #3 was installed below the midspan of the slab to measure slab deflection. This deflection was monitored to observe the effect of differential shrinkage between the top and bottom slab surfaces and the resulting curvature in the slab.

3.2 Compressive and splitting tensile strength tests

Cylinders for compressive strength tests were a nominal size of 102 mm diameter by 152 mm length. (Imperial size plastic molds: 4" diameter by 6" length.) All of the cylinders were moist cured in a fog room as specified by ASTM C 192. Strength tests were conducted in accordance with the specification ASTM C 39 and C 496. All cylinders for the 30 MPa slabs were sulfur-capped prior to testing. The HPC slab cylinders which were tested within three days were also capped. For HPC cylinders tested at ages later than three days, the ends were finished using an automatic grinding machine as recommended by ACI 363R-84. The improved accuracy resulting from grinding the ends of test cylinders is also noted by Lessard and Aïtcin (1992).

Cylinders for splitting tensile tests were also of 102 x 152 mm size. Tests were in accordance with the specification ASTM C 496.

3.3 Shrinkage and crack measurements

Shrinkage measurements were made using metal Demec points glued to the concrete surface. A grid of points at a 500 mm spacing was fixed to the top and side surfaces of each slab specimen. Points at 500 mm were also attached to the top and bottom surface of the free shrinkage specimens. The layout and numbering of the points is shown in Figure 3.10. For measuring crack width openings points at a 50 mm gauge were used. The location of these points is discussed later in relation to crack locations for the specific slabs. To directly measure crack width, a 50X crack microscope with 0.02 mm divisions was used.

To measure strains, precise instruments were used. An electronic digital micrometer with a 0.001 mm precision, mounted on a sliding steel beam, was used to measure distances for the 500 mm points. A mechanical dial gauge with a 0.002 mm precision, mounted on a steel bar with a pivoting caliper, was used for the points at a 50 mm gauge length.

The repeatability of measurements was checked for both instruments. In general, measurements using the electronic micrometer could be repeated within 0.002 mm. With the mechanical dial gauge, a 0.003 mm repeatability was achieved. In terms of strain, over the 500 and 50 mm gauge length repeatability was 4×10^{-6} and 60×10^{-6}, which is a satisfactory level of precision.

Shrinkage measurements commenced soon after casting of the slabs. Initial readings were taken within 36 hours after casting for slabs 30-2, 30-4, and 100-2. In order to determine the influence of early age shrinkage, which has been shown to be significant for HPC, readings for slabs 100-4 and 100-8 were started within 12 hours.

3.4 Temperature measurements within the slab section

To measure the rise in temperature during hydration several thermocouples were embedded in the test slabs. The location of these thermocouples is shown in Figures 3.11 and 3.12.

3.5 Reinforcement tensile tests

Samples from the steel reinforcement used in the test slabs were subjected to tensile tests. These tests were conducted to determine the yield stress and strain. Using the actual values for these steel properties, rather than imprecise material specifications, leads to a more accurate discussion of the effect of the reinforcement in restraining cracking.

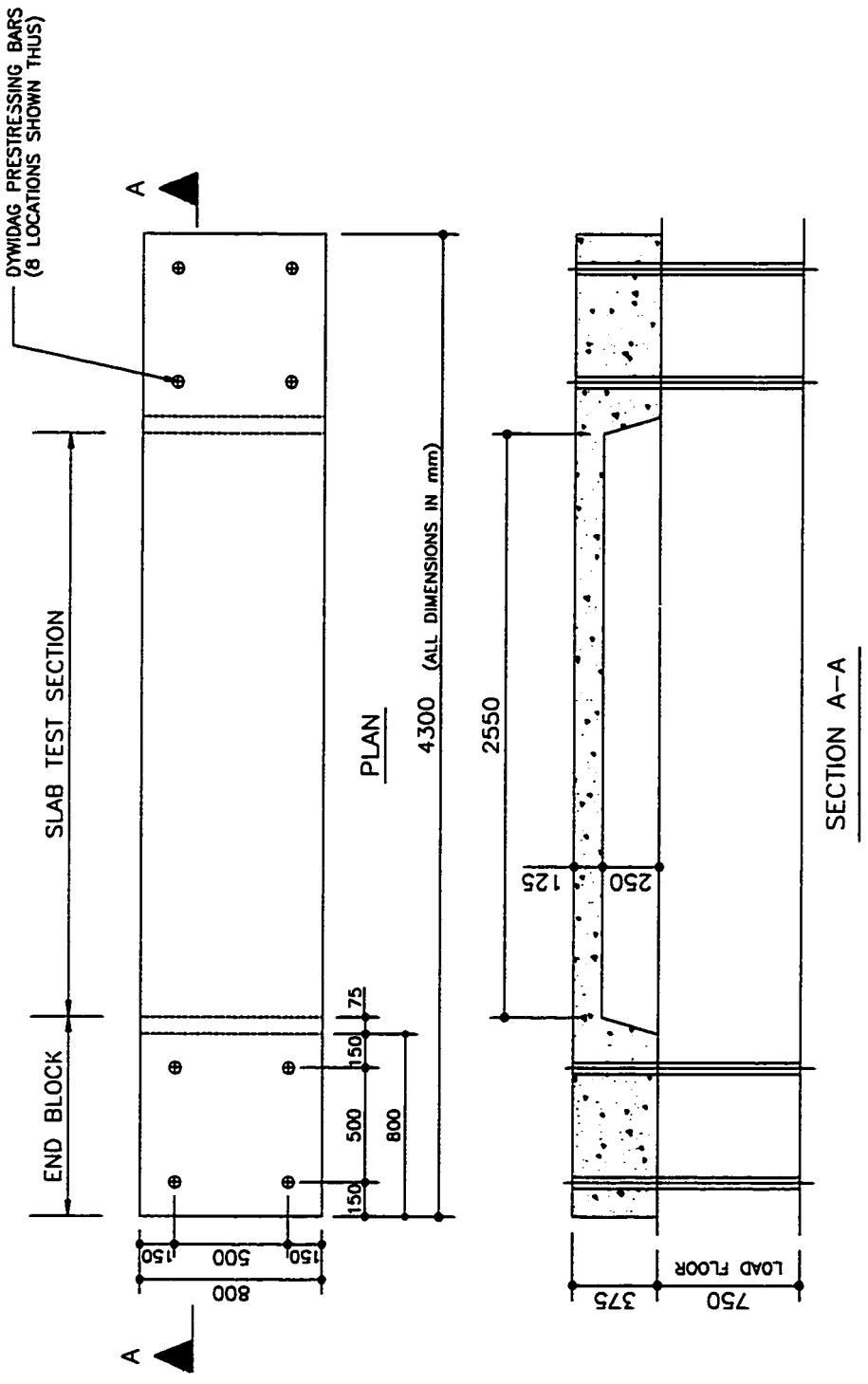

Figure 3.1 Restrained slab specimens

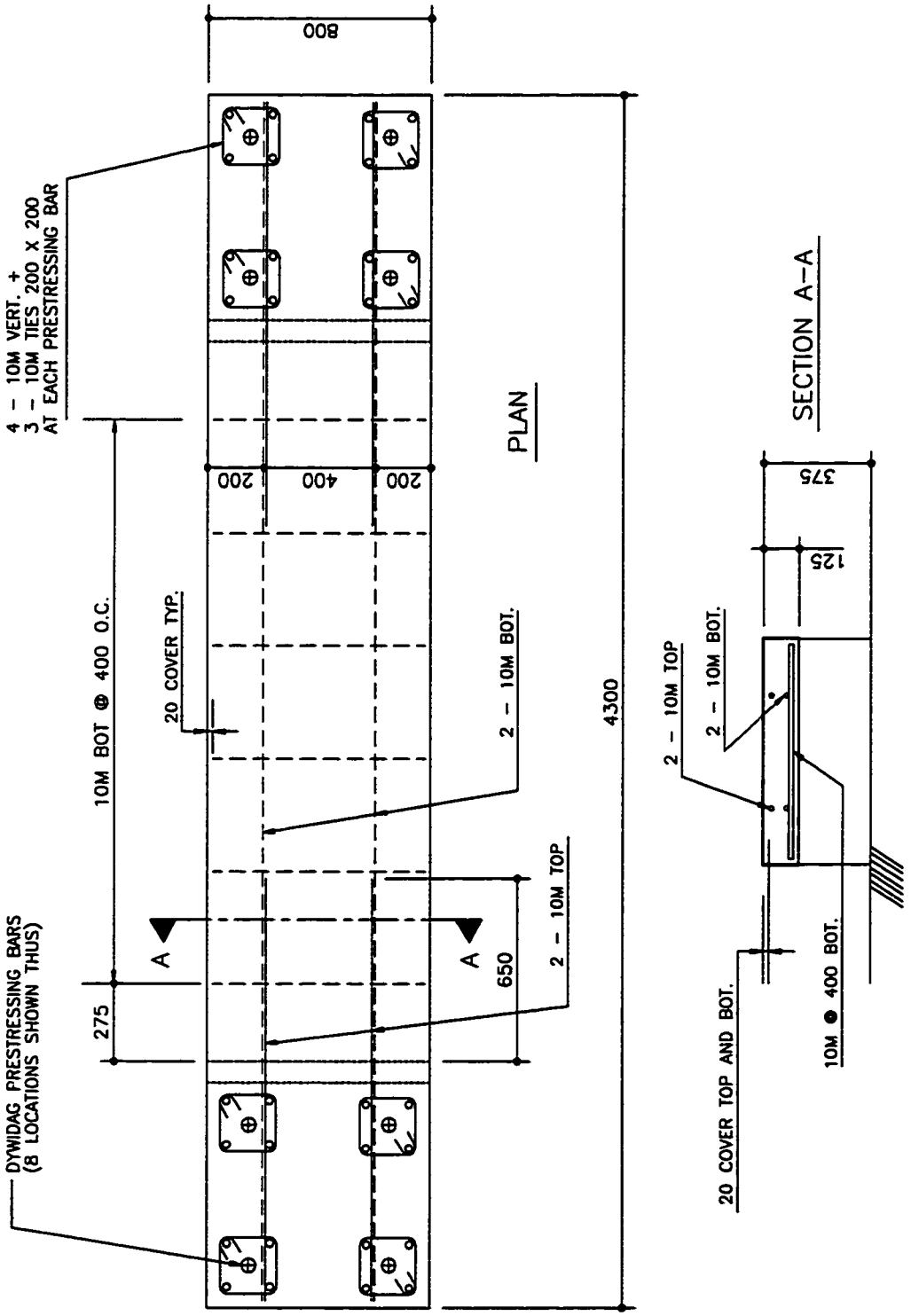

Figure 3.2 Reinforcement for slabs 30-2 and 100-2

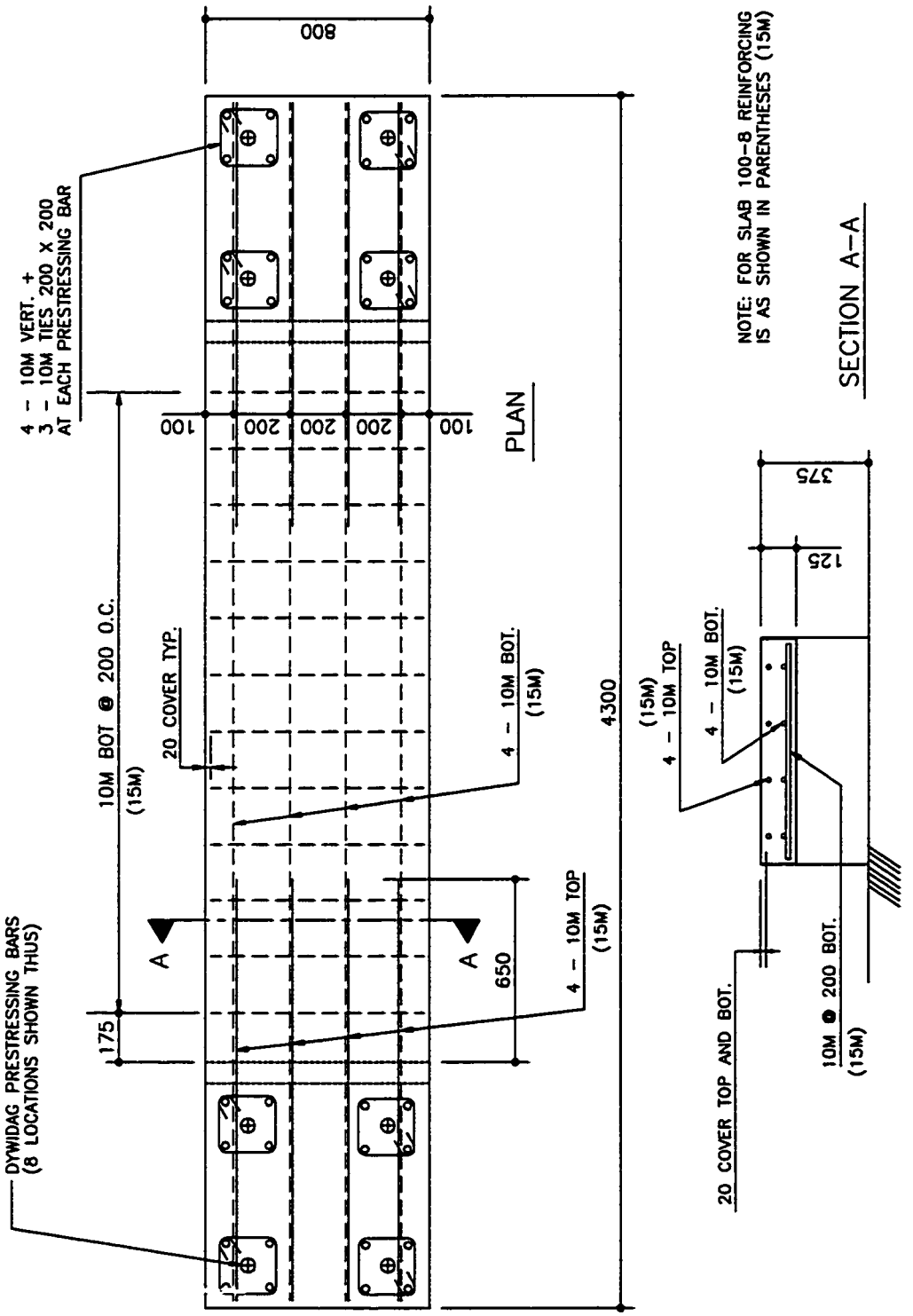

Figure 3.3 Reinforcement for slabs 30-4, 100-4, and 100-8

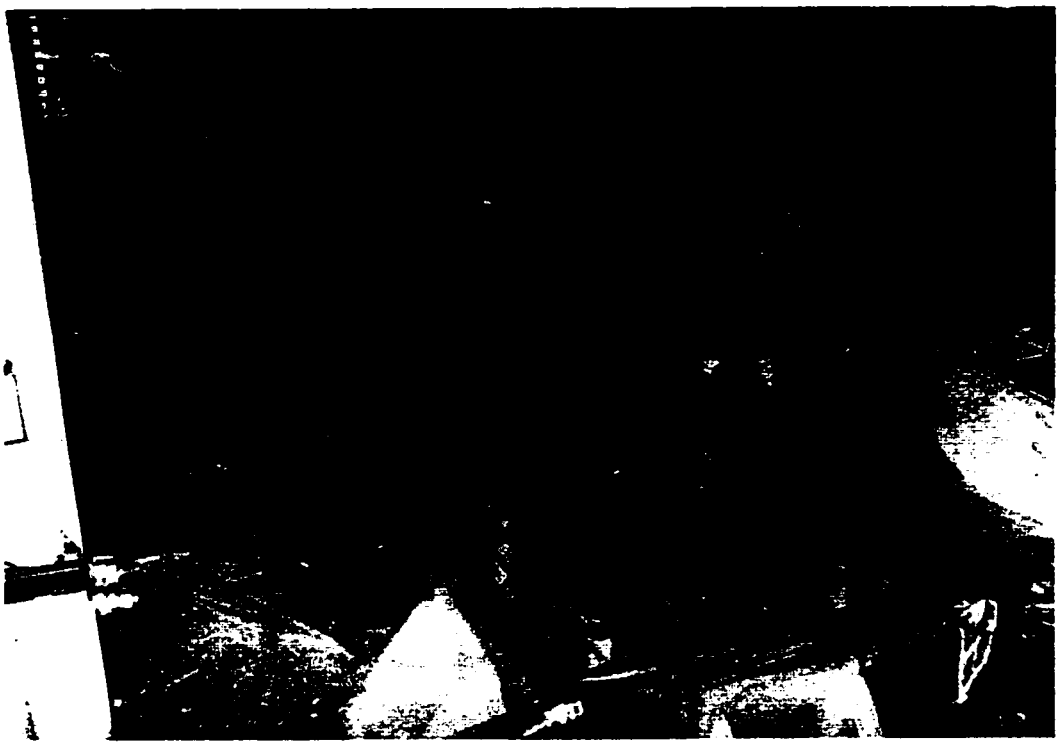

Figure 3.4 Slab 100-4 prior to casting concrete

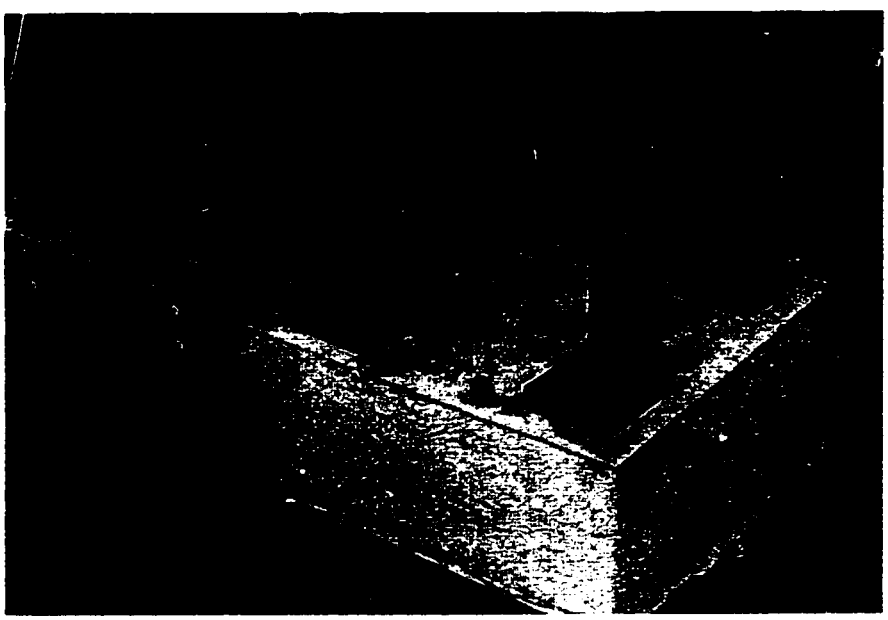

Figure 3.5 Slab 30-2: slab edge and end block

Figure 3.6 Dial gauges at slab end blocks
(tape lines shown were used to protect the dial gauges from being moved accidentally)

Figure 3.7 Free shrinkage specimens

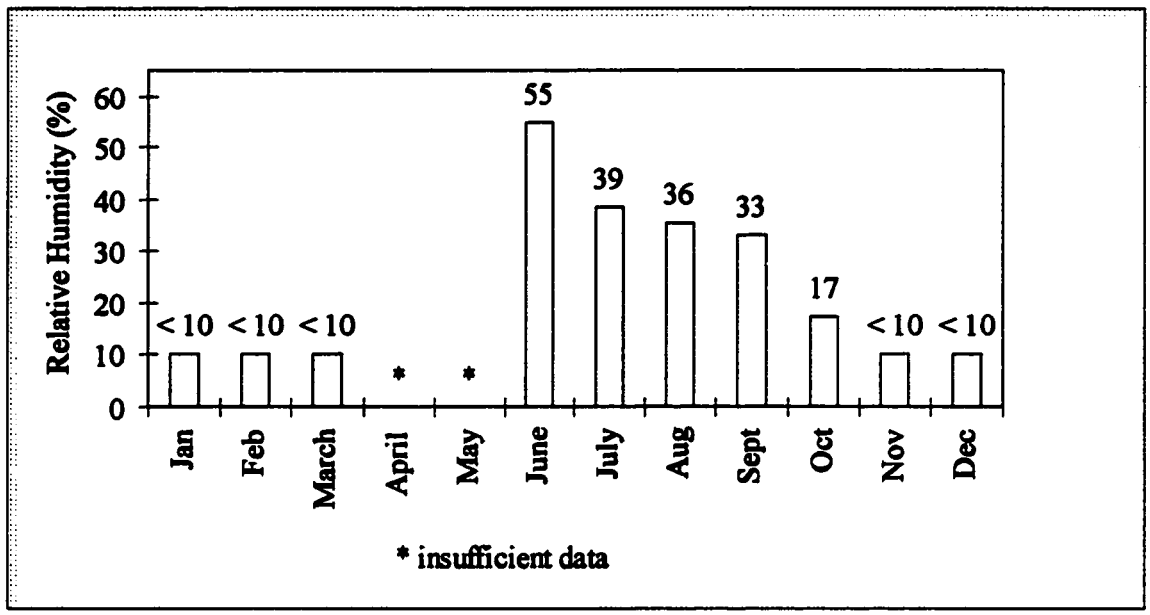

Figure 3.8 Monthly average humidity in laboratory

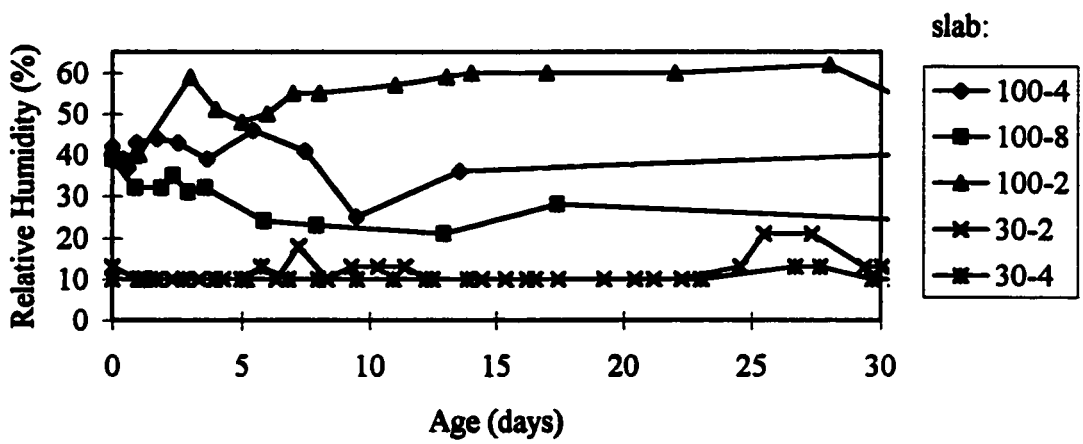

Figure 3.9 Curing humidity for test slabs

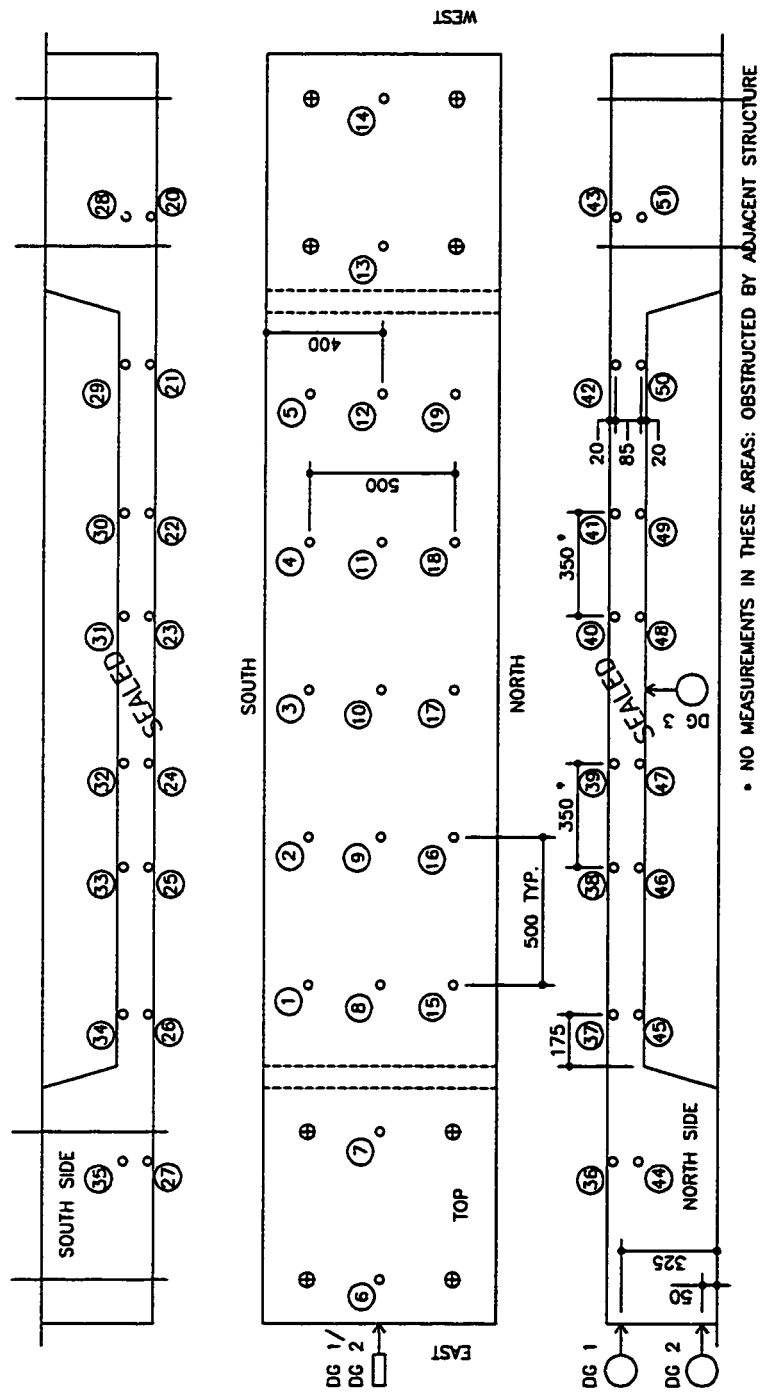

Figure 3.10 Demec point layout for shrinkage measurements

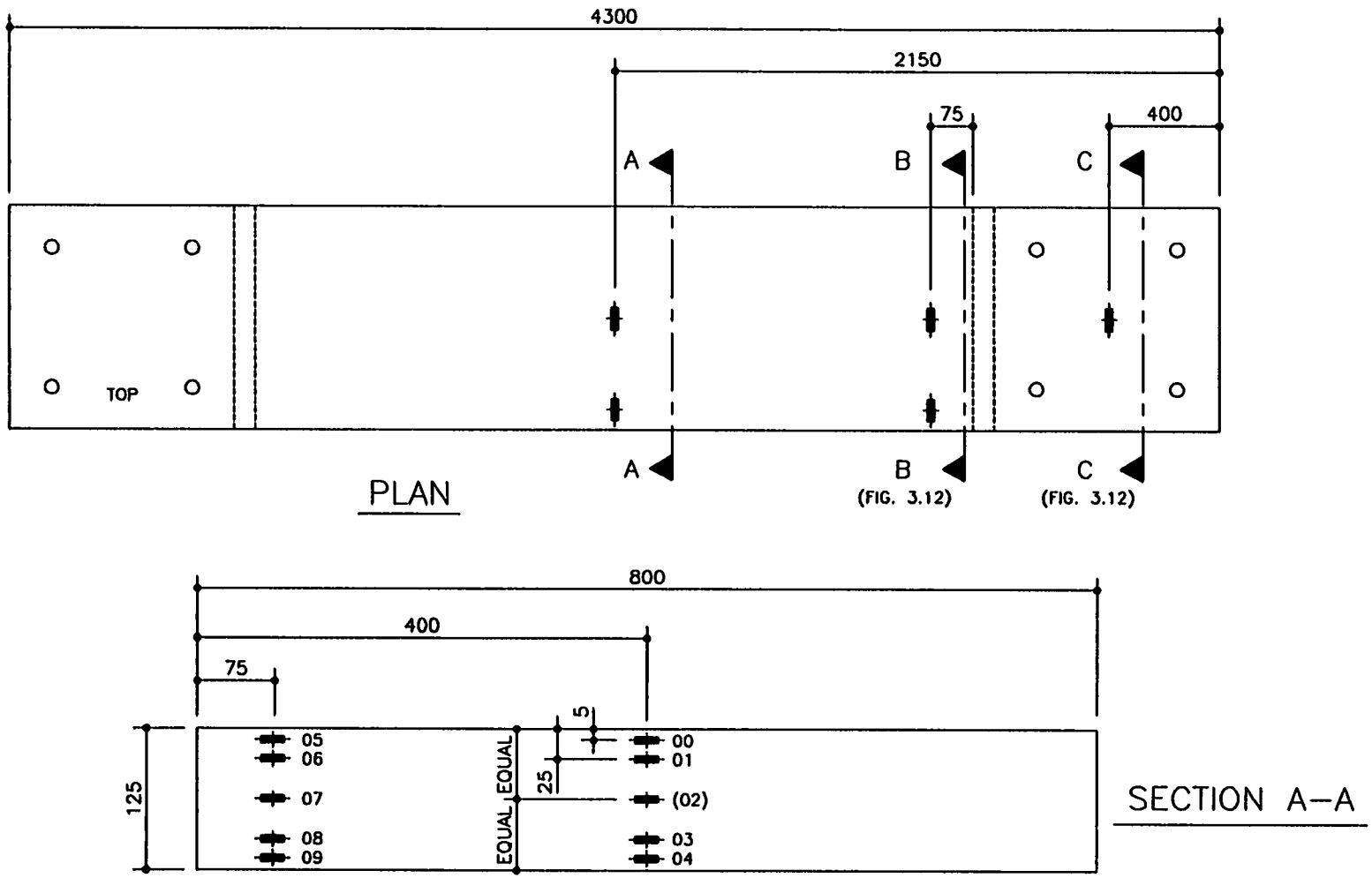

Figure 3.11 Thermocouple layout in slab specimens

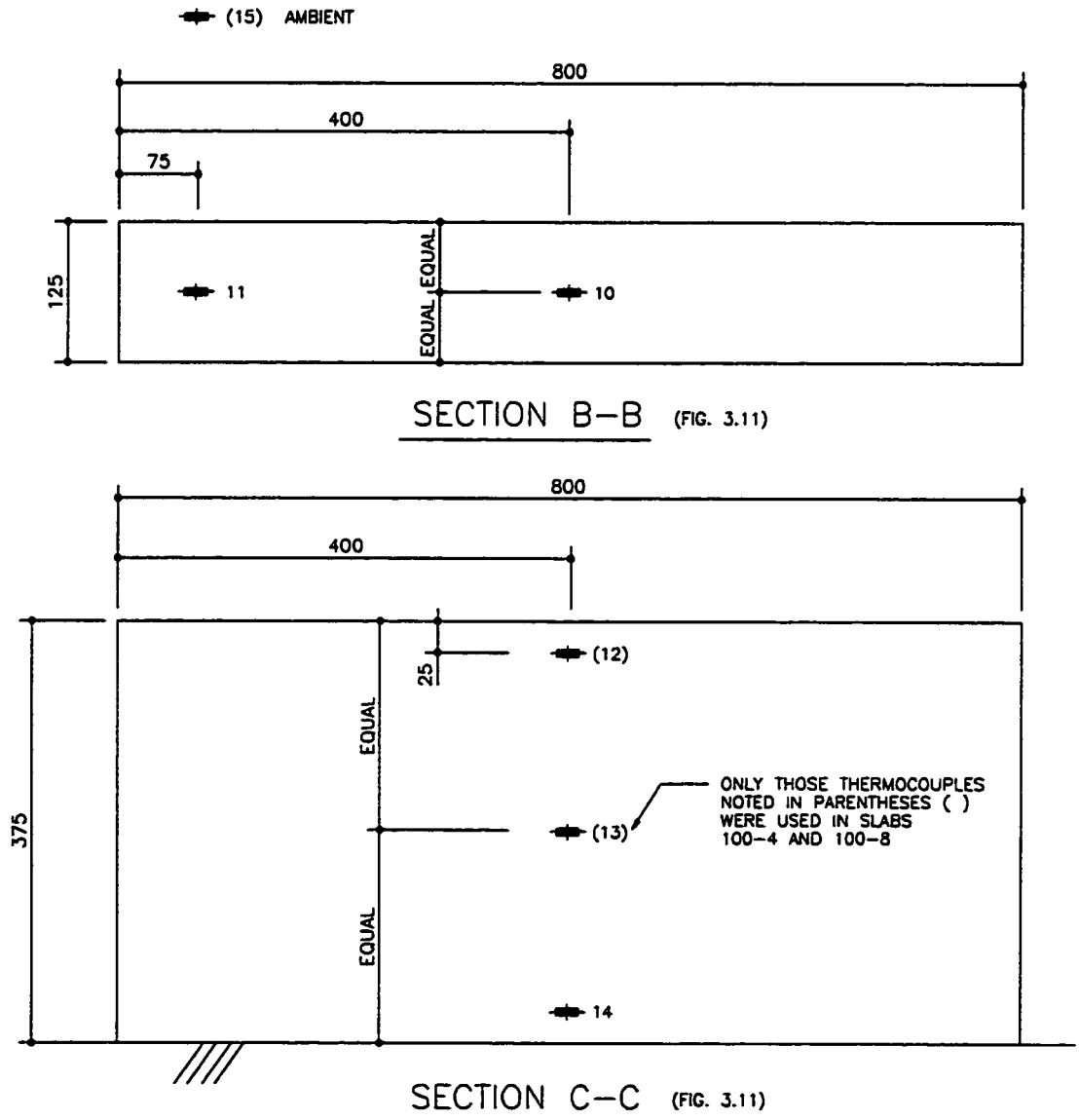

Figure 3.12 Thermocouple layout in slab specimens

CHAPTER 4

EXPERIMENTAL RESULTS

4.1 Fresh concrete properties

The following table lists the concrete properties for the different test slabs. Tests were done immediately after discharge from the mixer.

	30-2	30-4	100-2	100-4	100-8
slump (mm)	160	155	flowing	flowing	flowing
density (kg/m^3)	2390	2380	2425	2450	2435
temperature (°C)	20.0	20.0	23.5	23.5	22.0
air content (%)	1.2	1.2	0.9	0.9	1.1

Table 4.1 Fresh concrete properties

The properties achieved were fairly uniform from one batch to the next. However, the slump of the HPC was noted to be very sensitive to minor adjustments in the quantity of superplasticizer. Of note, the high-performance mixes had a much higher initial slump, although rate of slump loss was also higher. The density of the HPC was consistently higher by about 2%.

4.2 Compressive strength of concrete

A plot showing the development of compressive strength for the concrete used in the present research is shown in Figure 4.1. The NSC reached a nominal compressive strength of 30 MPa at 28 days, while the HPC reached 85 MPa.

The comparison of the development of compressive strength to the value predicted by the CEB MC90 (Equation 2.1) is also illustrated in Figure 4.1. Although the limit of validity for the prediction equation is 50 MPa, it is quite accurate for the 85 MPa HPC also. In general, predicted strength values were within 10 % of actual tests.

Some trends can be observed from the strength development curves. For the normal strength concrete, the CEB MC90 equation predicted strengths that are greater than actual for an age up to 28 days. Beyond 28 days, the CEB MC90 equation gives slightly lower than actual predictions.

For the high-performance concrete, the CEB MC90 equation predicted strengths that are greater than actual test results at ages beyond 28 days. The overestimation of later age strengths supports the observation that high-performance concrete gains strength more quickly than normal strength concrete, but development of strength at later ages is reduced. (FIP-CEB 1990)

4.3 Tensile strength of concrete

Although the property of concrete which is normally referenced is compressive strength, for the present study of minimum reinforcement, tensile strength is fundamental. Figure 4.2 shows the development of tensile strength for both types of concrete used.

The NSC reached a tensile strength of about 3.8 MPa at 28 days while the HPC reached 6.0 MPa.

The following table summarizes both the average 28 day test strengths as well as the predicted values of tensile strengths based on Equations 2.4 to 2.6. (FIP-CEB 1990)

	Test Results		FIP-CEB 1990 Predicted			ACI Predicted
Slab Group	f_{cm}	f_{sp}	f_{sp} (1)	f_{tk} (2)	f_r (3)	f'_{sp} (4)
30 (NSC)	30	3.8	3.0	2.3	4.2 to 4.7	3.2
100 (HPC)	85	6.0	5.0	4.3	7.0 to 7.9	5.4

(1) From Equation (2.4) (3) From Equation (2.6)

(2) From Equation (2.5) (4) From Equation (2.7)

Table 4.2 Concrete cylinder strength (in MPa)

Table 4.2 shows that the FIP-CEB 1990 predicted value of splitting tensile strength is up to 20 % less than the value from actual tests. For the cylinders tested here, a better prediction of split tensile strength is given by ACI 363R-84 (Equation 2.7). This expression gives values of 3.2 MPa and 5.4 MPa for the two slab groups. These values are 14 % and 10 % higher than test results.

Tensile strength development for the HPC was observed to occur more quickly than for the NSC. Figure 4.3 which plots strengths up to an age of 8 days, shows a steady rate of strength development for the NSC. The HPC, on the other hand, gains tensile strength more rapidly, especially for the first day. After one day the HPC had gained about 50% of its long term tensile strength, compared to about 30% for the NSC.

The rapid gain of tensile strength is an advantage is preventing cracking in young HPC. However, as will discussed later, other factors outweigh this advantage and make HPC susceptible to early-age cracks.

4.4 Modulus of elasticity for concrete

The modulus of elasticity for concrete is an important factor in analyzing the development of tensile stress due to shrinkage strain. It is much easier to measure surface strains on test specimens than attempt a direct measurement of tension. Since the assessment of cracking potential depends upon a comparison of tensile strength to applied stress at various ages, the modulus of elasticity of the concrete is needed to convert strain to stress.

Several expressions have been given to calculate a value of elastic modulus from a known compressive strength. Equations 2.12 to 2.15 have been presented, with Equations 2.13 and 2.15 in specific reference to high strength concrete. The upper limit of validity for Equations 2.12 and 2.14 is 80 MPa. Given the variability of elastic modulus, it seems reasonable to extend these ranges to include an HPC of 85 MPa. Table 4.3 shows the range of modulus values calculated for both the NSC and the HPC used in the present research.

		Elastic Modulus, E_c (MPa)			
Slab Group	f'_c (MPa)	Eqn. 2.12	Eqn. 2.13	Eqn. 2.14	Eqn. 2.15 *
30 (NSC)	30	25000	-	26500	-
100 (HPC)	85	37500	48500	36000	40000

* with $C_{ca} = 0.92$ (weighted average for coarse aggregate used, refer to Appendix B)

Table 4.3 Predicted elastic modulus for test concrete

The high degree of variability can be seen in the different prediction methods. For this reason, it is best to test the modulus of elasticity directly, when it is a critical parameter. The average of the values presented in Table 4.3 for E_c at 28 days is 25750 MPa and 40500 MPa for the NSC and HPC respectively. The predicted value for NSC can be considered reasonable owing to extensive testing on conventional concrete. However, tests for the particular HPC used have determined a much lower value of E_c = 32300 MPa at 28 days (Dilger and Wang, 1998). This test value is best suited for use in further analysis.

The development of elastic modulus over time is also valuable information in predicting tensile stress in concrete at early ages. Referring to Equations 2.1, 2.2, and 2.16, the CEB MC90 prediction uses the same time parameter, $\beta_{cc}(t)$, to predict both strength and modulus development. Using the average value of modulus for the NSC and the test value for the HPC, Figure 4.4 plots the predicted increase of elastic modulus over time. The two curves are seen to be parallel: this is because the CEB MC90 prediction equation is independent of concrete properties. Since cracking can occur at early ages in HPC, the value of elastic modulus of young concrete is important for analysis. Figure 4.5 shows the predicted increase in modulus within the first five days. For reference, test values obtained for the HPC at 1 and 3 days are also shown.

4.5 Tensile properties of steel reinforcement

The results of tensile tests on the steel reinforcement used in the four slabs 30-2, 4, and 100-2, 4 are as follows. From the average of six 10M bars tested, a yield stress of 450 MPa at a yield strain of 1900 x 10^{-6} was observed. The start of strain hardening was seen at a strain of about 5500 x 10^{-6}. A tensile stress-strain curve for the most representative test sample is shown in Figure 4.6.

Similar results were determined for samples of the 15M bars used to reinforce slab 100-8. An average value of 440 MPa was determined for the yield stress at an average yield strain of 2500 x 10^{-6}. The onset of strain hardening occurred at 8600 x 10^{-6} strain. Figure 4.7 plots stress-strain for a typical 15M sample.

4.6 Free shrinkage

4.6.1 *Slabs 30-2 and 30-4*

Figures 4.8 and 4.9 present the plots of free shrinkage for the NSC of slabs 30-2 and 30-4. The different curves are identified in the figure legends, and refer to the Demec point numbering given in Figure 3.10. For example, the curve "5657" refers to strain measurements made between points 56 and 57. These points are shown in Figure 3.10 as being on the top surface of the free shrinkage specimen with the sealed bottom. All other references in this thesis are made in the same manner.

The measured free shrinkage for the two NSC slabs showed similar characteristics. Long term shrinkage, after 500 days, approached a maximum value of about -800 x 10^{-6} for slab 30-2 and -700 x 10^{-6} for 30-4. Shrinkage on the top surfaces, curves 5253 and 5657, are essentially the same. This result shows that the top surface is not influenced by moisture loss from the bottom: top shrinkage is the same whether or not the bottom is sealed.

The top surfaces exhibited greater shrinkage than the unsealed bottom surface, 5455. A likely explanation for this is the increased amount of bleed water that would have risen to the top during casting and vibration. With more free water available for evaporation, drying shrinkage was increased. This effect ceased after about 100 days, at which point the curves 5253, 5657, and 5455 ran parallel.

The bottom sealed surface, 5859, experienced much less shrinkage since is was protected against moisture loss. It appears that the depth of penetration of drying was able to reach the sealed surface after about 100 days. At this age, shrinkage developed for 5859 at a rate comparable to the unsealed surfaces. Not coincidentally, the 100 day mark is the same time at which the rate of shrinkage in the unsealed specimen became equal top and bottom. Once drying was full depth there was no distinction between top and bottom, unsealed or sealed. Further shrinkage progressed at the same rate in all cases.

For slab 30-4 the sealed surface 5859 showed apparent swelling for the first 100 days. Since no water was added during this period, swelling could not have occurred. The reason for elongation on the surface is explained by the curvature induced due to differential shrinkage. As the top surface was shrinking and the bottom was not, a positive curvature developed. This curvature, about the neutral axis of the specimen, showed up as elongation on the bottom. The effect was much less pronounced for slab 30-2. Perhaps the membrane was not as effective in this case and some drying of the bottom occurred to reduce curvature.

Remarkably, the periods of higher humidity in the laboratory are reflected in the plots of free shrinkage. From 200 to 300 days for slab 30-2, and from 100 to 200 days for 30-4 (Figure 4.9), there is a definite reduction in the rate of free shrinkage, shown as a flattening of the curves.

4.6.2 *Slabs 100-2, 100-4, and 100-8*

The curves showing the free shrinkage measurements made for the HPC slab 100-4 is shown in Figure 4.10. Slab 100-8 data is very similar. Data for slab 100-2 is not presented because readings did not start until an age of 36 hours versus 12 hours for 100-4. In the period for 12 to 36 hours up to -200 x 10^{-6} strain was measured for 100-4. Rather than adjust the shrinkage for 100-2 to allow for this significant unmeasured strain, it is simpler to limit discussion to the other slab. Certainly, shrinkage development for 100-2 is very similar, and this simplification is reasonable.

The most significant observation for the HPC is the high rate of shrinkage at early ages. Table 4.4 compares the age at which various free shrinkage strains were reached for slab 30-2 versus 100-4.

	Strain (x 10^{-6})						
	-200	-300	-400	-500	-600	-700	-800
30-2	15 days	31	48	78	125	280	-
100-4	1.2	5	10	28	75	180	420

Table 4.4 Development of free shrinkage strain at 5253

Clearly, shrinkage developed much faster for the HPC: it reached -200 x 10^{-6} in 1.2 days as compared to 15 days for the NSC.

Several other results can be noted from Figure 4.10. The long-term shrinkage, after 400 days, for the HPC was over -900 x 10^{-6}. This value is about 20 % higher than for the NSC. Contrary to the NSC, shrinkage for 5657 of the HPC was consistently higher than 5253. This effect seems to suggest that the sealing of the bottom side, 5859,

(5859 being opposite to 5657) causes an increased loss of moisture from the unsealed surface, 5657, as internal water migrates through the section from the sealed side. It would have been expected that this phenomenon would be more noticeable in the NSC which has a much higher water content available for evaporation, and a more porous microstructure.

As well, the sealed surface, 5859, showed definite early age shrinkage which ceased to develop substantially after 15 days (Figure 4.10). Shrinkage on the sealed surface supports the notion that HPC undergoes significant basic shrinkage as reported in the literature.

Similar to the NSC, the top surface of the HPC, 5253, had higher shrinkage strain than the bottom (unsealed) surface, 5455.

4.7 Comparison to prediction models for free shrinkage

4.7.1 *CEB MC90 method*

Figure 4.11 shows a plot of the measured free shrinkage 5253 for slab 30-2, which is representative of both NSC slabs. Also shown is the CEB MC90 predicted shrinkage development for a 125 mm slab section of 30 MPa concrete cured at an average of 15% relative humidity. The CEB prediction model has a stated lower limit for humidity of 40%, and the curve for this limit is also shown. Although the curves follow a similar shape, the predicted strain is much less than actual. Curing for slab 30-2 was severe with measured humidity lower than 15% for the first six months.

Qualitatively, it can be seen that the shrinkage developed much more rapidly than predicted by the CEB. The low humidity conditions dried out the test slab quickly, and

this is not properly accounted for in the CEB method, even for the 15% humidity curve which is extrapolated beyond the method's limit of 40%.

Extending the CEB curve to an infinite time, gives a long-term predicted shrinkage strain of -700 x 10^{-6}. This value is reasonably close to the value extrapolated from measurements: -800 x 10^{-6}. In order to adjust the CEB equation, a faster development of shrinkage at low curing humidity needs to be modeled.

As shown on Figure 4.12, for the HPC the estimated shrinkage according to CEB is much lower than actual: basic shrinkage is not included. For the CEB method, an increase in concrete compressive strength gives a decrease in predicted shrinkage. This trend is opposite to what was observed in comparing slab 30-2 to 100-4.

4.7.2 *ACI Committee 209 recommendations*

The prediction of free shrinkage strain according to ACI 209, for the NSC concrete used, is also plotted on Figure 4.11. Contrary to the CEB, the ACI prediction greatly overestimates the shrinkage strain developed. The lower limit of validity for the ACI method is also 40% humidity. Two curves are shown: one at the limit of 40%, and the other extrapolated to the actual curing conditions of 15% humidity.

In terms of predicting the shrinkage of the HPC, Figure 4.12 illustrates that ACI 209 overestimates. The margin of error is even greater than for the NSC of slab 30-2. Whereas ACI 209 predicted a faster development of shrinkage for the NSC, the HPC definitely experienced quicker shrinkage than predicted, at early ages.

Neither method, CEB or ACI, seems to offer a reasonable prediction of free shrinkage for curing at low humidity. However, the actual shrinkage appears to at least be bracketed by an upper-bound ACI and a lower-bound CEB estimate. And the

bracketing is maintained over a wide range of concrete strengths (30 and 85 MPa tested). As might be expected, the bracket between the methods is somewhat tighter for the more conventional, 30 MPa, NSC.

4.7.3 *Dilger, Niitani, and Wang (1997)*

A much better prediction of shrinkage in HPC is given by Dilger, Niitani, and Wang (1997), as discussed in Section 2.5.2. The prediction curve for this method is also shown on Figure 4.12. The fit to the measured data for slab 100-4 is excellent. This can be attributed to the inclusion of basic shrinkage, which is very high in HPC, and to the method's consideration of data for low humidity tests.

4.8 Shrinkage of restrained test slabs

4.8.1 *Shrinkage across slab width*

Measurements which were made across the width of the large slabs (point sets 115, 216, 317, 418, and 519 on Figure 3.10) closely followed free shrinkage (5253). The plots shown on Figure 4.13, for slab 30-2, and on Figure 4.14, for slab 100-8, show this behavior. This result is predictable: since the slab is essentially unrestrained in the transverse direction, shrinkage across its width follows the same development as for free specimens.

Although the curves are shown only for 115, other sets of measurements, 216, 317, 418, and 519, were checked and seen to parallel free shrinkage. The only difference noted was that for points near the end blocks, 115 and 519, some restraint was apparent. That is, shrinkage for 115 and 519 was seen to be slightly less than for points in the middle of the slab. Factors contributing to the reduced shrinkage measured in this area

include 1) top and bottom reinforcement extended through this location and 2) the prestressed end blocks.

For slab 100-8 shrinkage across the slab was even greater than free shrinkage. To explain this there is eccentric restraint produced by having bottom-only reinforcement placed across the slab width. Thus, measured strains across the top of the slab should be higher than free shrinkage. The reason being that bottom restraint coupled with differential shrinkage - top greater than bottom - produces magnified top strain. The effect of magnified top strain is not significant for low reinforcement ratios, such as seen by the plot for slab 30-2.

4.8.2 *Level of restraint achieved*

In order to assess the amount of restraint that was lost in the test slabs, dial gauges were mounted to measure the deformation of the end blocks relative to the supporting load floor. The gauges were positioned as shown in Figure 3.10. A plot of end block deflection for slab 30-2 is presented in Figure 4.15. Negative dial gauge readings indicate a movement of the end block in a direction away from the dial gauge. In other words, a negative reading indicates a shortening of the overall slab length. The roughness in the curve indicates that the 0.01 mm precision of the dial gauges was not fine enough to smoothly follow the movement. For subsequent slabs 0.001 mm precision dial gauges were used instead.

The reason for the movement indicated by the dial gauges, is shear deformation in the end blocks. A tension force developed in the slab as it underwent shrinkage. This tension acted at the top of the end block as shown in Figure 4.16. Although the force was not large, because of the precision of the dial gauges, the shear deformation of the end block could be measured. (Note that the prestressing force is concentric to the end block,

and does not influence shear deformation.) As an example, for slab 30-2 an approximate calculation of shear deformation follows.

Assuming the final tension force in the cracked slab was equal to the yield force in the reinforcing (2 - 10M bars):

$$T = A_s F_y = 2 \text{ x } 100 \text{ mm}^2 \text{ x } 450 \text{ MPa} = 90 \text{ kN}.$$

From the well known expressions for shear modulus, G, shear stress, τ_{xy}, and shear strain, γ_{xy}, (Beer and Johnston, 1985):

$$G = \frac{E}{2(1+\nu)} \tag{4.1}$$

$$\tau_{xy} = G\gamma_{xy} \tag{4.2}$$

With, $E = 25750$ MPa (Section 4.4), Poisson's ratio, $\nu = 0.1$ to 0.15 (CEB MC90), and the area of concrete in shear, A_c:

$$G = 25750 \text{ MPa} / (2(1+0.15)) = 11200 \text{ MPa}.$$

$$\tau_{xy} = T / A_c = 90 \text{ kN} / (800 \text{ x } 800 \text{ mm}) = 0.14 \text{ MPa}.$$

Therefore,

$$\gamma_{xy} = 0.14 / 11200 = 13 \text{ x } 10^{-6}.$$

At the location measured by dial gauge 1, the elastic shear deflection is,

$$\Delta_{v,el} = (13 \times 10^{-6})(325) = 0.004 \text{ mm.}$$

Allowing for a creep coefficient equal to 3.0:

$$\Delta_{v,total} = (3.0 + 1)\ 0.004 = 0.016 \text{ mm.}$$

This estimated deflection is in the same order of magnitude as the final measured value shown on Figure 4.15, confirming that shear deformation accounts for this observation.

The partial loss of restraint which occurs because of the end block deformation, can be assessed by comparison to free shrinkage. For slab 30-2, the end block deflected by about 0.04 mm. Assuming that each end of the slab would deflect the same amount, the average strain over the full slab from this deflection would be,

$$\varepsilon_{end} = 2\ (-0.04) / 4300 = -19 \times 10^{-6}\ .$$

Compared to a free shrinkage strain of about -800×10^{-6}, the loss of restraint is approximately 19 / 800 or 2%. Thus, the slab can be considered as fully-restrained. The amount of pure slip, as represented by dial gauge 2 measurements on Figure 4.15, is, by the same calculation, less than 2%.

End block deformation was also measured for the HPC slabs. Expectedly, slab 100-8 had the highest movement. As shown in Figure 4.17, dial gauge 1 readings went to -0.10 mm within one day, and reached a maximum value over -0.15 mm within 30 days. Using the same explanation as given for slab 30-2, a deflection of -0.15 mm is reasonable. The tension force applied to the end block for 100-8 should be about 4 times

as great as for 30-2 since 4 times as much reinforcement was used. The resultant deflection of -0.15 mm is also about 4 times the -0.04 mm seen for 30-2. For a free shrinkage of -900 x 10^{-6} for the HPC, the end block deflection represents an 8% loss of restraint. As desired, the restraint was very high even for the most heavily reinforced slabs.

End block deflection developed rapidly for slab 100-8 in comparison to 30-2. This was a result of a more rapid shrinkage and development of tension for the HPC.

Slab 30-2 showed a surprising expansion in length at early ages, as measured at the level of dial gauge 2. The peak for the curve in Figure 4.15 at 0.01 mm occurred at about 20 days, and was followed by a drop to -0.005 mm just prior to the cracking of the slab at 30 days. Although this was originally thought to be an error in measurement, this behavior was evident in the HPC slabs as well. A possible explanation is that the end blocks tended to bulge in response to the vertical prestressing force. Since this effect was thought to be irrelevant to the behavior of the slab test section, no analysis was attempted.

4.8.3 *Shrinkage along length of slab*

4.8.3.1 *General*

The most important set of shrinkage measurements was that taken down the middle of the slabs along their full length. In Figure 3.10, the middle set of points are shown as 67, 78, 89, 910, 1011, 1112, 1213, and 1314. Not only did these points span across any potential lines of transverse cracking, but they also served as a reference check on the degree of restraint imposed on the slab. If full restraint was achieved, the distance between points 6 and 14 would remain the same. However, as described in Section 4.8.2, the end blocks deflected inwards due to shear deformation. The result was a measurable shortening in the overall length from 6 to 14.

Although the slabs were of significant length, 4300 mm, four distinct regions occurred along the length. Point sets 67 and 1314 were directly on the top of the end blocks. Across the intersection of the end blocks and the slab, points 78 and 1213 were located. The end regions of the slab, which included top reinforcement, were measured by points 89 and 1112. Finally, strain in the true test section of the slab, with bottom-only reinforcement, was measured by point sets 910 and 1011.

4.8.3.2 *Slab 30-2*

Figure 4.18 plots the development of strain for points along slab 30-2. For reference, free shrinkage 5253 is also shown. The time scale is limited to 60 days to highlight the period of interest. Beyond this time, development of strain paralleled free shrinkage. The data across the main crack, points 1011, is also shown separately, as change in length, on Figure 4.19. (Refer to Section 4.11 for a complete description of cracking.) The strain for points 78 and 1213 was negligible up to an age of about four days. At this time, visible cracks formed and positive strain began to develop. Due to imperfect symmetry, cracks between 7 and 8 were wider than between 12 and 13. These cracks opened up until the main crack formed between points 10 and 11, at 30 days. Then the secondary cracks began to close, and the strains for 78 and 1213 paralleled the curves for the other points.

As seen by the flat curves on Figure 4.18, very little strain developed for points 67 and 1314. This is understandable because the prestressing force applied to the end blocks produced a vertical compressive strain in the concrete and a corresponding horizontal tensile strain. Thus, the end blocks were greatly restrained, and shrinkage was not free to develop. Because the test region of the slab was at midspan, a detailed analysis of the stress-strain field in the end blocks is not of fundamental importance to the research, and is not discussed further.

The strain curves for points 89, 910, and 1112 all show a similar development. Prior to the main crack forming, the strains were restrained in comparison to the shrinkage of the free specimens. When the main crack formed at an age of 30 days, the restraint was released, and the curves showed a definite jump. After cracking, development closely followed free shrinkage, although not quite reaching as high a value, even after 280 days. The curves for 910 and 1011 were very close prior to cracking. There was no observable sign that the main crack would form within 1011. However, strain measurements flattened out between 25 and 28 days giving an indication of imminent cracking.

The development in the width of the main crack between points 10 and 11 is easily seen in Figure 4.19 as a jump in strain from negative (shrinkage) to positive (elongation) at 30 days. The development of crack width is very similar to the inverse of free shrinkage, as can be seen in comparing Figure 4.19 to Figure 4.13. Both free shrinkage and crack width had nearly reached final values by 300 days. The magnitude of crack width was, of course, much higher.

The series of strain measurements taken along slab 30-2 is shown in a different manner on Figure 4.20. The data is presented for four different ages close to the time when the main crack formed. This figure is useful in visualizing shrinkage because it presents strain values in left to right groups in the same position as the points on the slabs. In this way, certain trends can be more easily understood. Firstly, the end blocks, 67 and 1314, show essentially constant strain. Next to the end blocks, 78 and 1213, have positive strain values corresponding to cracks in these regions. Points in the middle of the slab, 78, 89, 910, and 1112, display fairly uniform shrinkage strain for the two ages before cracking, 26 and 28 days. Due to the higher restraint in the end regions of the slab, points 89 and 1112 had slightly lower strain. At the age of cracking, just prior to 30 days, accumulated shrinkage strains were redistributed. Across the main crack, strain jumped to a large positive value (points 1011). In a reverse manner, secondary cracks

began to close and strain decreased for 78 and 1213. In the middle uncracked portions of the slab, 89, 910, and 1112, restraint was released when the main crack formed. The release of the tensile stress which had built up in these areas caused a rapid elastic shortening and a negative step in strain values.

4.8.3.3 *Slab 30-4*

A plot of strain development up to an age of 60 days is shown in Figure 4.21 for slab 30-4. Unlike 30-2, no single main crack formed. As such, strain at all points along the slab developed smoothly. Secondary cracks still formed in the end regions 78 and 1213, and increasing positive strains were measured. However, these cracks did not close up. Other behavior was similar to 30-2.

The long term strain measurements for 30-4 uncovered an interesting behavior. As illustrated on Figure 4.22, strain in the region 1112 decreased after 350 days. From a visual inspection of the slab surface a new crack was discovered in this area. In the same time period the crack between points 12 and 13 closed slightly. Not surprisingly, the humidity at this time was very low. New cracking at such an advanced age highlights that drying shrinkage continued for a long time in the NSC slabs. No such behavior was observed for the HPC slabs.

Another plot of strain along slab 30-4, between 10 and 40 days, is given in Figure 4.23. Since a singular crack did not occur in slab 30-4, there is no strain reversal in any areas of the slab. Instead, all regions had an orderly change of strain, with the highest values across the secondary cracks in 78 and 1213.

4.8.3.4 *Slab 100-2*

Shrinkage strain along the HPC slab 100-2 developed much more quickly than for the NSC slabs. As illustrated on Figure 4.24, a main crack formed in the area 910 within 3 days after casting. The curve for 910 is almost vertical and reached a strain of over 500 x 10^{-6} immediately after cracking. Since restraint was released so soon, with the formation of the crack in 910, strain curves in other areas along the slab closely followed free shrinkage 5253. The strain for 89, 1011, and 1112 is greater than free shrinkage, on Figure 4.24. As explained in Section 4.8.1, differential shrinkage combined with bottom-only reinforcement is the reason for this magnified top strain.

In order to better describe the early age behavior of slab 100-2, plots of strain up to 5 days are shown in Figures 4.25 and 4.26. Between 2 and 3 days, as the crack formed in 910, restraint was released and the curves for 78, 89, 1011, 1112, and 1213 go from zero strain to about -50 to -100 x 10^{-6}. Unlike the NSC slabs, strain on top of the end blocks 67 and 1314 shows significant development because of the HPC's high early shrinkage. For the first 3 days, as shown on Figure 4.25, end block strain is higher than for other areas along slab 100-2. After about 5 days, this order reverses and strain for 67 and 1314 is less (Refer to Figure 4.24.) This lower long-term shrinkage for the end blocks is consistent with the NSC. Lateral strain due to the prestressing force, present in all of the slabs, is superimposed on shrinkage. The result is an apparent reduction in strain.

4.8.3.5 *Slab 100-4*

Figure 4.27 shows the development of strain along slab 100-4. Significant strain was measured between 0.5 and 1.5 days. This data was not recorded for 100-2, as seen on Figure 4.25, because measurements did not start until after this time. For 100-4, an

early peak in shrinkage was noted at 1.1 days. This peak was followed by a small drop, then by steady strain, and finally an increase in strain as the main crack formed at 3 days, and restraint was released. The early peak was caused by prestressing, which took place just after 1.1 days. When the prestress force was applied to the end blocks, they were vertically compressed. Correspondingly, the end blocks expanded horizontally. This expansion had the effect of imposing a strain on the slab which gave the apparent reduction in shrinkage. Of course, the early peak in strain did not occur in the non-prestressed free shrinkage specimens, as confirmed by the curve 5253 on Figure 4.27.

The flat portion of the curves on Figure 4.27 between 1.2 and 2.2 days shows that a high degree of restraint was present in slab 100-2. After cracking, this restraint was released and the curves develop in a manner similar to free shrinkage.

4.8.3.6 *Slab 100-8*

A plot of strain measurements for slab 100-8 up to 60 days is given as Figure 4.29. The development of shrinkage is very similar to slab 100-2 (Figure 4.24) except for the points 1011. As was the case for slab 100-2, shrinkage for 1011 is substantially higher than for 5253, free shrinkage. Because of the even higher amount of reinforcement for 100-8, the strain for 1011 is magnified to a greater degree. (An intermediate effect was seen for slab 100-4, but the plot is not presented here.)

Once again, early age shrinkage is vital to understanding the behavior of the HPC slab 100-8. To better see this, Figure 4.30 shows strain along 100-8 up to an age of 5 days. The peak in strain prior to prestressing, at 1.2 days, is seen here as well. An observation which is different than 100-4 is that significant strain values were measured immediately for 100-8. The initial (zero) measurements were taken at 13.8 hours, with the next set at 14.3 hours. Shrinkage of nearly -170×10^{-6} developed over the 30 minute time period. This rapid shrinkage explains the near vertical curves in Figure 4.30. Prior

to the initial measurements, the expected shrinkage would be about -150 x 10^{-6}, as measured by Dilger and Wang (1998). In comparison, for slab 100-4, initial measurements were made at 12.0 hours and the second set at 22.5 hours. Thus, very rapid shrinkage may have occurred but it was not recorded. In a similar way, the magnitude of shrinkage strains for slab 100-2 are not directly comparable with 100-4 and 100-8, because initial measurements were not taken until 36 hours after casting.

The importance of starting shrinkage measurements as early as possible can not be overstated. Significant strength, and stiffness, developed quickly in the HPC: up to 15 MPa in the first 12 hours. Thus, early age shrinkage puts high tensile stress on the restrained slabs. As seen for all three HPC slabs, this led to cracking within three days, regardless of the amount of reinforcement used.

4.8.4 *Shrinkage and curvature along sealed edge of slab*

4.8.4.1 *General*

The most complex time-dependent behavior was observed by strain measurements along the edges of the slab. Referring to Figure 3.10, the point sets in this series are from 2021 to 3435 on the south edge of the slab, and 3637 to 5051 on the north edge. The effect of differential shrinkage is evident in these measurements since one line of points was located along the top of the slab and the other along the bottom.

A comparison was made between north and south side shrinkage for all of the slabs. It was found that corresponding sets of points experienced similar shrinkage. This result confirms that the sealing of both edges was sufficient and that shrinkage was relatively uniform across the width of each slab. As such, further discussion will be presented for the south edge points only.

The measurements made on the slab edges provide data for a direct calculation of curvature along the slab. The examination of curvature is useful in understanding the effects of differential shrinkage and of eccentric reinforcement. These two factors are almost always present in structural slabs. The normal practice of consolidating concrete causes bleed water to rise to the surface leading to differential shrinkage. As well, areas which require only a minimum amount of reinforcement are generally areas of positive bending (tension on the bottom fiber). Thus, minimum reinforcement is generally placed in the bottom of the slab only.

The curvature in the test slabs was calculated directly from the strain measurements using data from top and bottom points at the same location. For example, for slab 30-2 at an age of 28 days, curvature in the slab at midspan (points 2324) is determined as follows:

ε_c (2324) = -212×10^{-6}

ε_c (3132) = $+36 \times 10^{-6}$

γ (2324) = $-(-212 \times 10^{-6} - (+36 \times 10^{-6})) / (0.085\ m) = +2918 \times 10^{-6} / m$,

where the vertical distance between the point sets 2324 and 3132 is 0.085 m, and a negative sign is introduced to arrive at the sign convention of positive curvature being concave upwards.

4.8.4.2 *Slab 30-2*

Figure 4.31 shows the strain development for the regions of slab 30-2 near the end blocks, against a logarithmic time scale. The cracks which developed near the edge of the end blocks are the reason for the positive strain values. (Cracking is discussed in detail in a Section 4.11.) The penetration of the crack was from the top towards the bottom of the slab. Correspondingly, the bottom point measurements, 2829 and 3435, are

lower than for the top points, 2021 and 2627. (The drop in strain for 3435 at 2 days was caused by the application of prestress.) The effect of reinforcement is not the cause of smaller bottom crack width in this region: equal amounts of top and bottom reinforcement were used near the end blocks.

As discussed previously, when the main crack formed, the secondary cracks near the end blocks began closing. A reverse in strain development, toward negative, resulted for the edge points. This can be seen as a sharp cusp in the curves of Figures 4.31 at an age of about 30 days. After cracking, the curves follow a fairly normal shrinkage development curve. Figure 4.31 plots corresponding points for the west and east end: 2021 / 2829, and 2627 / 3435 respectively. Although the curves show similar behavior, some difference in the magnitude of strains is apparent. A possible cause for this difference is the influence of prestressing, which was not applied simultaneously at all locations. Thus, the end sections of the slab may have been left with different values of stress-strain after prestressing. Since the end sections are not in the critical region of study, near midspan, further discussion of the prestressing effect is not relevant.

The strain along the edge of slab 30-2 near the main crack, and free shrinkage 5253, are plotted on Figure 4.32, up to an age of 50 days. As for the region near the end blocks, the strain at the bottom of the slab (2930) is lower than for the top (2122) after cracking at 30 days. However, both of these areas remained uncracked. Formation of the main crack is evident in the curves for 2324 and 3132 as a vertical drop in strain just prior to 30 days. Conversely, the curve for points 2122 shows a definite increase in shortening after the release of restraint due to cracking.

The effect of reinforcement in the cracked region of slab 30-2, can also be seen on Figure 4.32. The reinforcement, which was present in the bottom only in this region of the slab, restricted crack width and likewise reduced the strain measured for points 3132, as compared to the top points 2324. Prior to the main crack forming bottom strain (3132)

was already positive. The positive curvature in the uncracked slab, and differential shrinkage accounts for positive bottom strain. The restraint of the reinforcement is only evident after cracking when the tensile force which had developed in the slab is transferred to the steel. To explain this in another way, the center of restraint drops from the centroid of the uncracked section down to the level of the reinforcement once the slab becomes fully cracked.

Curvature along slab 30-2 is plotted in Figure 4.33 for a range of ages near the time of cracking. Prior to cracking, the slab at midspan (2324) had positive, or sagging, curvature. Positive curvature resulted from greater shrinkage on the top of the slab. If the slab had been reinforced equally top and bottom, post-cracking curvature would have remained positive. The jump in strain as the crack formed would be equal top to bottom and curvature would be unaffected. However, since the slab, had bottom-only steel, midspan curvature was greatly affected by the crack. Upon cracking, the tension previously acting on the uncracked concrete was immediately transferred to the reinforcement. The resulting eccentric tension reversed the slab into a negative, or hogging, curvature. The abrupt reversal in curvature is shown at the location 2324 with a drop in curvature from nearly 3000 x 10^{-6} / m at 28 days to less than 1000 x 10^{-6} / m at 30 days.

The slab near the end blocks remained at a relatively constant negative curvature. This is shown on Figure 4.33 in the measurements for points 2021 and 2627. The high degree of restraining end moment imposed by the end blocks did not permit a great deal of reflex when the slab cracked. (The curvature calculated for 2021 and 2627 was based on the 125 mm slab thickness. This is not absolutely correct because these points cross over into the 375 mm pedestal thickness. However, relative discussions on the development of curvature in this area are still valid.)

The behavior at midspan was observed in a different way from the measurements of a dial gauge (designated DG 3 on Figure 3.10) installed under the slab. The plot given in Figure 4.34 shows that prior to cracking the slab deflected downward, in agreement with a sagging curvature. As soon as the main crack occurred, the slab began to deflect upwards, with negative curvature. Dial gauge readings for the other slabs show a similar behavior and are not presented here.

4.8.4.3 *Slab 30-4*

A long term plot of strain development along the sealed edge for slab 30-4 is shown in Figure 4.35. Free shrinkage 5253 is also given for reference. The presence of a crack on the underside of the slab between points 31 and 32 is indicated by the positive strain values on the curve 3132. The crack remained small and stable throughout the test period. Other cracks formed in the region 2930 at 100 days, and in 2122 around 200 days. The strain across these cracks changed smoothly, as opposed to the sharp peaks shown for slab 30-2 in Figure 4.31. The smooth strain change indicated a controlled and stable crack formation which is the behavior desired in a slab with sufficient reinforcement to control cracking.

A smooth change in curvature for slab 30-4 was also measured. Figure 4.36 plots curvature along the slab over a range of age similar to that shown for slab 30-2 in Figure 4.33. Comparing the two figures, 30-4 shows a steady increase in both positive curvature at midspan and negative at the end blocks, while the curvature at the midspan of 30-2 changed rapidly due to sudden cracking at an age of 30 days.

4.8.4.4 *Slab 100-2*

Strain on the edge of the HPC slab 100-2, up to 50 days, is shown on Figure 4.37. The crack which developed at 3 days in the middle of the slab gave rise to the near-

vertical drop in the curve for 2324. The curve for 3132, at the bottom of the slab, is also indicative of cracking. However, strains are lower for 3132 because of the crack control provided by reinforcement in the bottom of the slab. Points near to end of the slab, 2122 and 2930 showed strain which followed free shrinkage development 5253. Strains for 2930 were lower due to differential shrinkage, as explained in detail for slab 30-2.

The development of curvature is plotted in Figure 4.38 for ages near the time of cracking. Initial curvature is negative at the slab ends and positive at midspan, as it was for the NSC slabs. However, because cracking, and curvature reversal occurred at a very early age, curvature immediately prior to cracking was slight. With the main crack forming between observations at 2.2 and 3.4 days, slab curvature sharply reversed.

4.8.4.5 *Slab 100-4*

The formation of the main crack was not apparent in measuring the development of strain on the edge of slab 100-4. The reason for this was that the crack appeared between points 24 and 25, where no measurements were possible because of interference with an adjacent structure. However, referring to Figure 4.39, several secondary cracks effected the strain values. The curves for 3132 and 4546 both show a positive increase in strain after an age of about 5 days. This indicated cracking. Indeed, small cracks were visible on the underside and edge of the slab in these areas. As observed for the other slabs, strains in the uncracked portions of slab 100-4 followed free shrinkage, once restraint was released by the main crack.

Curvature along slab 100-4 was more difficult to interpret than for the other slabs because the main crack formed in an area where strains were not measured. From Figure 4.40, a definite offset in the line of symmetry for curvature, towards the east end of the slab, 2627, is noticeable. Data for 2425 was estimated such that maximum negative

curvature occurs at this location, and such that a realistic development of curvature for 2.2 to 4.2 days is depicted.

4.8.4.6 *Slab 100-8*

The influence of a much higher percentage of reinforcement for slab 100-8 is clearly seen in the development of strain along the slab edge. As shown in Figure 4.41, the main crack formed in the region 2324 (top) and 3132 (bottom) at an age of about 3 days. As for slab 100-2, strain for 2324 increased rapidly as the crack formed and widened. Due to the higher reinforcement , bottom strain at 3132 was limited to a value just over +200 x 10^{-6} after cracking. This is much different than for slab 100-2, where strain at 3132 was over +800 x 10^{-6} after 15 days (refer to Figure 4.37).

With the much higher total tension force at the level of reinforcement, post - cracking curvature for slab 100-8 was also much higher. Curvature reached over -5000 x 10^{-6} / m immediately after cracking (age of 3.5 days on Figure 4.42). At the same age, slab 100-2 had a curvature of less than -3000 x 10^{-6} / m (age 4.3 days on Figure 4.38). Thus, the undesirable effect of increased reinforcement, placed eccentrically, was to greatly increase the deflections of the cracked slab. In fact, upward deflection was so pronounced for slab 100-8, after cracking, that it was easily visible to the unaided eye.

4.8.5 *Effect of slab edge*

Since a fairly narrow slab strip, 800 mm width, was used for the test specimens, measurements were taken to check for edge effects. These consisted of sets of strain readings along the length of the slab in three lines: center, between point 8 and 12, outside south between 1 and 5, and outside north between 15 and 19. (Refer to Figure 3.10).

The difference in shrinkage measurements between the center of the slab and the edges was found to be negligible in all cases. The widest band between curves was observed for slab 30-2 near the west end block. Figure 4.43 plots the three sets of data. The maximum variation in strain is about 100 x 10^{-6}, comparing 1112 to 45. For a long term value of about -700 x 10^{-6}, this variation is only 15 %. The majority of the other curves studied showed a maximum variation in strain of 50 x 10^{-6}.

The uniform shrinkage at different lines along the slabs showed that the waterproof membrane was effective in preventing additional drying along the slab edges. As intended, the test specimens represented a full-width slab section without significant edge effects.

4.9 Thermal strains

4.9.1 *General*

It is important to consider the effect of thermal strains when investigating the potential for cracking, especially in slabs with low amounts of reinforcement. Due to the high heat of hydration in HPC, significant thermal strains can develop during cooling. These strains are superimposed on the shrinkage strains also developing rapidly at early ages. To accurately include for thermal strains, temperature within the test slabs was directly measured using embedded thermocouples. The location of the thermocouples is shown in Figures 3.11 and 3.12.

At the completion of its hydration heating and subsequent cooling, a restrained concrete structure will be left in a state of tensile stress. This phenomenon is explained by Ghali and Favre (1986) as follows. When the concrete temperature increases during hydration the structure expands and compressive stresses are developed against the restraint. If the concrete elastic modulus was constant and creep was insignificant, stress

would return to zero upon cooling. However, the concrete is less stiff and creep is greater at earlier ages. Thus, heating produces less stress than cooling and the structure is left in tension after it returns to ambient temperature.

4.9.2 *Measured temperatures*

Internal temperatures were measured for all of the HPC slabs: 100-2, 100-4, and 100-8, and were found to be very similar. For the NSC slabs, temperatures were measured for 30-4 only. For analysis, slabs 30-4 and 100-8 will be considered as representative.

The development of temperature is plotted in Figure 4.44. The curves show that the HPC slab 100-8 reached its maximum temperature about 20 hours after casting. The peak temperature within the center of the end block (thermocouple 13) was 42.2 °C. The interior of the slab at midspan (thermocouple 02) reached 36.6 °C. By comparison, the NSC slab 30-4 showed lower peak temperatures of 33.5 °C and 30.4 °C at the same locations. The maximum values were reached at an age of 15 hours for 30-4.

Variation of temperature within the slab cross section was also measured for slabs 100-2 and 30-4. For 30-4 the maximum difference in temperature between the middle of the cross section and the thermocouple located 5 mm from the surface was 1.0 °C. The same comparison was 1.7 °C for slab 100-2.

The difference in temperature across the slab width was checked. For 30-4, the middle reached a peak temperature of 0.9 °C higher than the edge. Specifically, thermocouple (02) registered 30.4 °C at 15 hours, while (07) on the slab edge reached 29.5 °C. The same comparison of peak temperatures for the HPC slab 100-2 had (02) with a peak of 36.3 °C at an age of 14 hours, and (07) at 34.3 °C. Thus, the maximum temperature difference across the slab was 2.0 °C. The larger temperature gradient for the

HPC is predictable since the difference between ambient temperature and the interior of the concrete is much higher in the HPC. For more massive structures, such a thermal gradient can give rise to thermal cracking. However, for the fairly thin slab differential thermal stresses are less of a factor.

4.9.3 *Calculation of thermal strains during hydration*

4.9.3.1 *General*

As discussed above, temperature was relatively constant within the slab cross-section and across the slab width. To simplify the calculation of thermal strains, a uniform temperature equal to that measured at the middle of the slab (thermocouple 02) will be used. To determine overall effects, and not internal stress-strain gradients, this is a reasonable approach.

The development of thermal strain and stress in concrete during hydration is complex. Since the concrete is gaining strength at early ages, rapidly for HPC, the elastic modulus is changing during hydration. Any method used to determine thermal strains must obviously account for this change in stiffness. From the thermal coefficient of expansion for concrete, temperature change can be converted to strain. Then, by using an expression for the development of elastic modulus, stress can be calculated. Of course, the effects of creep must be included.

For the HPC tested, a coefficient of thermal expansion, $\alpha_T = 8 \times 10^{-6}$ /°C has been determined by other researchers (Dilger et al. 1996). This value agrees with an average value for concrete as suggested by Ghali and Favre (1986). As reported by CEB MC90, thermal expansion is dependent primarily on the type of coarse aggregate. Since the NSC

used had the same aggregate as the HPC, the same value for the coefficient of thermal expansion can be used for analysis.

A time step analysis to determine stress development due to temperature changes has been given by Ghali and Favre (1986). The expression for the stress increment in the *i*th time interval is:

$$(\Delta\sigma_{res})_i = -\frac{E_c(t_i)}{1+\phi(t_{i+1/2},t_i)}\left(\alpha_T\sum_{j=1}^{i}(\Delta T)_j + \sum_{j=1}^{i-1}\frac{(\Delta\sigma_{res})_j}{E_c(t_j)}\left[1+\phi(t_{i+1/2},t_j)\right]\right) \quad (4.3)$$

The terms in the above equation are defined as follows:

$(\Delta\sigma_{res})_i$	=	restrained stress increment in the *i*th time interval
$E_c(t_i)$	=	elastic modulus of concrete at the middle of the *i*th time interval
$\phi\,(t_{i+1/2},t_i)$	=	creep coefficient for stress applied at t_i, and sustained to $t_{i+1/2}$
α_T	=	coefficient of thermal expansion
$(\Delta T)_j$	=	temperature increment in the *j*th time interval.
t_i	=	age of concrete at the middle of the *i*th interval
$t_{i+1/2}$	=	age of concrete at the end of the *i*th interval
$t_{i-1/2}$	=	age of concrete at the beginning of the *i*th interval

4.9.3.2 *Thermal stress-strain development in NSC slabs*

Using the time step analysis presented in Equation 4.3 above, a prediction of thermal stress development for the NSC slabs was made. The first step is to divide the temperature curve into a number of intervals. These intervals should be sufficiently small so that the measured temperature can be approximated by a series of linear increments. Figure 4.45 shows the division of the temperature curve for slab 30-4 (thermocouple 02). As shown, three linear intervals give a reasonable fit. The resulting time and temperature data points are given in the following table:

i	0.5	1	1.5	2	2.5	3	3.5
t_i (days)	0.00	0.30	0.60	1.05	1.50	1.75	2.00
T_i (°C)	18.4		30.4		18.0		19.4

Table 4.5 Time and temperature data for slab 30-4 ($t = 0$ is age at casting)

Creep coefficients need to be calculated for the various time intervals. The method described by CEB MC90 can be used (CEB Equations 2.1-64 to 2.1-71), with the loading in this case being thermal. For example, to calculate the creep coefficient for an age at loading of 0.30 days up to an age of 2.00 days:

Input:

RH	=	40% * =	relative humidity
A_c	=	125 x 800 = 100000 mm^2 =	concrete cross-sectional area
u	=	2 x 800 = 1600 mm^2 =	exposed surface area
t	=	2.00 days =	age at time considered
t_0	=	0.30 days =	age at loading
f_{cm}	=	30 MPa =	concrete compressive strength

* 40% is the lower limit of validity for the CEB method, and was used for calculations; results are not reasonable when extrapolated to actual humidity of 15%.

Output:

h = 125 = notional size of member in mm

$\beta(t_0)$ = 1.129 = coefficient for age at loading

$\beta_c(t-t_0)$ = 0.189 = coefficient for development of creep from time t_0 to t

$\beta(f_{cm})$ = 3.06 = coefficient for concrete compressive strength

ϕ_{RH} = 2.21 = coefficient dependent on RH and h

ϕ_0 = 7.64 = notional creep coefficient

$\phi(t, t_0)$ = 1.44 = ϕ (2.00, 0.30) = creep coefficient.

Other values of the creep coefficient over different time intervals were calculated in the same way to give the following results:

ϕ_{CEB} (2.00, 0.30) = 1.44

ϕ_{CEB} (2.00, 1.05) = 0.97

ϕ_{CEB} (2.00, 1.75) = 0.59

ϕ_{CEB} (1.50, 0.30) = 1.30

ϕ_{CEB} (1.50, 1.05) = 0.77

ϕ_{CEB} (0.60, 0.30) = 0.86.

The subscript *CEB* indicates CEB MC90 as the source of the creep coefficients. This is a necessary distinction because Equation 4.3 was derived with normalized creep coefficients:

$$\phi \text{ (Eqn. 4.3)} = \phi_{CEB}\, E_c(t_0) / E_c(28) \qquad (4.4)$$

where $E_c(t_0)$ = elastic modulus at age t_0

$E_c(28)$ = elastic modulus at age of 28 days = 25750 MPa, for the NSC (Section 4.4).

Also using CEB MC90 to determine the development of elastic modulus (CEB Equations 2.1-57 and 58) gives:

$E_c(0.30) = 0.339\ E_c(28)$

$E_c(1.05) = 0.594\ E_c(28)$

$E_c(1.75) = 0.687\ E_c(28)$.

Thus, for use in Equation 4.3,

$\phi\ (2.00, 0.30) = 1.44 \times 0.339 = 0.49$

$\phi\ (2.00, 1.05) = 0.97 \times 0.594 = 0.58$

$\phi\ (2.00, 1.75) = 0.59 \times 0.687 = 0.41$

$\phi\ (1.50, 0.30) = 1.30 \times 0.339 = 0.44$

$\phi\ (1.50, 1.05) = 0.77 \times 0.594 = 0.46$

$\phi\ (0.60, 0.30) = 0.86 \times 0.339 = 0.29$.

With all of the required values calculated the time step analysis can be carried out.

<u>First interval,</u> $i = 1,\ t_i = 0.30$ days

$\phi\ (t_{i+1/2}, t_i) = \phi\ (0.60, 0.30) = 0.29$

$$\sum_{j=1}^{i} (\Delta T)_j = 30.4 - 18.4 = +12.0\ ^\circ C$$

$$(\Delta\sigma_{res})_i = -\frac{(0.339)(25750)}{1+0.29}\left(+8\times10^{-6}(12.0)+0\right)$$

$$= -0.65\ \text{MPa (compression)}.$$

Second interval, $i = 2$, $t_i = 1.05$ days

$\phi\,(t_{i+1/2}, t_i) = \phi\,(1.50, 1.05) = 0.46$

$$\sum_{j=1}^{i} (\Delta T)_j = (18.0 - 30.4) + (30.4 - 18.4) = -0.4\ ^\circ C$$

$$(\Delta\sigma_{res})_i = -\frac{(0.594)(25750)}{1+0.46}\left(+8\times10^{-6}(-0.4) + \frac{-0.65(1+0.44)}{0.339\times25750}\right)$$

$$= +1.16 \text{ MPa (tension).}$$

Third interval, $i = 3$, $t_i = 1.75$ days

$\phi\,(t_{i+1/2}, t_i) = \phi\,(2.00, 1.75) = 0.41$

$$\sum_{j=1}^{i} (\Delta T)_j = (19.4\text{-}18.0) + (18.0 - 30.4) + (30.4 - 18.4) = +1.0\ ^\circ C$$

$$(\Delta\sigma_{res})_i = -\frac{(0.687)(25750)}{1+0.41}\left(+8\times10^{-6}(1.0) + \frac{-0.65(1+0.49)}{0.339\times25750} + \frac{+1.16(1+0.58)}{0.594\times25750}\right)$$

$$= \text{-0.21 MPa (compression).}$$

The total restrained stress in slab 30-4 at an age of 2.00 days, due to thermal effects, is the sum of the three calculated stress increments:

$$\sigma_T(2.0) = \text{-0.65 + 1.16 - 0.21 = +0.3 MPa (tension).}$$

The development of predicted thermal stress is plotted on Figure 4.47. Considering that the tensile strength of the NSC was measured at about 2 MPa at 2 days, the calculated thermal stress of 0.3 MPa is 15% of the strength. The predicted risk of thermal cracking in the NSC slabs is negligible, given that early age shrinkage was not high. This was confirmed with the test specimens which did not develop cracks until long after the slab returned to ambient temperatures. The reinforcement which was provided was sufficient to prevent thermal cracking. Further discussion of tensile stress due to shrinkage is given in Section 4.10.

4.9.3.3 *Thermal stress-strain development in HPC slabs*

The development of thermal stress in the HPC slabs can be calculated in the same way as for the NSC slab. Shown on Figure 4.46 is the division of the temperature curve for slab 100-8. For this slab, three intervals give a reasonable linear fit. Temperature may be considered constant between an age of 0.00 (time of casting) and 0.30 days. Over this period the concrete was in a pre-hydration dormant stage. Thus, the development of thermal stresses were insignificant in this interval and are not included in the analysis. The time and temperature data are shown in the following table.

i	0.5	1	1.5	2	2.5	3	3.5
t_i (days)	0.30	0.55	0.80	1.35	1.90	2.45	3.00
T_i (°C)	22.4		42.0		26.3		22.8

Table 4.6 Time and temperature data for slab 100-8 ($t = 0$ is age at casting)

Calculation of creep coefficients for the HPC slab 100-8 is in accordance with the model of Dilger, Niitani, and Wang (1997) (subscript *DNW*) using $f_{cm} = 85$ MPa:

$\phi_{DNW}(3.00, 0.55) = 1.34$

$\phi_{DNW}(3.00, 1.35) = 0.88$

$\phi_{DNW}(3.00, 2.45) = 0.50$

$\phi_{DNW}(1.90, 0.55) = 1.20$

$\phi_{DNW}(1.90, 1.35) = 0.67$

$\phi_{DNW}(0.80, 0.55) = 0.80$

Using interpolated values from a curve fit to test data for elastic modulus of the HPC (Wang 1997):

$E_c(0.55) = 0.656\, E_c(28)$

$E_c(1.35) = 0.748\, E_c(28)$

$E_c(2.45) = 0.809\, E_c(28)$.

Hence, creep coefficients are:

$\phi\,(3.00, 0.55) = 1.34 \times 0.656 = 0.88$

$\phi\,(3.00, 1.35) = 0.88 \times 0.748 = 0.66$

$\phi\,(3.00, 2.45) = 0.50 \times 0.809 = 0.41$

$\phi\,(1.90, 0.55) = 1.20 \times 0.656 = 0.79$

$\phi\,(1.90, 1.35) = 0.67 \times 0.748 = 0.50$

$\phi\,(0.80, 0.55) = 0.80 \times 0.656 = 0.53$.

Using the calculated values above and $E_c(28) = 32300$ MPa (Section 4.4), the time step analysis can be carried out.

First interval, $i = 1$, $t_i = 0.55$ days

$\phi\,(t_{i+1/2}, t_i) = \phi\,(0.80, 0.55) = 0.53$

$$\sum_{j=1}^{i} (\Delta T)_j = 42.0 - 22.4 = +19.6\ ^\circ\mathrm{C}$$

$$(\Delta\sigma_{res})_i = -\frac{(0.656)(32300)}{1+0.53}\left(+8\times10^{-6}(19.6)+0\right)$$

$= -2.17$ MPa (compression).

Second interval, $i = 2$, $t_i = 1.35$ days

$\phi\,(t_{i+1/2}, t_i) = \phi\ (1.90, 1.35) = 0.50$

$$\sum_{j=1}^{i} (\Delta T)_j = (42.0 - 22.4) + (26.3 - 42.0) = +3.9\ ^{\circ}C$$

$$(\Delta\sigma_{res})_i = -\frac{(0.748)(32300)}{1+0.50}\left(+8\times10^{-6}(3.9) + \frac{-2.17(1+0.79)}{0.656\times32300}\right)$$

$$= +2.45 \text{ MPa (tension).}$$

Third interval, $i = 3$, $t_i = 2.45$ days

$\phi\,(t_{i+1/2}, t_i) = \phi\ (3.00, 2.45) = 0.41$

$$\sum_{j=1}^{i} (\Delta T)_j = (+3.9) + (22.8 - 26.3) = +0.4\ ^{\circ}C$$

$$(\Delta\sigma_{res})_i = -\frac{(0.809)(32300)}{1+0.41}\left(+8\times10^{-6}(0.4) + \frac{-2.17(1+0.88)}{0.656\times32300} + \frac{+2.45(1+0.66)}{0.748\times32300}\right)$$

$$= +0.40 \text{ MPa (tension).}$$

The total restrained stress in slab 100-8 at an age of 3.0 days, due to thermal effects, is the sum of the three calculated stress increments:

$$\sigma_T(3.0) = \quad -2.17 + 2.45 + 0.40 = +0.7 \text{ MPa (tension).}$$

For reference, the predicted development of thermal strains in slab 100-8 is also shown on Figure 4.47. With a measured split cylinder tensile strength of about 5 MPa at 3 days, the tensile thermal stress in the restrained HPC slab is equal to about 15% of the strength. As will be discussed in Section 4.10.3, in combination with shrinkage at an early age, which was very high in the HPC slabs, thermal strains were a contributor to the cracks which occurred.

4.10 Analysis of shrinkage stress-strain development

4.10.1 *General*

A time step analysis, which is of the same form as that presented above for thermal strains, can be carried out to determine the effect of shrinkage in a fully-restrained member. As discussed in Section 4.8.2, "fully-restrained" is a reasonable assumption for the test slabs. A general equation which describes the time step analysis is given by Neville, Dilger, and Brooks (1983) as follows:

$$\sigma_{i+1} = \sigma_{i-1} + \frac{E_i}{1+\phi_{ii}}\left(\sum_{j=1}^{i}\Delta\varepsilon_j - \sum_{j=1}^{i-1}\left(\sigma_{j+1}-\sigma_{j-1}\right)\frac{1}{E_j}\left(1+\phi_{ij}\right)\right) \qquad (4.5)$$

The concrete parameters are:

$\sigma_{i+1}, \sigma_{j+1}$	=	stress at the end of the *i*th , *j*th interval
$\sigma_{i-1}, \sigma_{j-1}$	=	stress at the beginning of the *i*th , *j*th interval
E_i, E_j	=	modulus of elasticity at the middle of the *i*th , *j*th interval
$\Delta\varepsilon_j$	=	change in strain over the *j*th interval
ε_j	=	ε_{sh}, free shrinkage strain (for this analysis)
ϕ_{ii}	=	$\phi\,(t_{i+1},t_i)$ = creep coefficient at the end of the *i*th interval for load applied at the middle of the *i*th interval
ϕ_{ij}	=	$\phi\,(t_{i+1},t_j)$ = creep coefficient at the end of the *i*th interval for load applied at the middle of the *j*th interval

4.10.2 *NSC test slabs*

To begin the stress-strain analysis, the free shrinkage curve obtained for the NSC must be divided into a reasonable number of intervals. Since the purpose of this analysis is to estimate the tensile stress in the slab prior to cracking, the duration is taken up to age of 28 days, when the main crack formed. Neville, Dilger, and Brooks (1983) suggest intervals which are of equal width when plotted on a logarithmic scale. With reference to the plot of free shrinkage for slab 30-4 shown on Figure 4.48, four intervals were selected. The values required for analysis are presented in Table 4.7 below, beginning with the baseline shrinkage measurements which were made at an age of 0.9 days. The calculated stress due to shrinkage is also given in Table 4.7. (For a detailed presentation of calculations refer to Appendix C.)

i		1		2		3		4	
t_i (days)	0.9	1.5	2.1	3.7	5.2	9.1	13.0	20.5	28.0
$\varepsilon_{sh}(t_i)$ x 10^{-6}	0	-8	-16	-52	-88	-138	-188	-234	-280
σ (MPa) tensile			0.076		0.84		1.72		2.35

Table 4.7 Free shrinkage data for NSC (slab 30-4) and calculated stress in fully-restrained member

The predicted development of stress due to shrinkage is plotted on Figure 4.49, up to the age of cracking (for slab 30-2) of 28 days. Thermal stress is also depicted. Because shrinkage strain developed slowly for the NSC there is virtually no overlap between shrinkage and thermal stress development. Hence, a superposition of these two stresses is irrelevant to a discussion of cracking. The main crack which developed in slab 30-2 was caused by shrinkage stress alone.

Curves are shown on Figure 4.49 for the development of direct tensile strength, which defines the force resisting cracking. To convert from mean splitting tensile strength, $f_{ct,sp}$, which was determined from cylinder tests, to mean axial (direct) tensile strength, f_{ctm}, the following equation from CEB MC90 was used:

$$f_{ctm} = 0.9 f_{ct,sp} \tag{4.6}$$

It is well known that the tensile strength of normal strength concrete is dependent on curing conditions. Since drying causes tensile stresses to form on the surface of the member, dry-cured tensile strength is substantially lower. Some sources have reported a 50% loss of strength from moist-cured to dry-cured (Dilger 1993). Knowing that the test slabs were cured under very low humidity, it can be presumed that their tensile strengths would be much less than the tested cylinders which were cured in a fog room. The curve for dry-cured tensile strength, shown on Figure 4.49, was taken as being 70% of that for moist-cured. This strength reduction was arrived at by equating the tensile strength at 28 days to the predicted tensile stress in the slab: the condition at which cracking will occur. The intersection of the two curves at an age of 28 days is seen on Figure 4.49.

4.10.3 *HPC test slabs*

The development of tensile stress in the HPC test slabs prior to cracking is more difficult to predict. Since cracking occurred at such an early age, estimated values of elastic modulus and tensile creep will be less accurate: time intervals being very small. The analysis is aided, however, by using actual elastic modulus test results by Wang (1997), and creep coefficients according to Dilger, Niitani, and Wang (1997). Shrinkage development for slab 100-4 is divided into intervals for analysis as shown on Figure 4.50. Table 4.8 summarizes the shrinkage data and the resulting prediction of stress development. (For a detailed presentation of calculations refer to Appendix C.)

i		1		2		3		4	
t_i (days)	0.3	0.4	0.5	0.7	0.9	1.2	1.4	2.2	3.0
$\varepsilon_{sh}(t_i)$ x 10^{-6}	0	-60	-120	-200	-278	-308	-338	-356	-374
σ (MPa) tensile			0.72		2.61		3.08		3.03

Table 4.8 Free shrinkage data for HPC (slab 100-4) and calculated stress in fully-restrained member

For the HPC slabs, shrinkage stress developed significantly during the same period as thermal stress. The plots of predicted values are given on Figure 4.51. A superposition of shrinkage and thermal stress gives total stress, which is also plotted on the figure. To illustrate the potential for cracking, the development of direct tensile strength for the HPC is shown. This curve was derived by using average values of splitting tensile strength determined in cylinder tests (Section 4.3). To convert to direct tensile strength, FIP-CEB 1990 equations for HPC were used. (Equations (2.4) and (2.5) in Section 2.4.2)

Clearly, from Figure 4.51, the HPC slabs experienced total tensile stress which exceeded the tensile strength of the concrete section at an age of about 2 days. The observed formation of cracks between 2 and 3 days was the direct result. (The crossing of the three curves for total stress, shrinkage stress, and tensile strength at an age of 1.7 days is a coincidence.) Thermal stress became tensile only after the age of cracking. However, if the slabs had been less fully-restrained, cracking may have been delayed to

an age where thermal stress would have had an influence. There is definitely a potential for early-age cracking caused by the combination of shrinkage and thermal stress in HPC.

4.11 Crack development

4.11.1 *Patterns of cracking*

4.11.1.1 *General*

During the aging of the test slabs, significant cracks were carefully observed, marked, and measured. The general criteria for a "significant" crack was that it was visible to the unaided eye and had a length of at least 20 mm. The width of a barely visible crack was determined to be about 0.05 mm, using a 50X crack microscope. For comparison, the limit for acceptable crack width is given as 0.3 mm by the FIP-CEB for normal structures. Thus, not all cracks which were noted on the test slabs can be considered as structurally objectionable. However, the primary cracks, which penetrated the full slab thickness, reached widths up to 2.5 mm. Such cracks are definitely not acceptable, and will be discussed herein. A more quantitative presentation of crack width measurements is given in Section 4.11.2.

4.11.1.2 *Slab 30-2*

Diagrams showing the cracks which developed on slab 30-2 are given as Figure 4.52 and 4.53. For reference, the locations of reinforcing steel is noted on the underside surface. As seen on Figure 4.52, the first significant cracks developed at an age of 15 days. These cracks were located near the bearing plates at the prestressing points, and are thought to be the result of horizontal tensile strain produced during vertical prestressing. Two groups of cracks were observed on the underside of the slab near the pour breaks

(the slab was cast using four batches). These cracks were fairly random and did not develop into major cracks.

As shown in Figure 4.53, a major crack running the full width of slab 30-2 was observed at 30 days near the slab midspan. This crack was located directly at a cross section which was weakened by a transverse reinforcing bar. After the main crack formed, no other significant cracks developed. Presumably, the main crack released the restraint in the slab. Subsequently, the two sections of the slab on either side of the crack were free to shrink away from the crack.

4.11.1.3 *Slab 30-4*

Figure 4.54 shows the crack pattern which formed for slab 30-4 up to an age of 35 days. Unlike, slab 30-2, a single predominant crack did not occur. Instead, a series of cracks, only visible on the underside, developed in the test section of the slab. These cracks were generally oriented along the transverse reinforcement, although some propagated in line with the longitudinal bars. A few of the transverse cracks penetrated up the sides of the slab, but none reached the top surface other than near the prestressing in a similar location to slab 30-2.

Even after 35 days, additional cracks formed and propagated in slab 30-4. This is consistent with distributed and controlled cracking: restrained shrinkage continued. Unexpectedly, at 300 days a more major crack was noted on the top of the slab near the right end block (Figure 4.55). This crack was in line with a transverse reinforcing bar, and went through the full slab thickness. From a review of humidity and free shrinkage measurements, it is believed that this late crack occurred due to accelerated shrinkage over a seasonal period of very dry conditions. Although this crack was full depth, its width was much smaller than the crack at the midspan of slab 30-2. Since top reinforcement was also present in this region, crack width was better controlled.

4.11.1.4 *Slabs 100-2, 100-4, and 100-8*

The crack patterns for the three HPC slabs were remarkably similar. As shown in Figures 4.56, 58, and 60, a major crack formed in each slab at an age of 3 days. Prior to this, the only cracks to appear in slab 100-2 were those shown on the top of the slab. These shorter, randomly oriented cracks, were caused by the overworking of the surface during finishing. Unfortunately, these cracks, which were formed in the rapidly hardening concrete by trowelling, could not be closed up by further trowel pressure. The other two HPC slabs, 100-4 and 100-8 did not have these cracks because finishing was done more quickly and with lighter pressure.

Within the first day after casting, cracks near the bearing plates for prestressing showed up in slabs 100-4 and 100-8. Similar cracks in 100-2 were not as numerous, and did not develop until an age of 5 days.

The main crack in slabs 100-2 and 100-4 followed a transverse reinforcing bar, whereas in slab 100-2 the main crack occurred between two bars. On close inspection, it was noted that the crack in 100-2 was in line with a slight step in the concrete bottom surface which had been caused by a joint in the formwork. Although the net concrete section at a transverse bar may have been less, the crack initiation favored the notch created by the step.

Even though each slab had an unacceptably wide single crack, the effect of reinforcement ratio on crack distribution was evident. Comparing Figures 4.56, 58, and 60, the underside of 100-8 showed more distributed cracking than 100-4, and 100-4 showed more than 100-2. As will be discussed in Section 4.11.3, the width of the main crack, at the level of reinforcement, was also greatly reduced with each increase in reinforcement ratio.

The long term crack patterns for the HPC slabs are given in Figures 4.57, 59, and 61. The underside surface of all three slabs was covered in cracks, although 90% of these were structurally insignificant (less than 0.1 mm in width). Each slab had a reduced crack density next to the main crack, as expected in this locally unrestrained region. In the same area, short longitudinal cracks had propagated along the longitudinal bars from the main crack. The most noticeable effect of the higher reinforcement ratios used in slabs 100-4 and 100-8 is that cracking was strongly oriented along the transverse bars. Whereas for slab 100-2, cracks were shorter and more randomly distributed.

The greatest difference between slabs 100-4 and 100-8 can be seen by the crack patterns on the slab edges. Slab 100-8 had many more cracks which propagated from the underside up the slab edge. One edge crack even extended out onto the top of the slab near the right end block (refer to Figure 4.61). The more advanced edge cracking for slab 100-8 is indicative of a greater width for secondary cracks. This being a result of a more restrained, and less wide, main crack. Hence, an increase in reinforcement ratio from 0.4% to 0.8% had some effect on crack patterns.

Slabs 100-4 and 100-8 both showed some minor longitudinal cracking on their top surfaces. Figure 4.59 overemphasizes the top longitudinal cracks which occurred on 100-4. The majority of these were barely visible.

4.11.2 *Crack widths*

4.11.2.1 *Slab 30-2*

Figure 4.62 shows the locations where the cracks on slab 30-2 were measured. Measurements were made with a microscope and across 50 mm gauge Demec points. The plot of crack width development is given in Figure 4.63. Strain readings are shown by

the curves, and widths are given as discrete points. (Note that the vertical axes are logarithmic to better show the much smaller values at 6869.) Since measurements of the main crack at points 7475, 7677, and 7879 were all very consistent, only 7677 is plotted.

Prior to the formation of the main crack, at an age of 30 days, the width of the secondary cracks at 6263, and 6869 increased steadily. As soon as the main crack formed these secondary cracks closed up slightly. The closing of cracks is indicated in Figure 4.63 by the drop in the curves from the peak width just before 30 days. Further shrinkage strain was then concentrated at the full-width main crack and secondary crack width stabilized. For 6869 the crack began to close as indicated by the steady decrease in the strain curve for this location.

The width of the main crack at the slab midspan was initially 0.3 mm at 30 days. Prior to the slab's removal at an age of 280 days, maximum crack width was 1.5 mm. As seen on Figure 4.63, the crack microscope readings of width closely paralleled the strain readings.

4.11.2.2 *Slab 30-4*

Although a single concentrated crack did not develop in slab 30-4, several distributed cracks were observed and measured. The cracks which were present on the top surface of the slab were located near the end blocks. The points of measurement for these cracks are shown in Figure 4.64. The full width crack which formed to the left of points 5-12-19 was monitored, but no crack growth was observed. Most likely, this crack was first detected long after it occurred, since the slab was not checked frequently at this late age.

Due to the existence of many parallel cracks, the increase in crack width over time is less smooth for slab 30-4 than for the other slabs. Figure 4.65 plots crack development,

in terms of strain and width. At points 6061, crack width development is fairly smooth from an initial value of 0.08 mm at 25 days to 0.50 mm at 200 days. The line for strain across 6061 parallels crack width but is offset to a lower absolute value. (The strain and width axes on Figure 4.65 are equivalent.) This offset occurs because crack width measurements began at a non-zero value initially, whereas strain is relative to a zero initial strain. The curve for 6869 flattens out at an age of about 30 days. This is a result of new parallel cracks having formed, as shown on Figure 4.64 to the left of 6869. A similar behavior occurred at an age of 200 days for 8081, as the crack to the left of points 5-12-19 opened up across the full slab width.

4.11.2.3 *Slabs 100-2, 100-4 and 100-8*

The location of crack measurements for the HPC slabs is shown in Figure 4.66. Since the main crack formed in a the same position for all three of the HPC slabs, crack widths at points 7475, 7677, and 7879 are directly comparable. To check the variance of crack width over the thickness of the slab, and especially to determine the effect of bottom reinforcement, measurements were also made on the side of slabs 100-4 and 100-8.

The increase in crack width over time is plotted in Figure 4.67 for all of the HPC slabs. For reference, the NSC slabs, 30-2 and 30-4, are also included. As noted, the largest crack, at points 8081, is charted for 30-4. (Refer to Figure 4.64 for location.). The curves for all of the HPC slabs are remarkably similar. Any variance can not be attributed to the different reinforcement ratios used. In fact, the crack width for 100-4 was consistently larger than for 100-2, even though 100-4 had twice as much reinforcement. The only conclusion that is apparent is that the amount of bottom reinforcement was irrelevant in terms of its effect on restraining crack width on the top of the HPC slabs.

The HPC slabs developed cracks which were much wider than for the NSC slabs. As well, cracks occurred at an earlier age and grew more rapidly. On Figure 4.67 this can be seen by the sharp rise in the curves at early ages. The NSC slabs, on the other hand, showed a more gradual increase in crack width.

4.11.3 *Crack profiles*

The variation in crack widths over the thickness of the test slabs was recorded and analyzed. Variation over the width of the slabs was also measured. This was done in an attempt to better understand the effect of the reinforcement on restricting crack width. Because of the relatively small amounts of reinforcement used, cracks on the top of the slabs did not reflect the presence or quantity of steel. That is, top cracks had a constant width at all locations across the slab. Figure 4.68 shows the profiles of main crack widths over the slab thickness. The age of slabs 30-2, and 100-2, 4, and 8 for this figure was 280, 460, 420, and 360 days respectively. Since the increase in crack width at these ages had practically stopped (refer to Figure 4.67) these profiles can be directly compared, even though the ages are different. The effect of a larger amount of reinforcement can be seen by comparing the curve for 100-2 to that of 100-4. At the level of reinforcement, crack width was 1.0 mm for 100-2 and 0.4 mm for 100-4. There appears to be no benefit to a further increase in reinforcement. The crack profiles for 100-4 and 100-8 are almost identical. The NSC slab 30-2 also had a significant decrease in crack width from the top of the slab (1.5 mm) to the bottom (0.6 mm). Since no principal crack formed for slab 30-4, measurements of crack width along the slab edge were not taken.

Inspection of the underside surface of the slabs showed a defined variation in crack width. The data plotted as Figure 4.69 shows that cracks became noticeably narrower at each reinforcing bar and wider in the unreinforced regions. This effect emphasizes the need for a maximum bar spacing criteria to achieve acceptable crack widths. Even if a

minimum reinforcement ratio is used, if bars are too widely spaced, cracks between the bars may become excessively wide.

4.12 Effect of creep

The effect of creep on the restrained slabs must be considered in any study of time-dependent behavior. As the concrete shrunk, tensile stress developed due to the restraint of the end blocks. The end blocks could not move appreciably: they were clamped to the load floor by prestressing. As for any structure subject to a constant strain, the effect of creep is to produce a relaxation of stress. For a slab undergoing restrained shrinkage, this relaxation is beneficial in reducing the build-up of tensile stress. Ultimately, a concentrated crack will form, if the tensile strength of the concrete, and the tensile yield of the reinforcement, is exceeded.

The quantitative effect of creep was considered in the strain analysis of the slabs discussed in Section 4.9.3, and 4.10.1. Since the test program did not include creep measurements, a prediction of creep using the method presented by CEB MC90 was used for the NSC. For the HPC, the model developed by Dilger, Niitani, and Wang (1997) was used.

4.13 Minimum reinforcement

4.13.1 *NSC Slabs 30-2 and 30-4*

In answer to the main question of this research, the 0.2% reinforcement ratio used for slab 30-2, the minimum as prescribed by CSA A23.3, was not sufficient. For the highly-restrained test slab, a single crack was formed with an unacceptable width of 1.5 mm. However, when a reinforcement ratio of 0.4% was used, for slab 30-4, the results

were favorable. A distributed pattern of cracks with a maximum width of 0.6 mm resulted.

An estimate of the tension force in the NSC slabs at the time of cracking, using the values for tensile stress in the slab established in Section 4.10.2, is as follows:

$$T_{concrete} = \sigma_{total} A_g = \quad (2.35 \text{ MPa})(125 \text{ mm})(800 \text{ mm}) = 235 \text{ kN} \ (28.0 \text{ days}).$$

Comparing this force to the resistance of the reinforcing steel for slab 30-2:

$$T_{reinf} = A_s f_y = \quad 2(100 \text{ mm}^2)(440 \text{ MPa}) = 88 \text{ kN} = 35\% \ T_{concrete}$$

Thus, it is understandable that a single large crack opened up, since the steel yielded and began to exhibit large strain.

With twice as much reinforcement, the tensile resisting force for slab 30-4 was twice as high as for 30-2:

$$T_{reinf} = 176 \text{ kN} = 75\% \ T_{concrete}$$

This resistance was close enough to the developed tensile stress to provide good crack control. Rather than yielding and stretching at a single location as for 30-2, the reinforcement in 30-4 was able to relieve the tensile stress due to shrinkage by forming distributed cracks.

4.13.2 *HPC Slabs 100-2, 100-4, and 100-8*

None of the HPC slabs had acceptable crack control. Even with a relatively high ratio of reinforcement, 0.8% for 100-8, a single crack with a width of up to 2.1 mm occurred. No reasonable level for bottom-only minimum reinforcement was established for the HPC slabs. Ratios greater than 0.8% were considered impractical, and testing was concluded with slab 100-8.

For the underside of the HPC slabs, the reinforcement ratios tested produced a reasonable distribution of cracks, and control of crack width. The reinforcement, which was located at 20 mm from the bottom of the slab, restricted crack width to a maximum value of 0.3 mm for 0.2% steel. The use of 0.2% top and bottom reinforcement would have likely given good overall crack control, and is considered much more practical than large amounts of bottom-only reinforcement.

As for the NSC slabs, the tension force at the time of cracking can be estimated for the HPC slabs (stress values are calculated from an addition of thermal stress, Section 4.9.3.3, and shrinkage stress, Section 4.10.3):

$$T_{concrete} = \sigma_{total} A_g = \quad (3.38 \text{ MPa})(125 \text{ mm})(800 \text{ mm}) = 338 \text{ kN} \quad (1.9 \text{ days})$$
$$(3.71 \text{ MPa})(125 \text{ mm})(800 \text{ mm}) = 370 \text{ kN} \quad (3.0 \text{ days}).$$

The maximum resisting force, provided by the reinforcing steel for slab 100-8 was:

$$T_{reinf} = A_s f_y = \quad 4(200 \text{ mm}^2)(440 \text{ MPa}) = 352 \text{ kN} = 95\% \, T_{concrete}.$$

Thus, the maximum amount of reinforcement used for the test slabs (0.8%) was very close to providing the force needed to prevent large cracks from forming. In fact, in

terms of tensile resistance versus predicted tensile stress, it would appear that 100-8 should have offered better crack control than 30-4 (95% of $T_{concrete}$ versus 75%). However, tension developed in the HPC slab so quickly that there was no time for a series of cracks to form and relieve the developing stress. The first crack to penetrate the top surface of the slab rapidly opened up. Only after the main crack was of a significant width, did a distributed series of bottom cracks form.

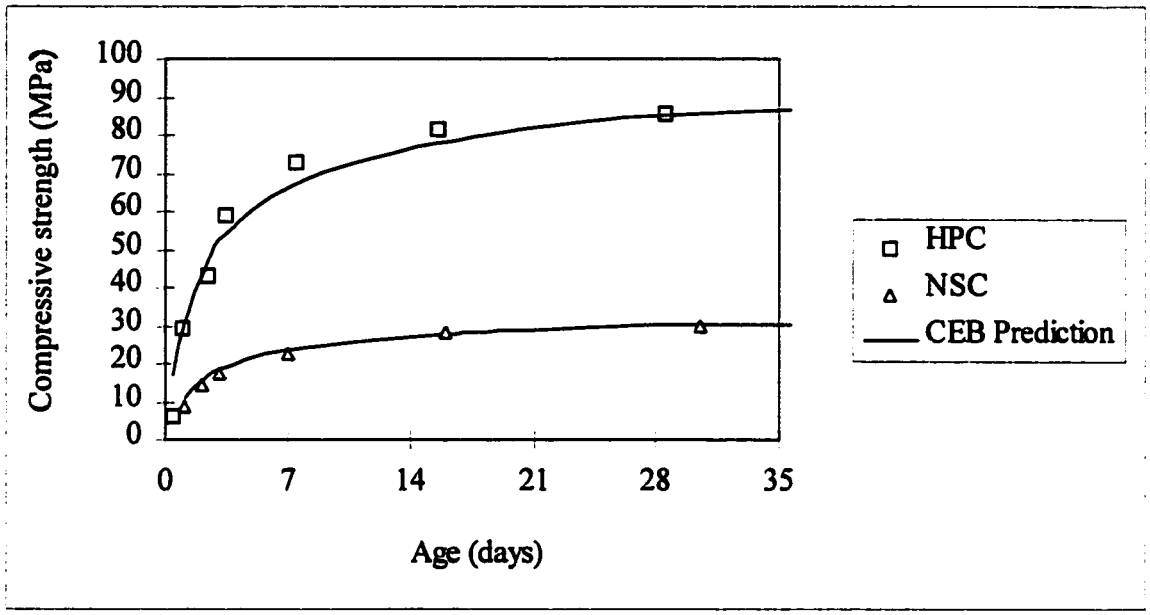

Figure 4.1 Compressive strength development: measured vs. predicted

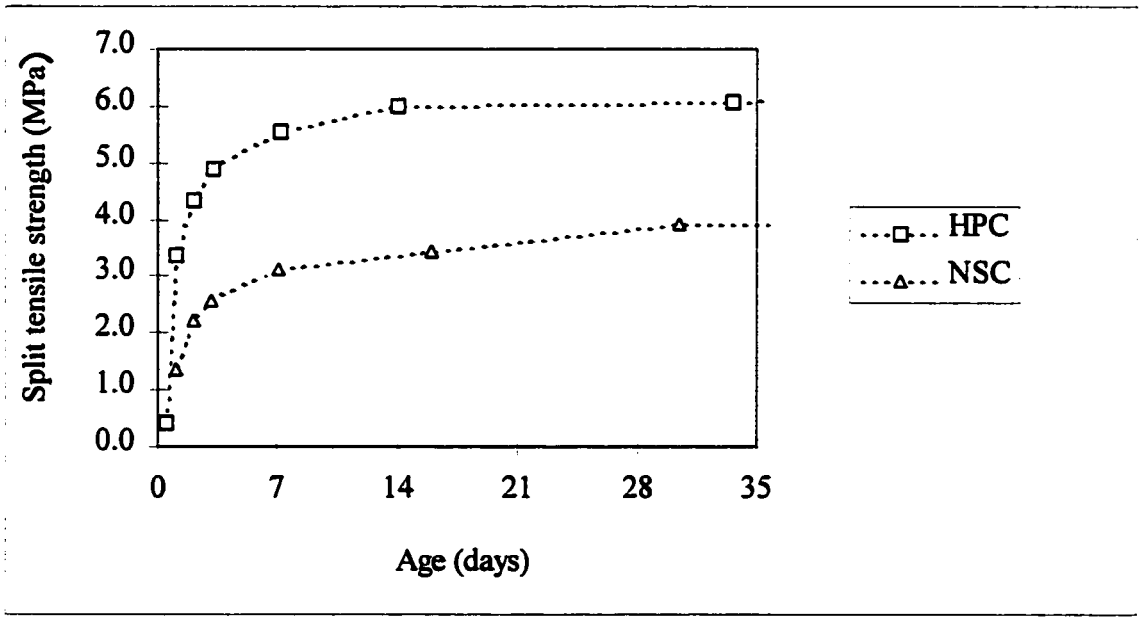

Figure 4.2 Split tensile strength development: measured

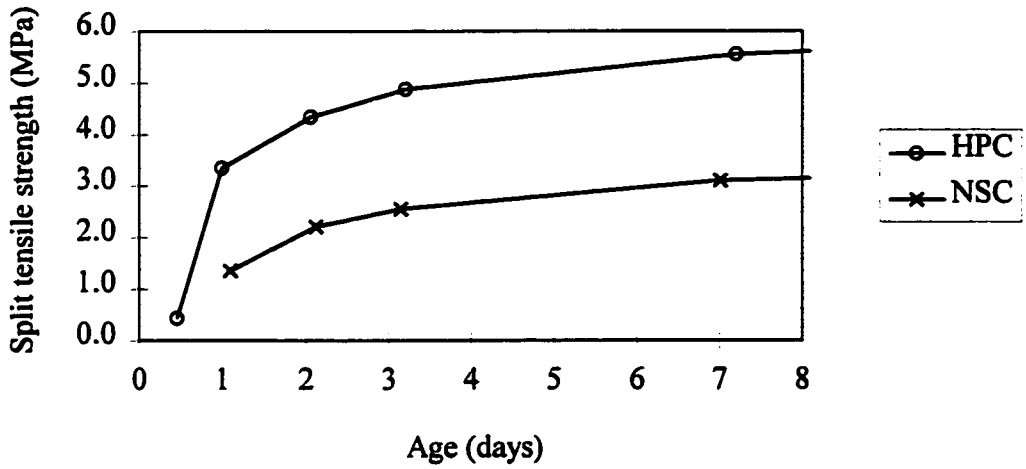

Figure 4.3 Split tensile strength: development at early age

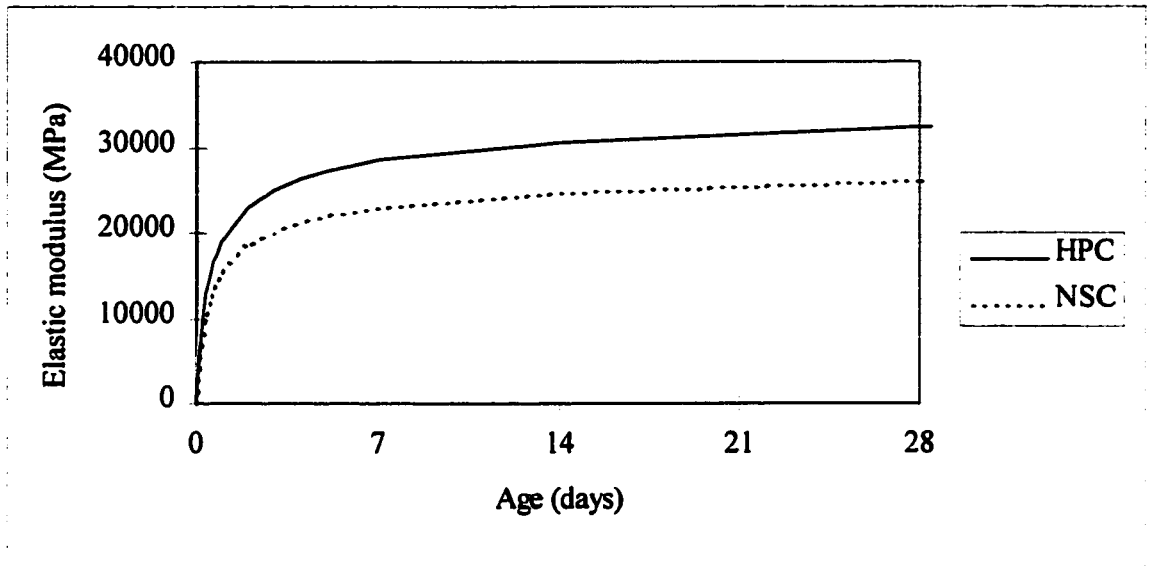

Figure 4.4 Predicted development of elastic modulus (According to CEB MC90)

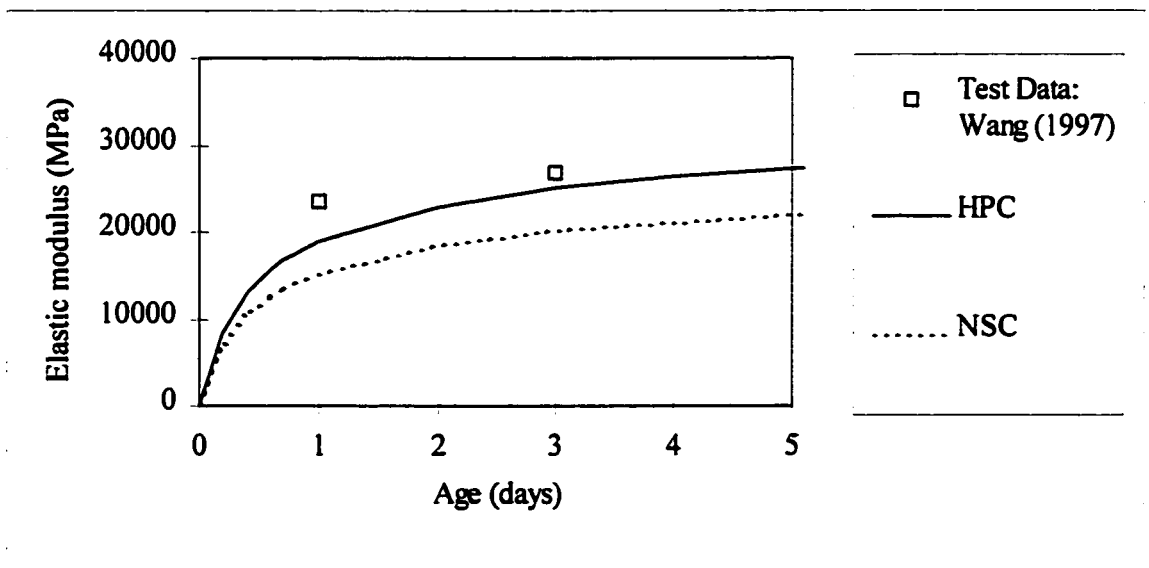

Figure 4.5 Predicted elastic modulus at early ages (According to CEB MC90)

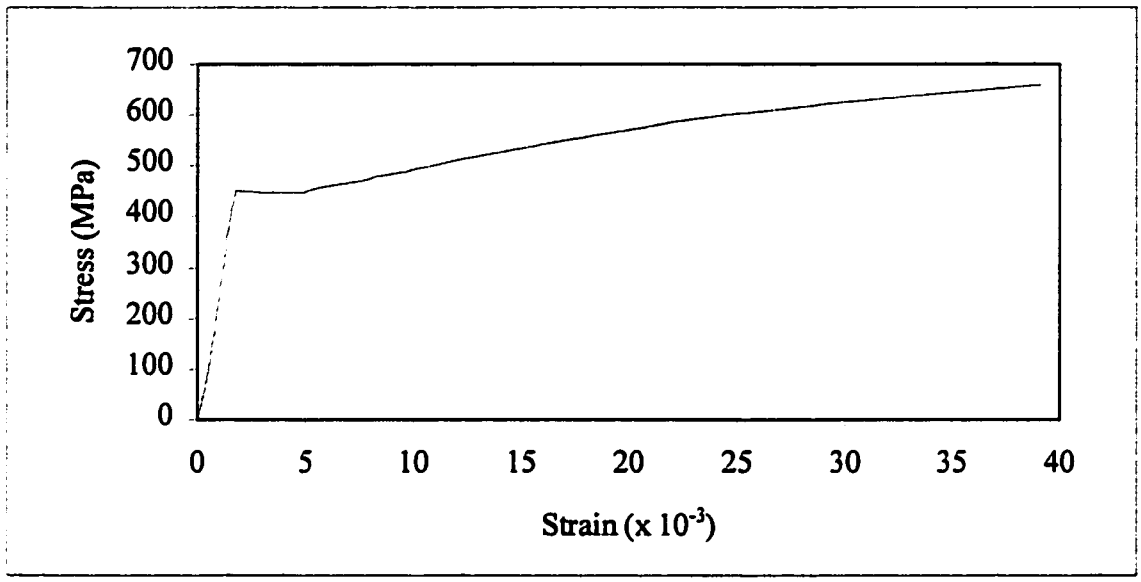

Figure 4.6 Tensile test for 10M steel reinforcing bar

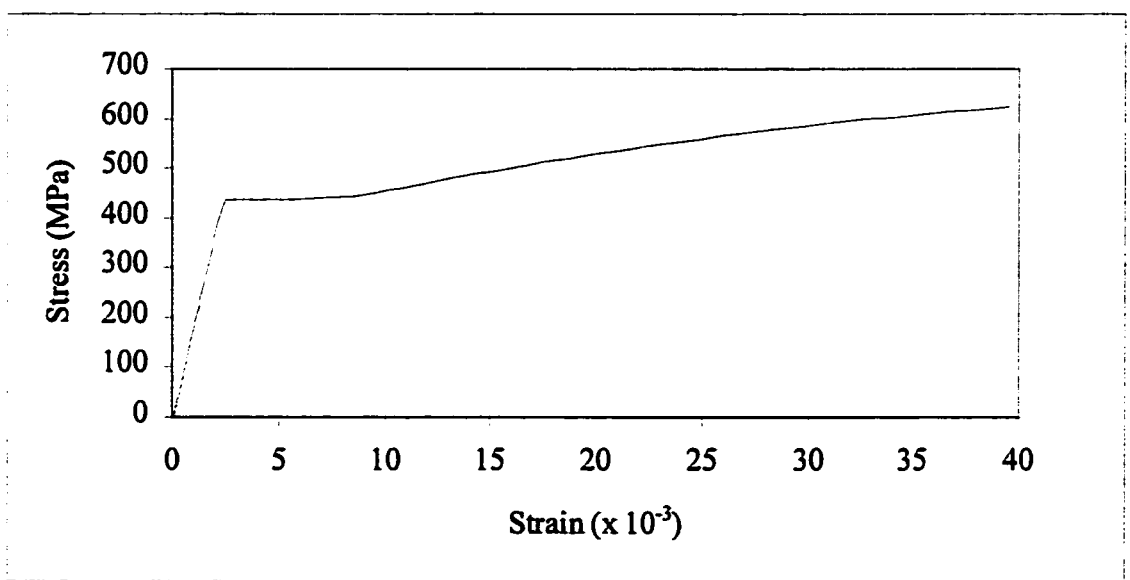

Figure 4.7 Tensile test for 15M steel reinforcing bar

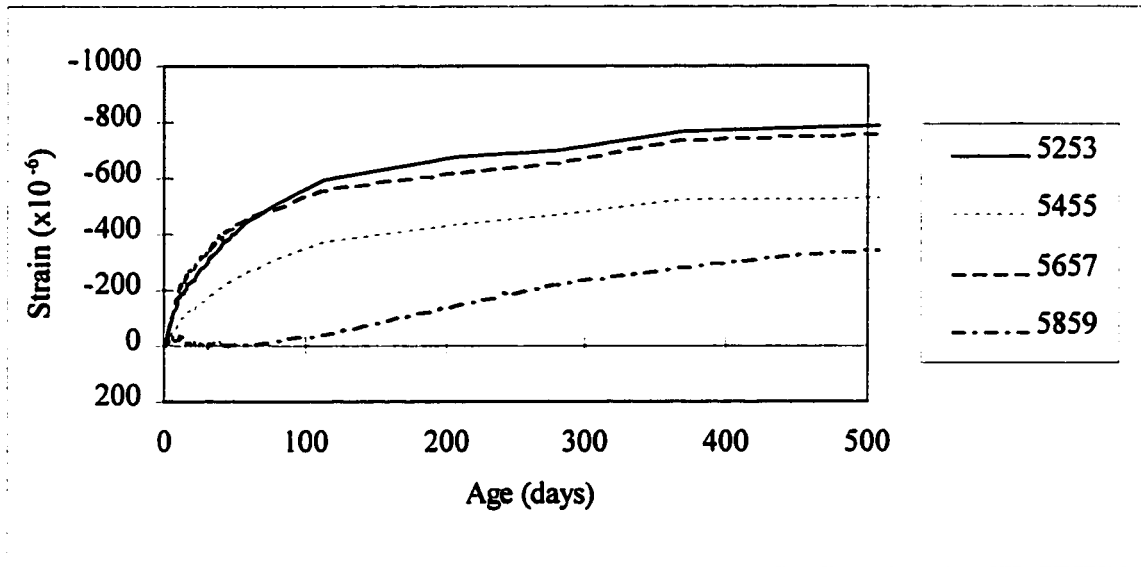

Figure 4.8 Free shrinkage for slab 30-2

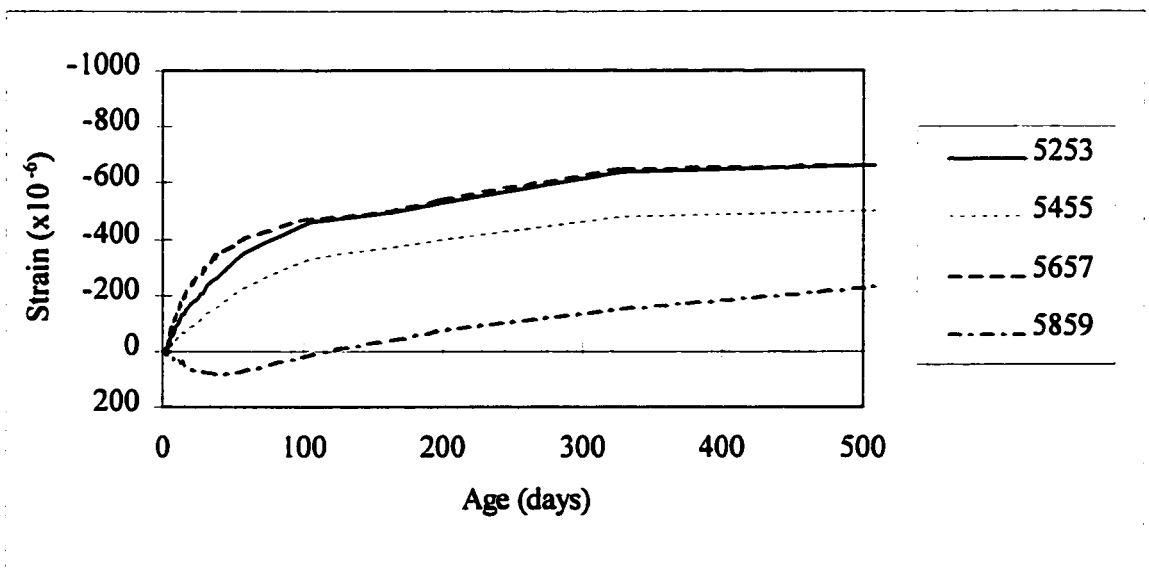

Figure 4.9 Free shrinkage for slab 30-4

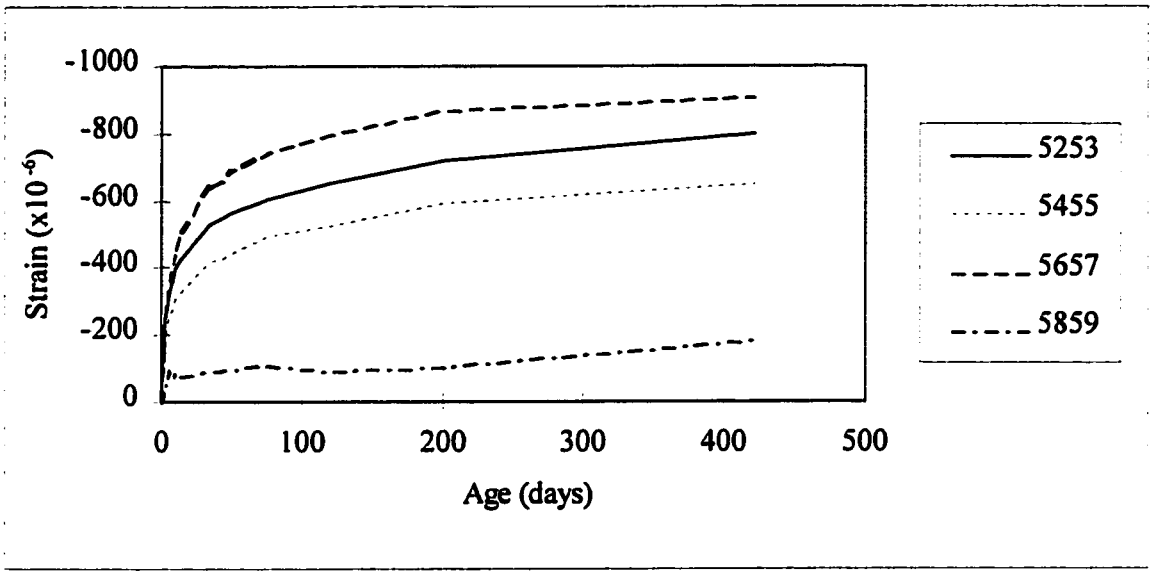

Figure 4.10 Free shrinkage for slab 100-4

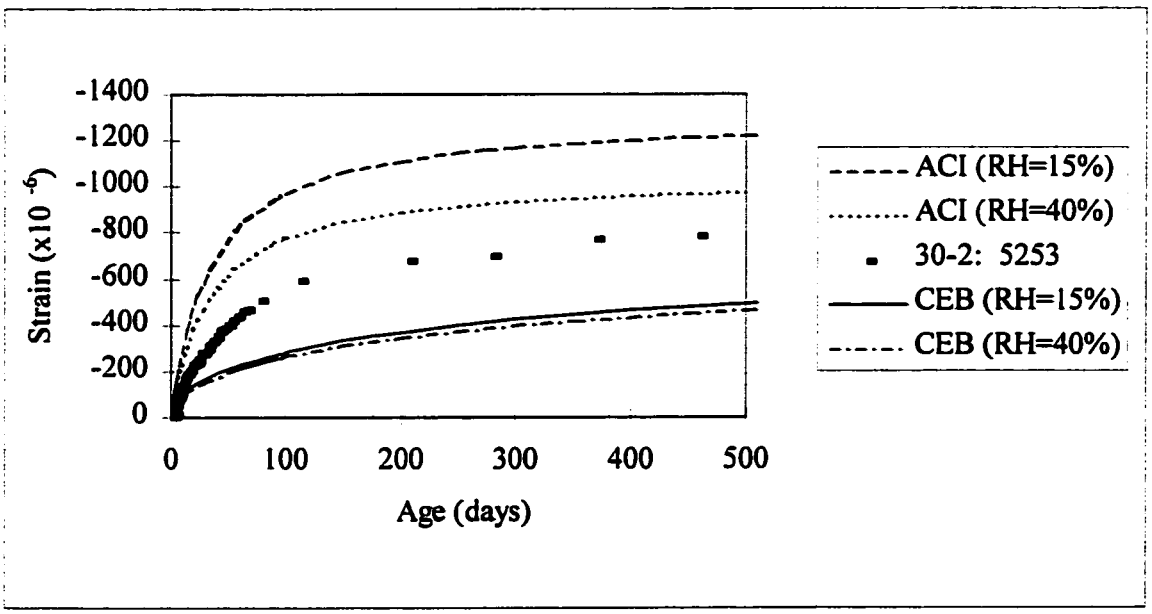

Figure 4.11 Shrinkage prediction by ACI 209 and CEB MC90
(for parameters as per slab 30-2)

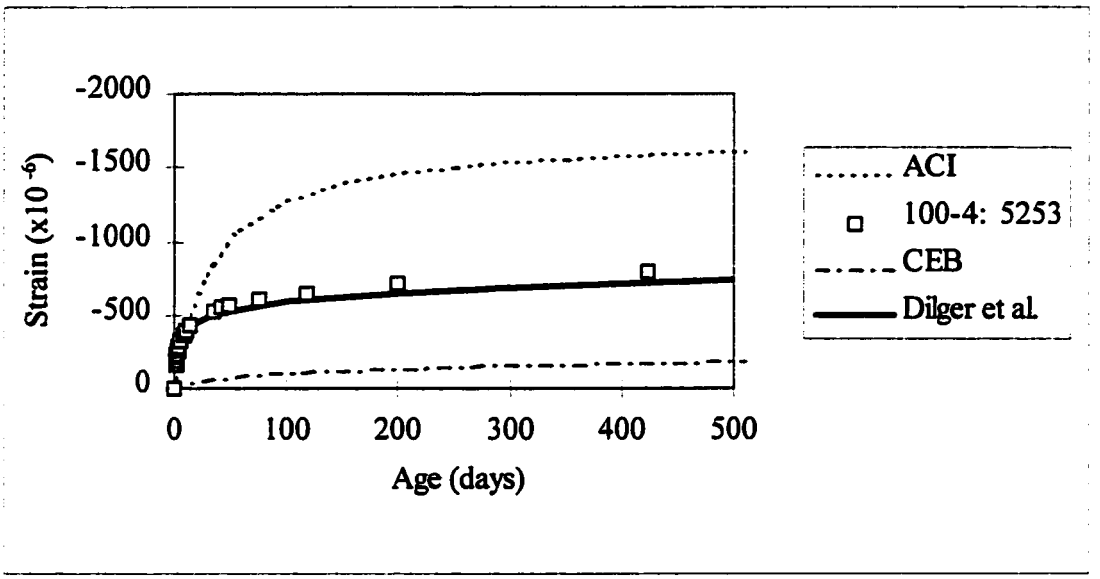

Figure 4.12 Shrinkage prediction by ACI 209, CEB MC90, and Dilger et al (1997) (for parameters as per slab 100-4)

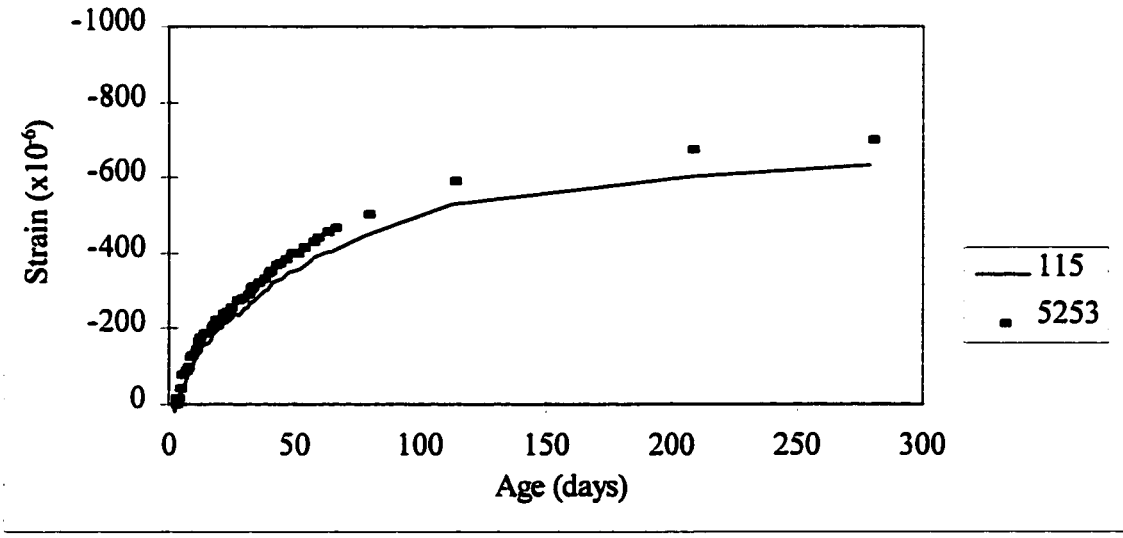

Figure 4.13 Shrinkage strain across slab width compared to free shrinkage (slab 30-2)

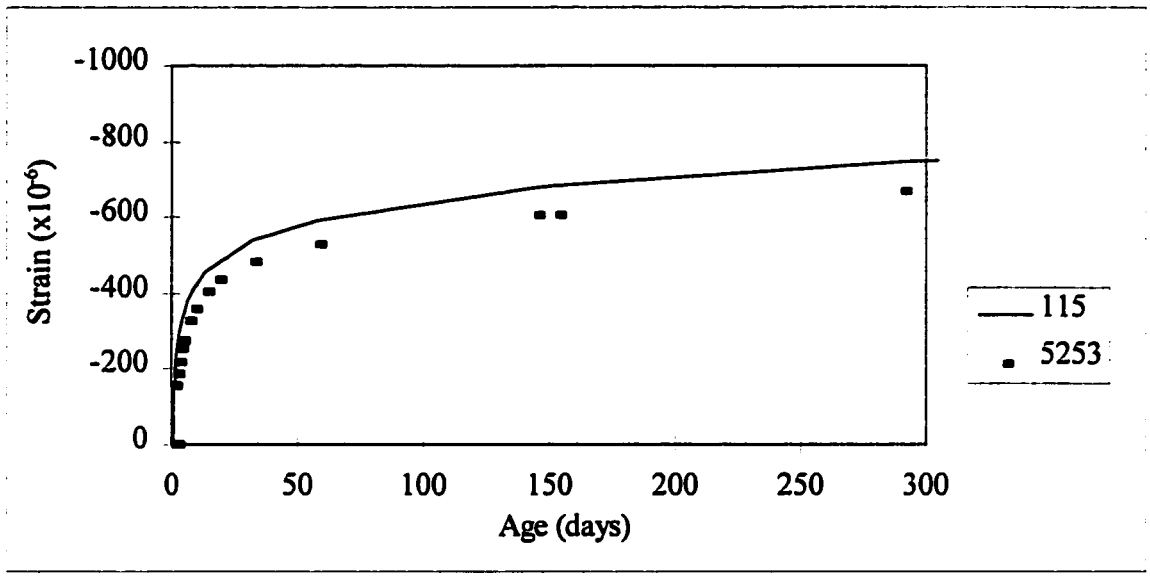

Figure 4.14 Shrinkage strain across slab width compared to free shrinkage (slab 100-8)

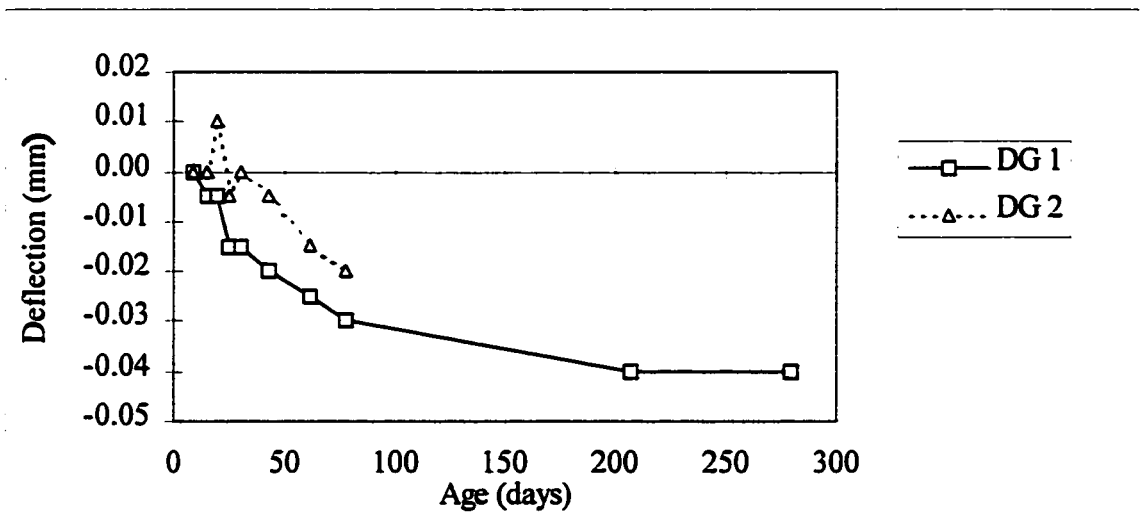

Figure 4.15 Deflection at end block: slab 30-2

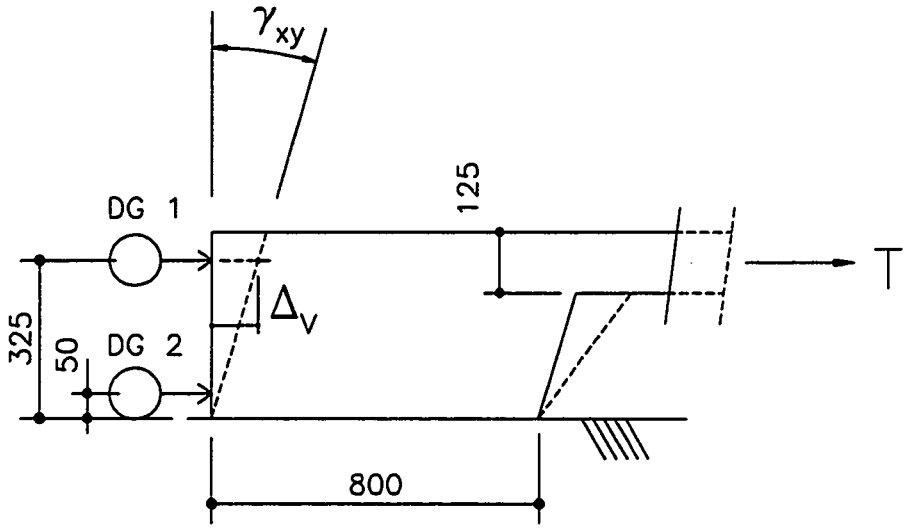

Figure 4.16 Shear deformation of slab end block: schematic

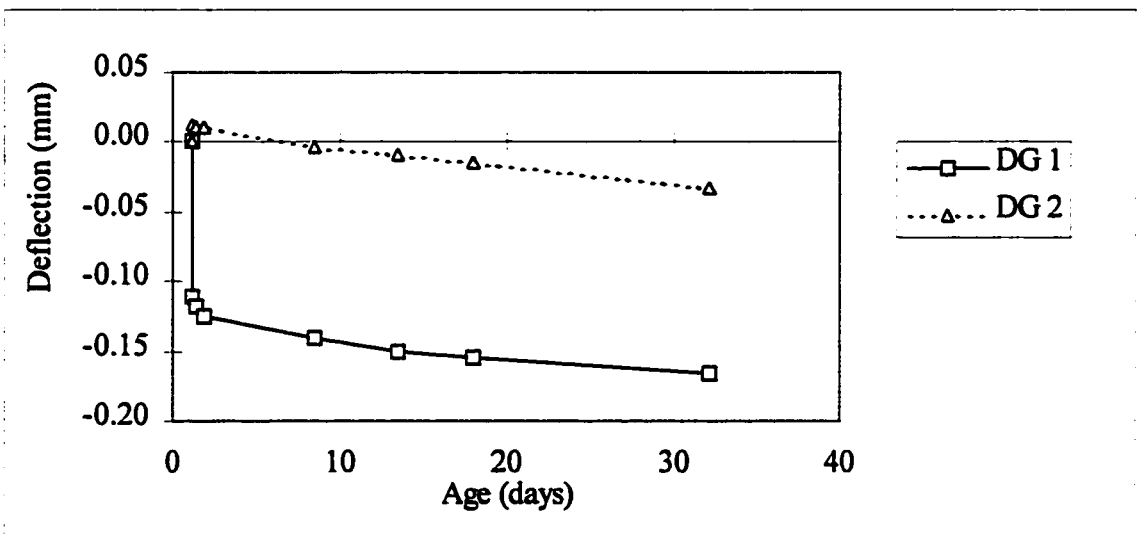

Figure 4.17 Deflection at end block: slab 100-8

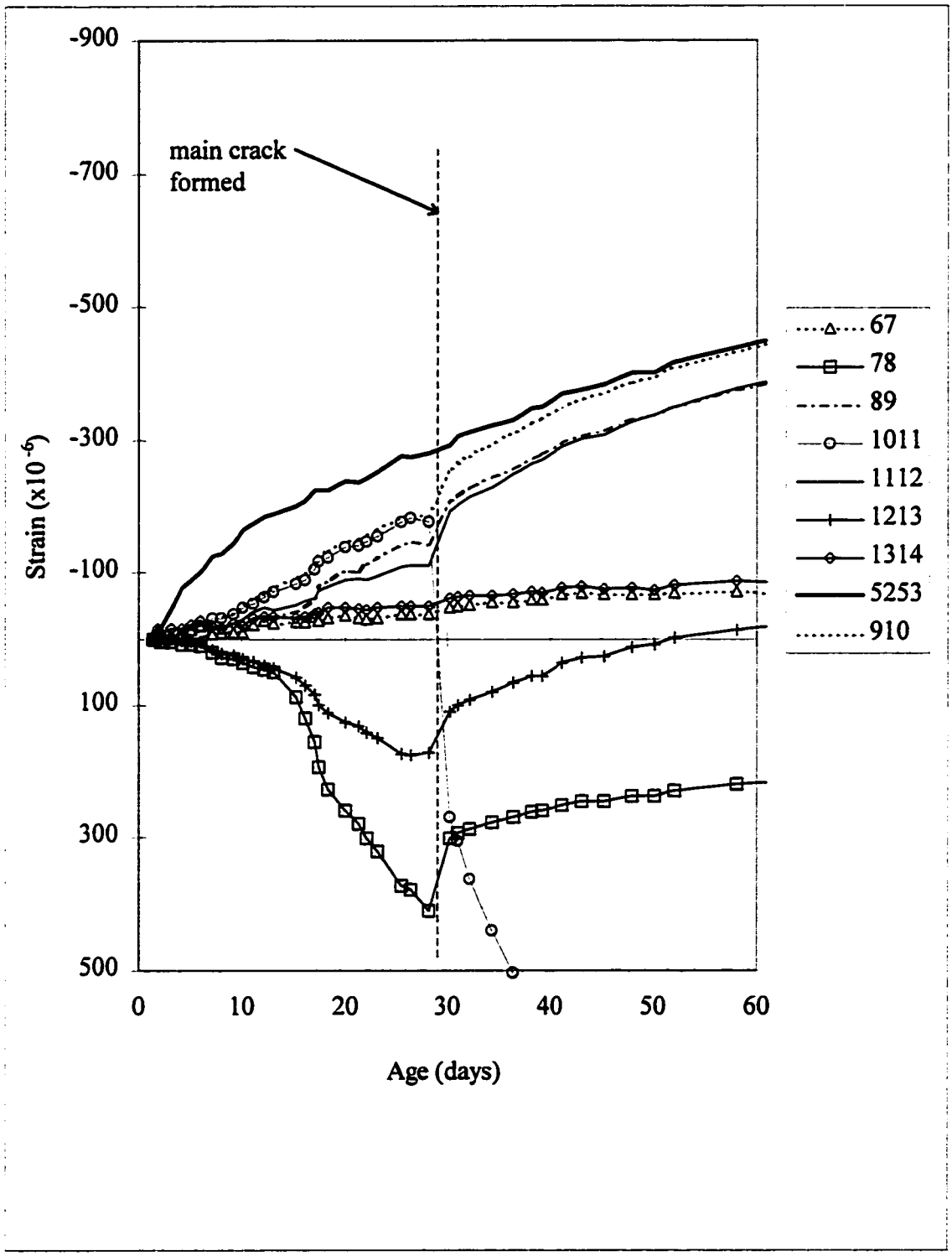

Figure 4.18 Strain development along middle of slab 30-2

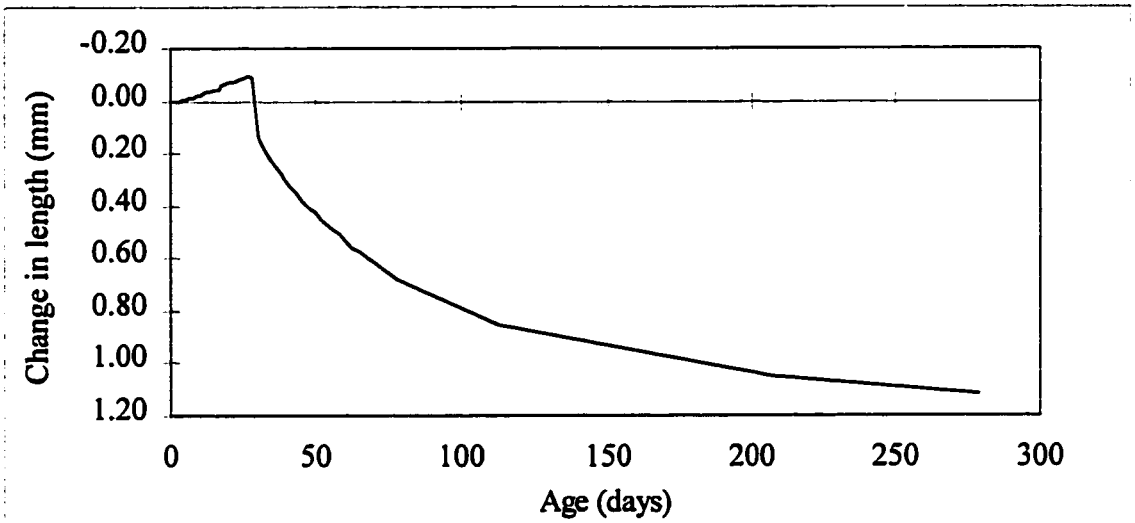

Figure 4.19 Development of change in length for slab 30-2 across main crack (as measured between points 1011)

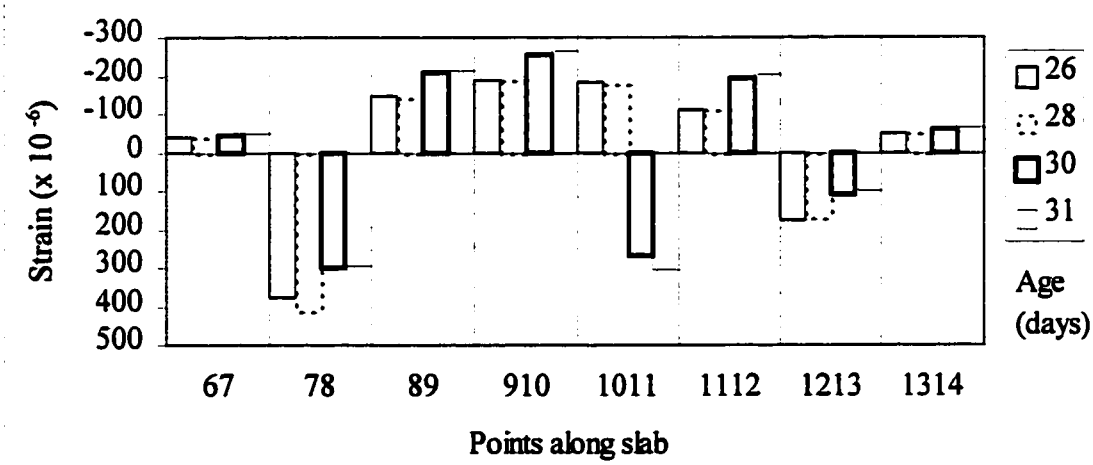

Figure 4.20 Strain development along slab 30-2 near age of main cracking (main crack formed at 30 days)

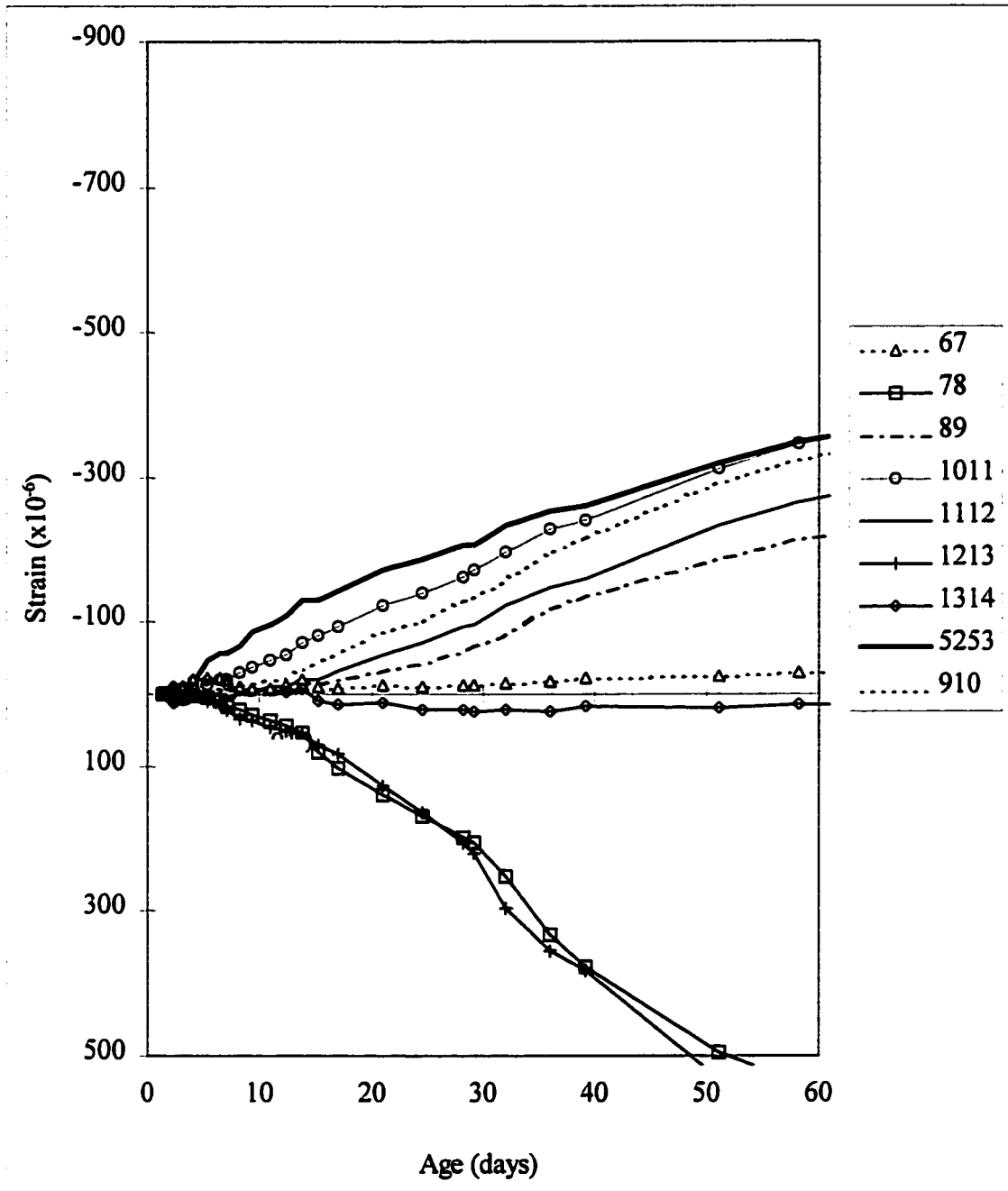

Figure 4.21 Strain development along middle of slab 30-4, to 60 days

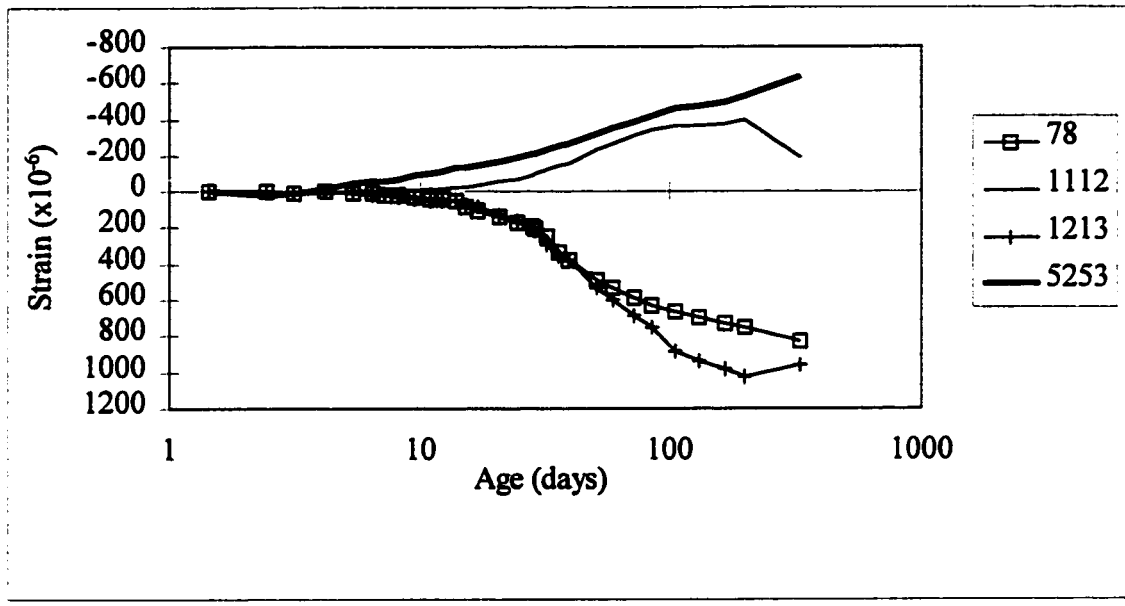

Figure 4.22 Strain development along middle of slab 30-4, to 350 days

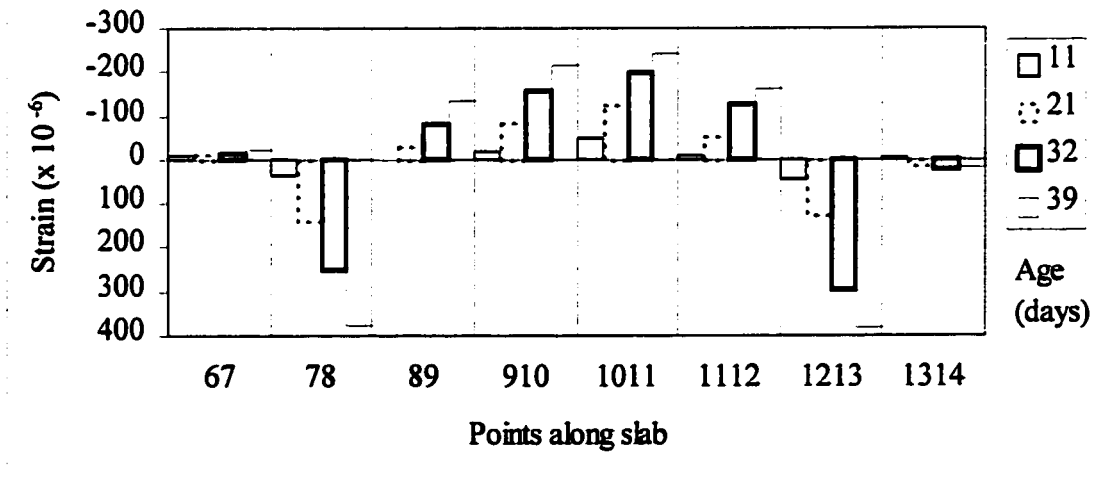

Figure 4.23 Strain development along slab 30-4 between 10 and 40 days

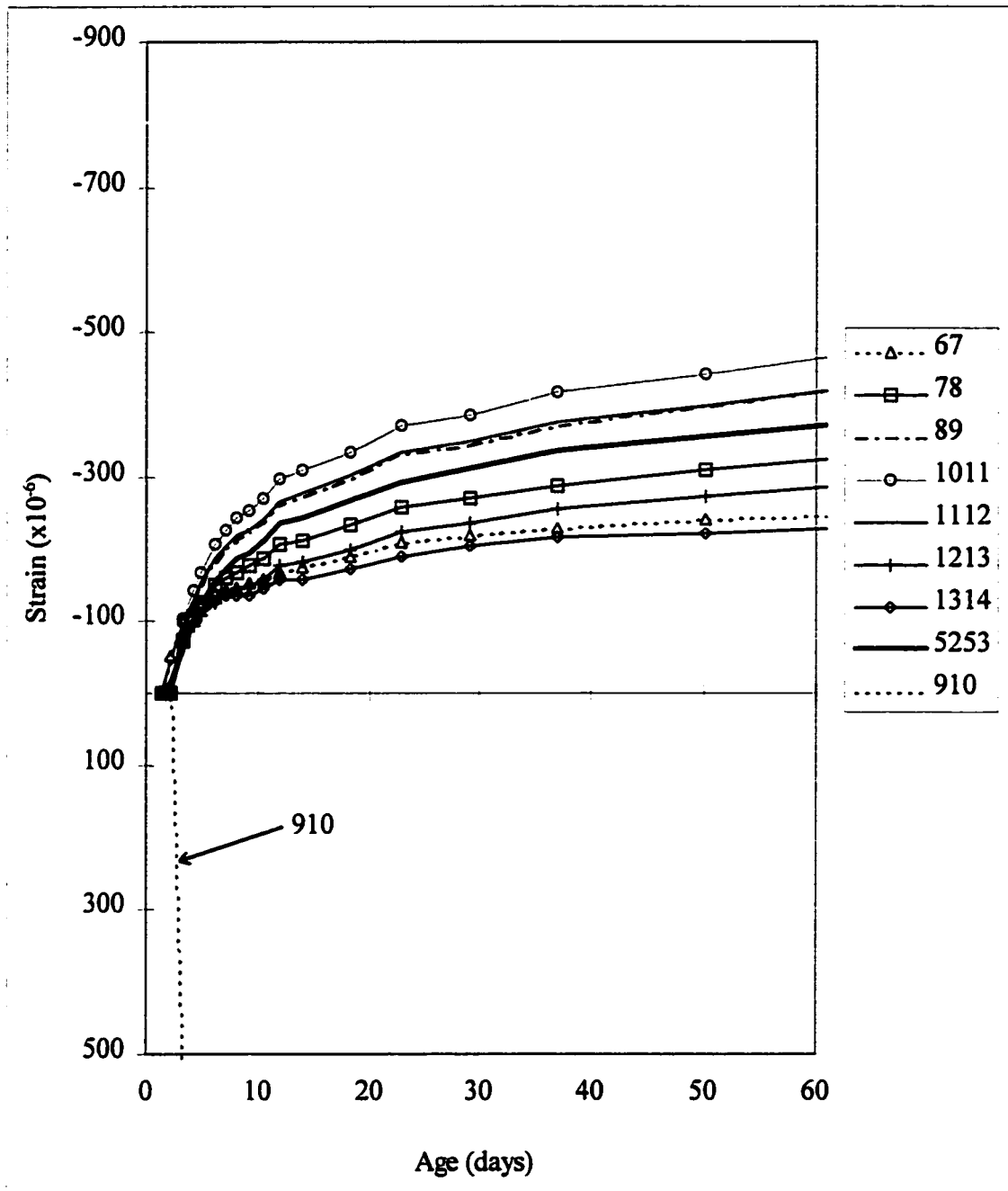

Figure 4.24 Strain development along middle of slab 100-2, to 60 days

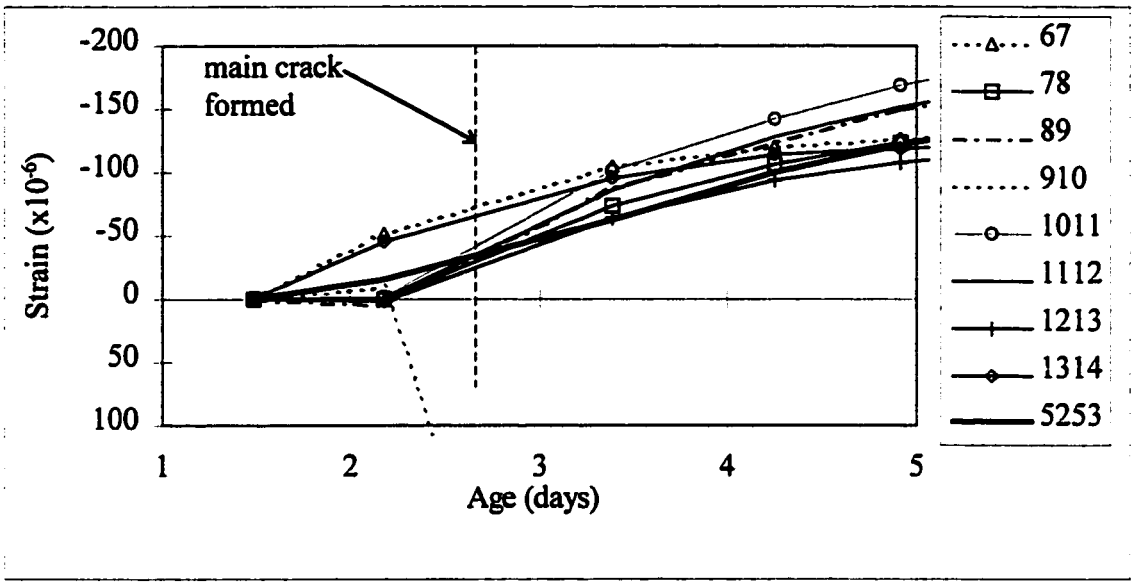

Figure 4.25 Strain development along middle of slab 100-2, to 5 days

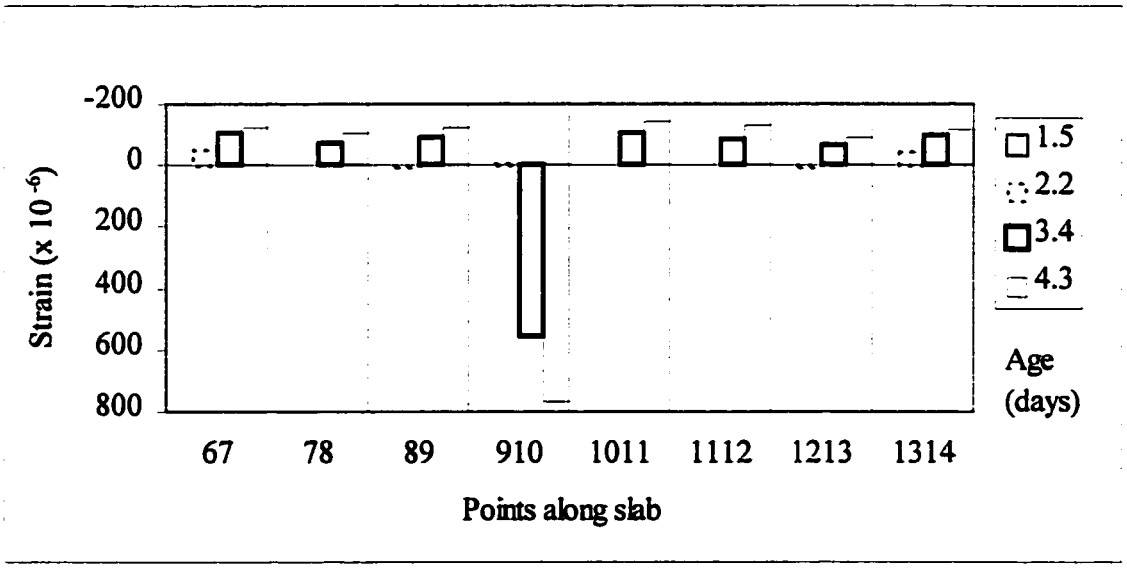

Figure 4.26 Strain development along slab 100-2 between 1 and 5 days

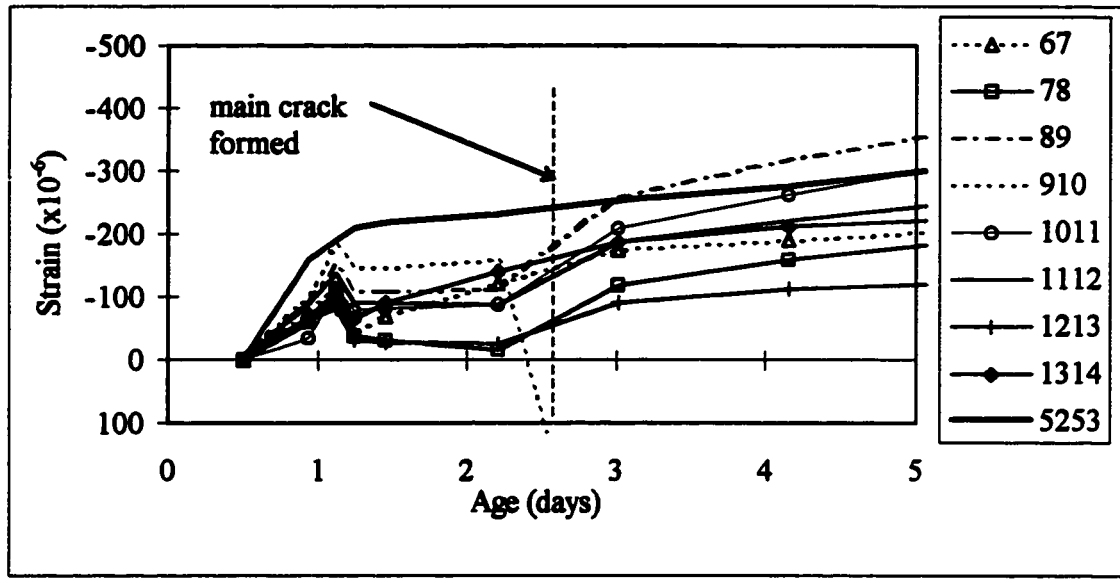

Figure 4.27 Strain development along middle of slab 100-4, to 5 days

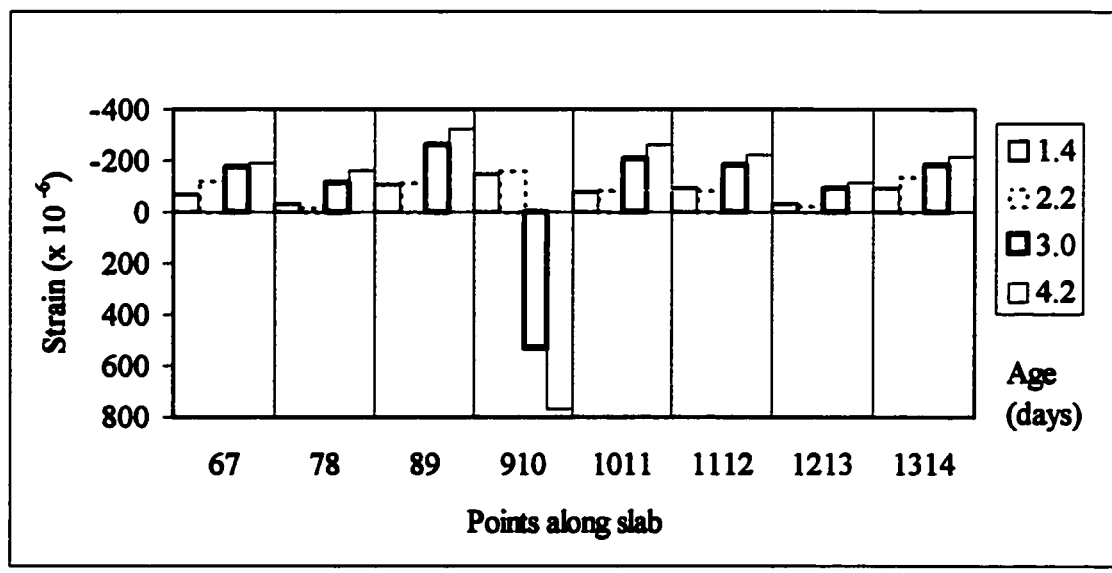

Figure 4.28 Strain development along slab 100-4 between 1 and 5 days

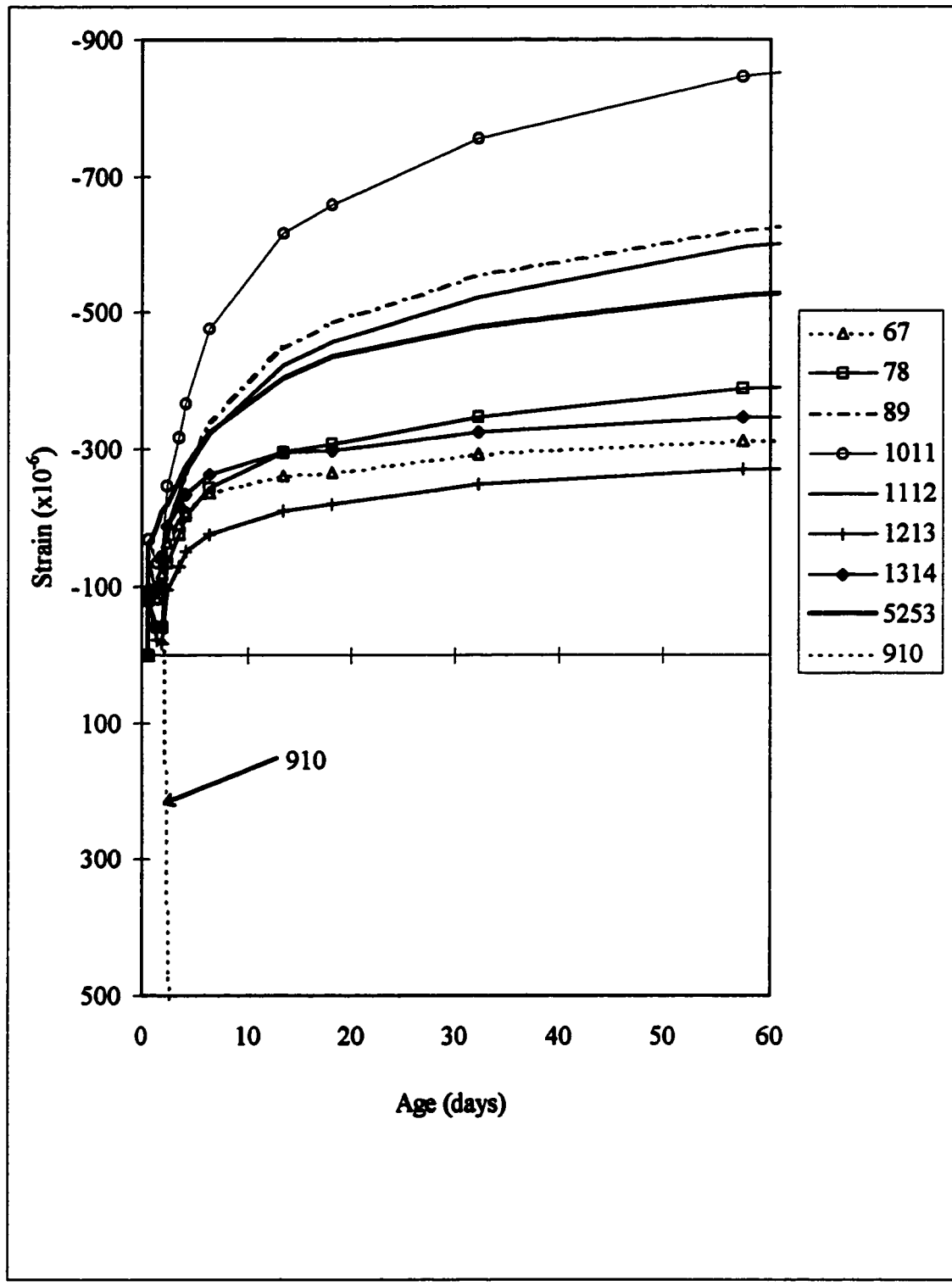

Figure 4.29 Strain development along middle of slab 100-8, to 60 days

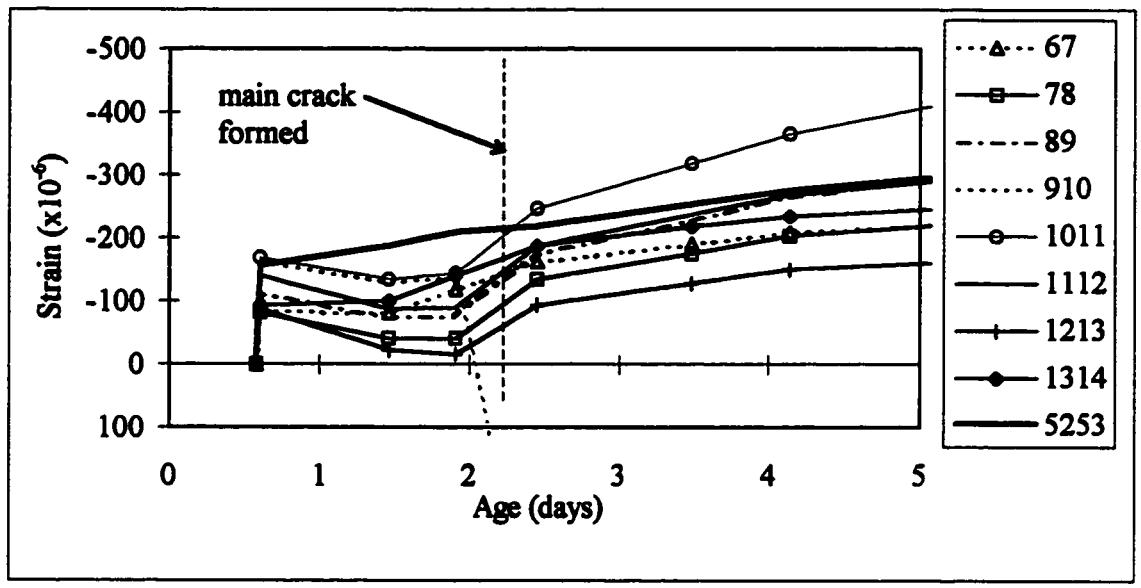

Figure 4.30 Strain development along middle of slab 100-8, to 5 days

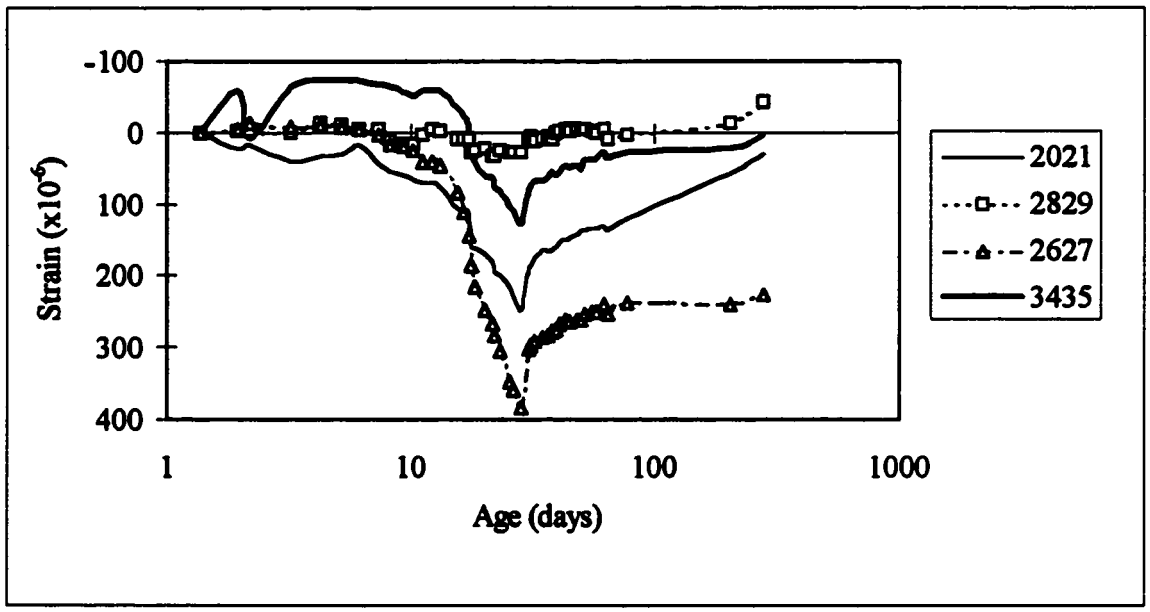

Figure 4.31 Strain measurement of south edge near end blocks: slab 30-2

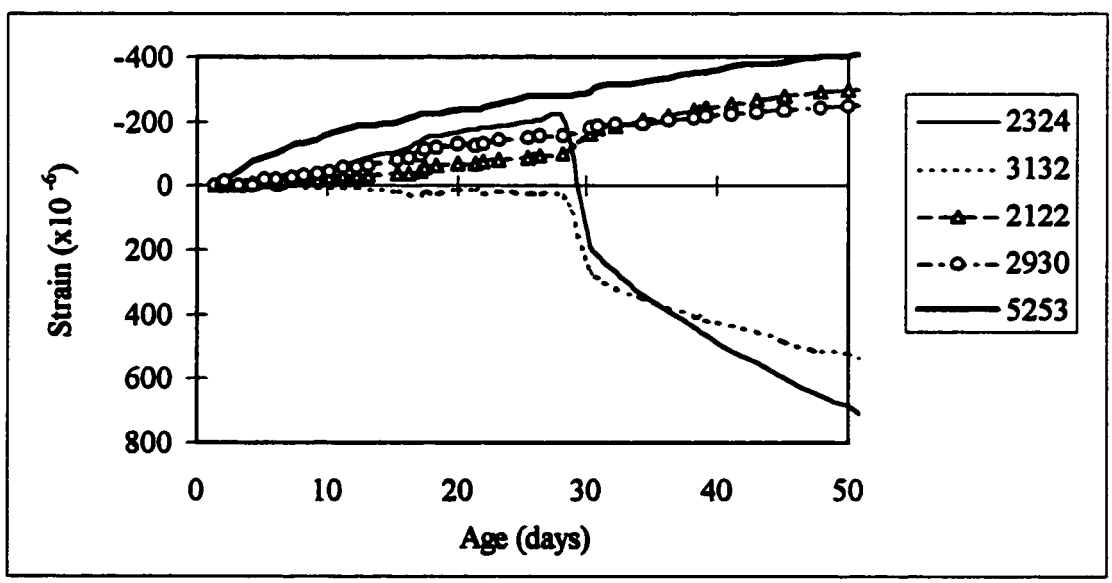

Figure 4.32 Strain development along edge of slab 30-2, up to 50 days

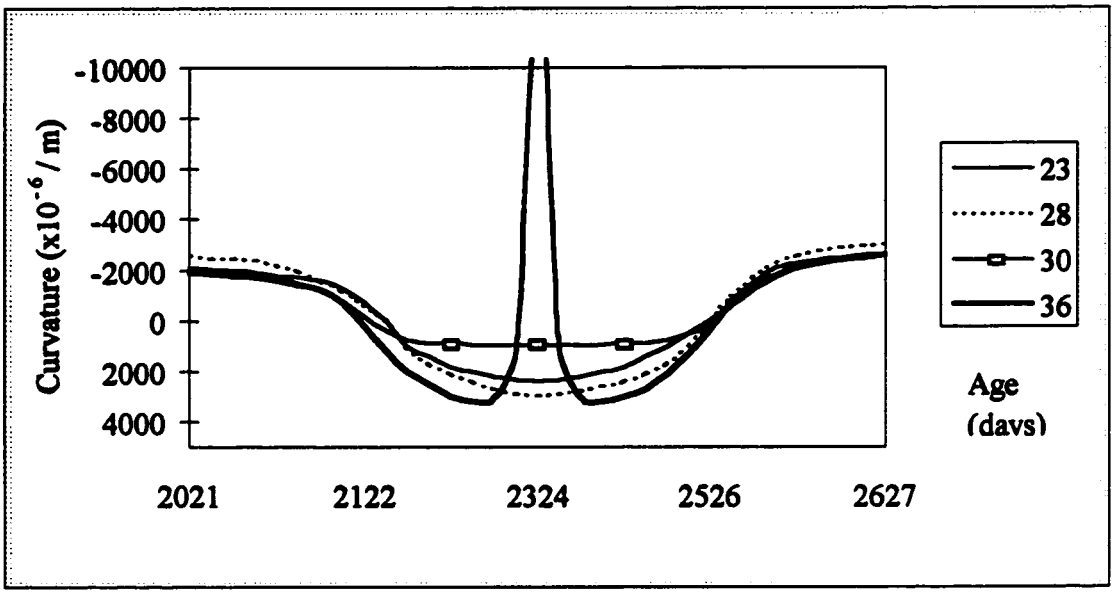

Figure 4.33 Curvature development along slab 30-2
(+ve curvature is concave upwards)

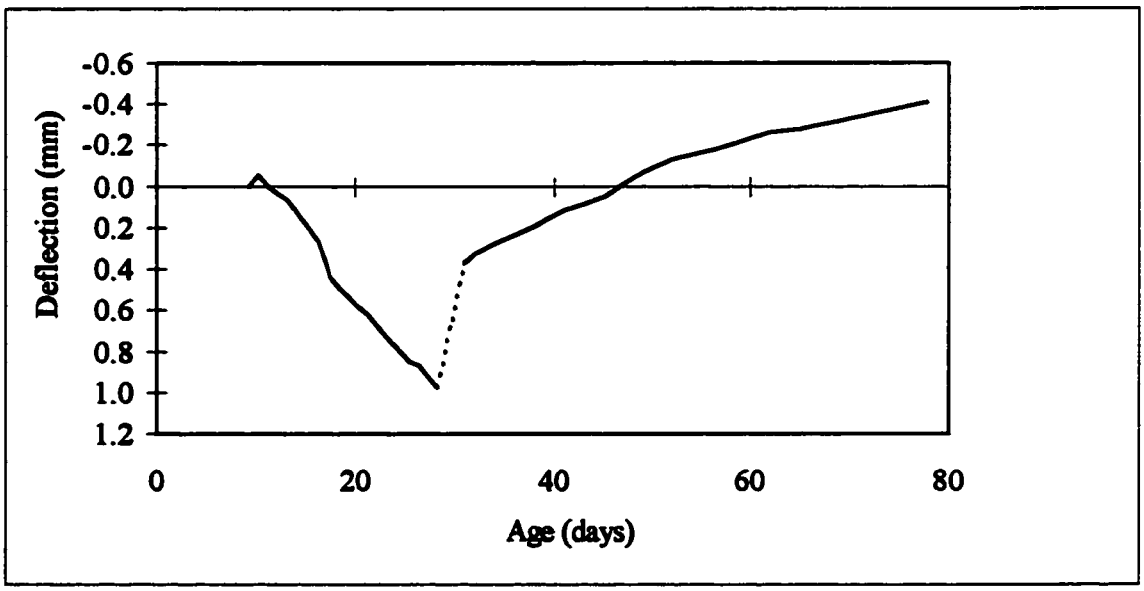

Figure 4.34 Deflection at middle of slab 30-2 as measured by dial gauge 3
(+ ve deflection is downwards)

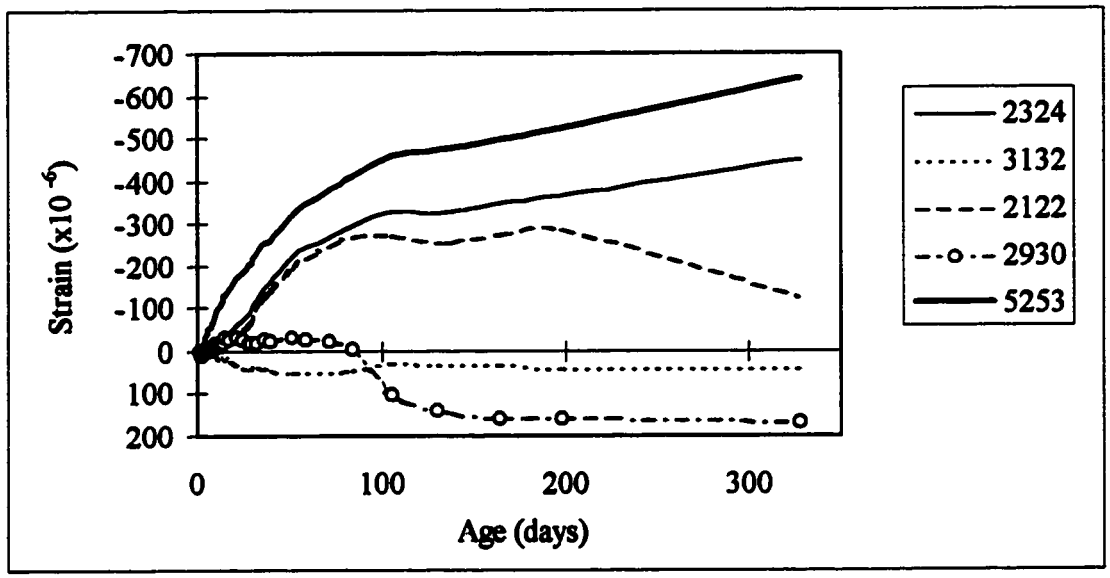

Figure 4.35 Strain development along edge of slab 30-4

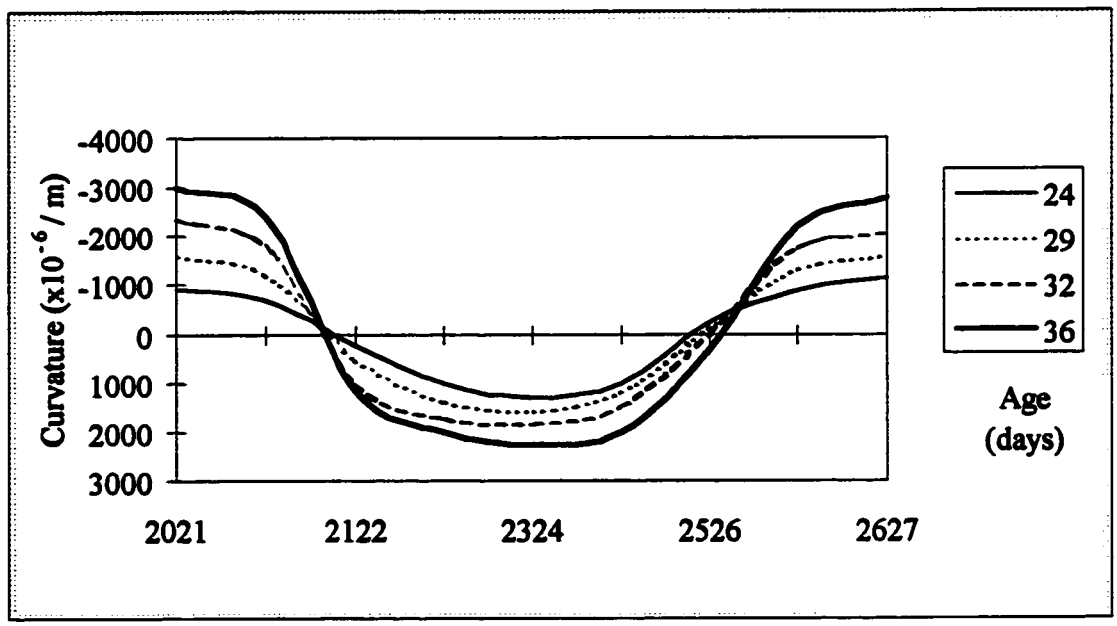

Figure 4.36 Curvature development along slab 30-4
(+ve curvature is concave upwards)

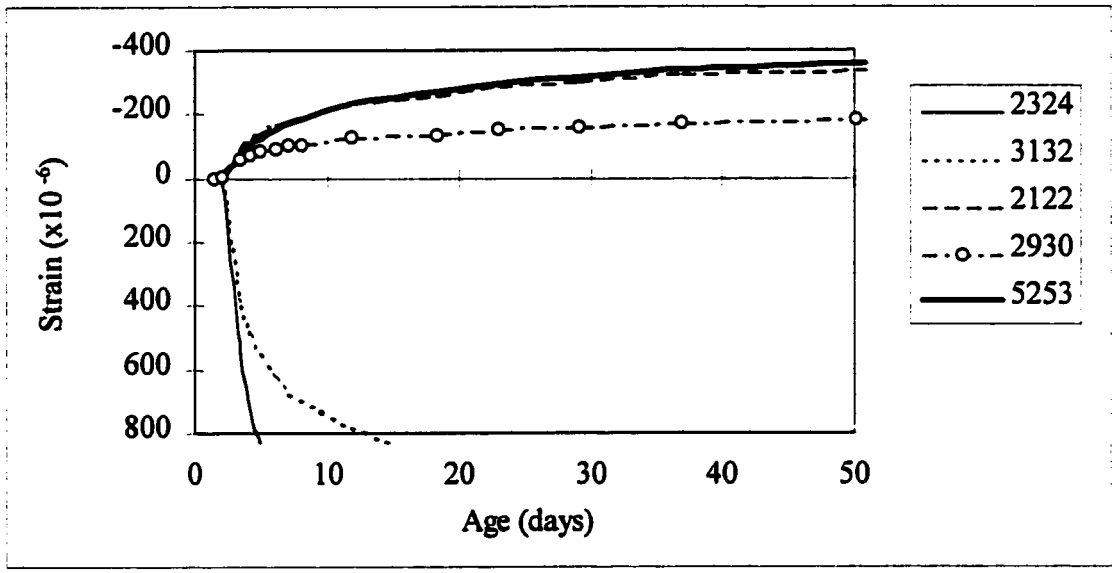

Figure 4.37 Strain development along edge of slab 100-2, up to 50 days

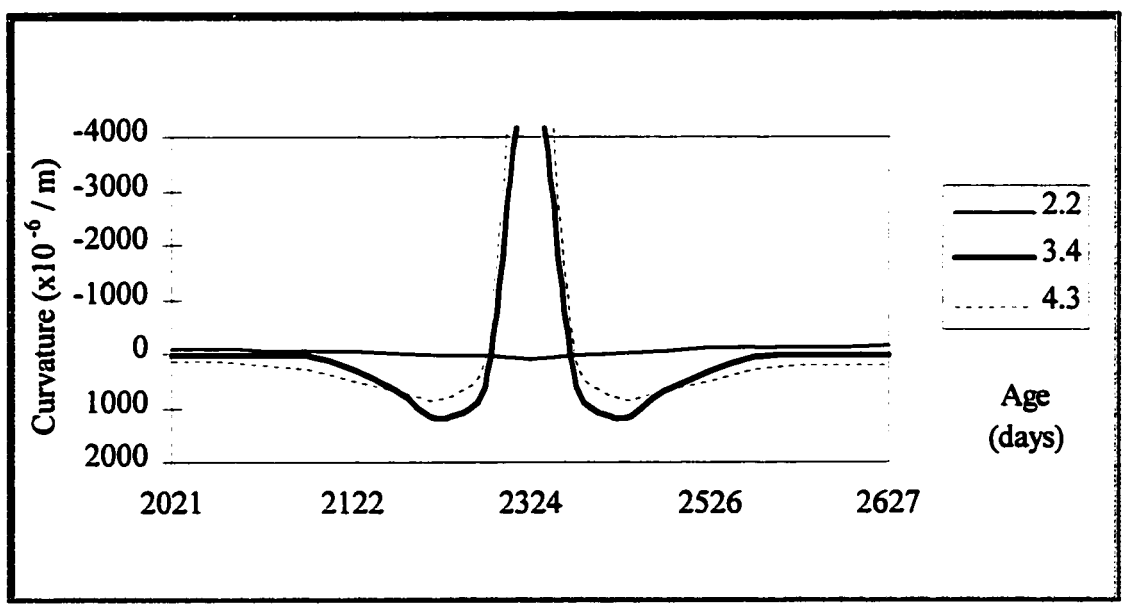

Figure 4.38 Curvature development along slab 100-2
(+ve curvature is concave upwards)

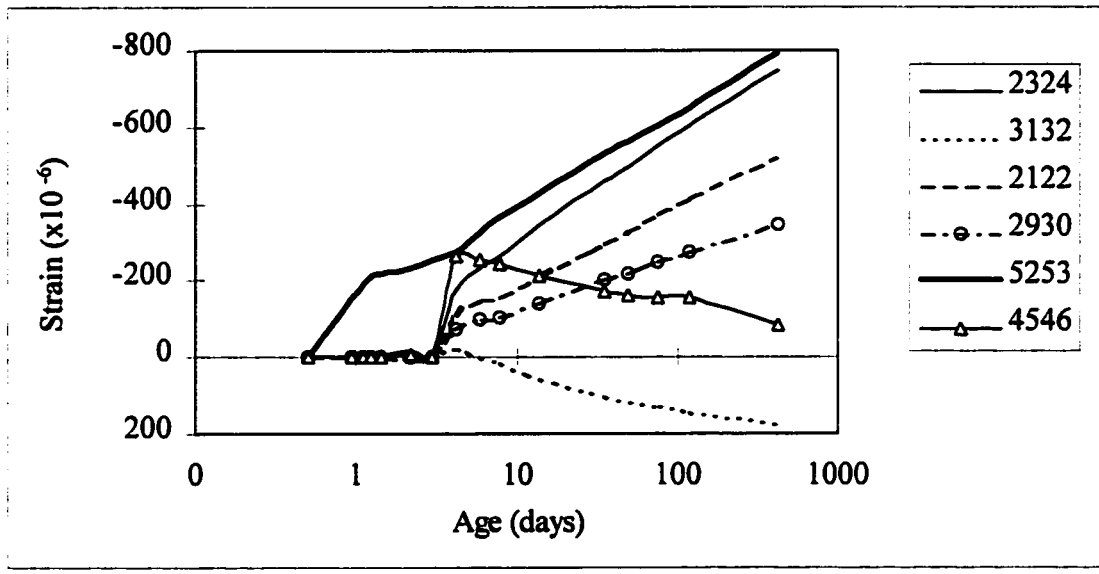

Figure 4.39 Strain development along edge of slab 100-4

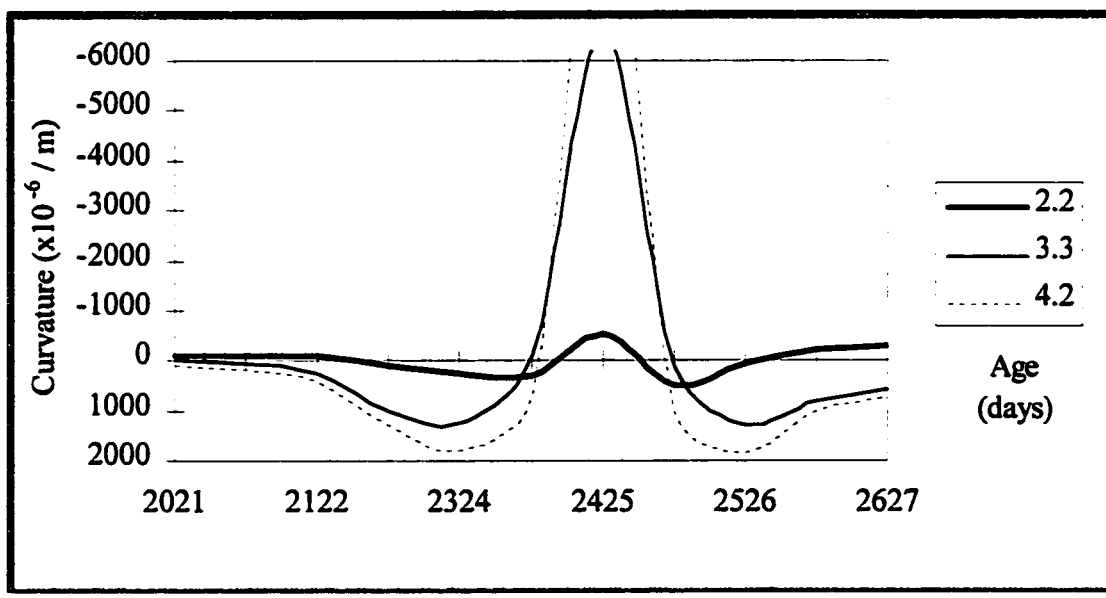

Figure 4.40 Curvature development along slab 100-4
(+ve curvature is concave upwards)

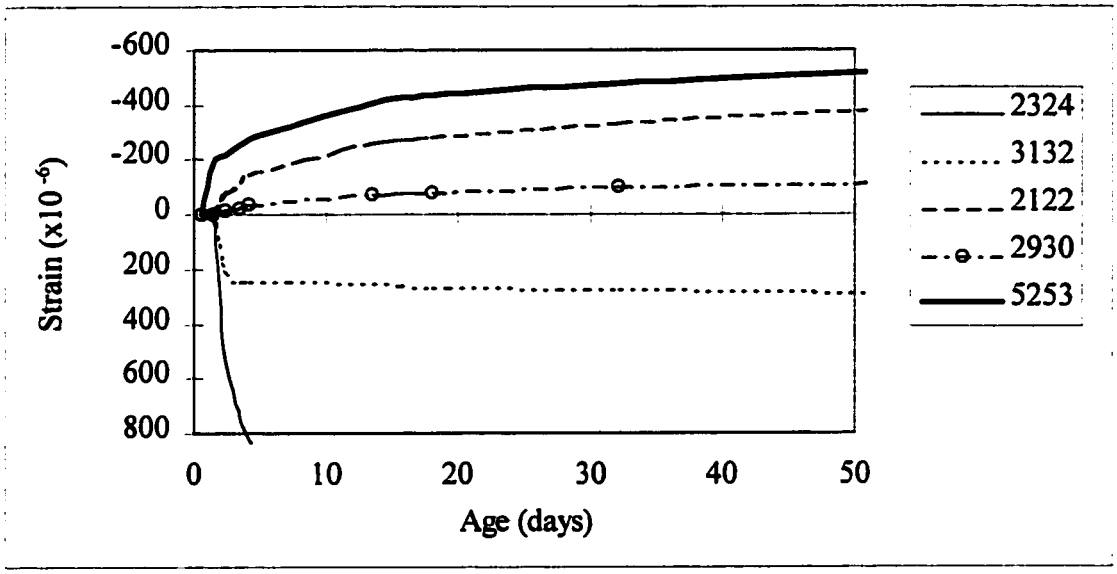

Figure 4.41 Strain development along edge of slab 100-8, up to 50 days

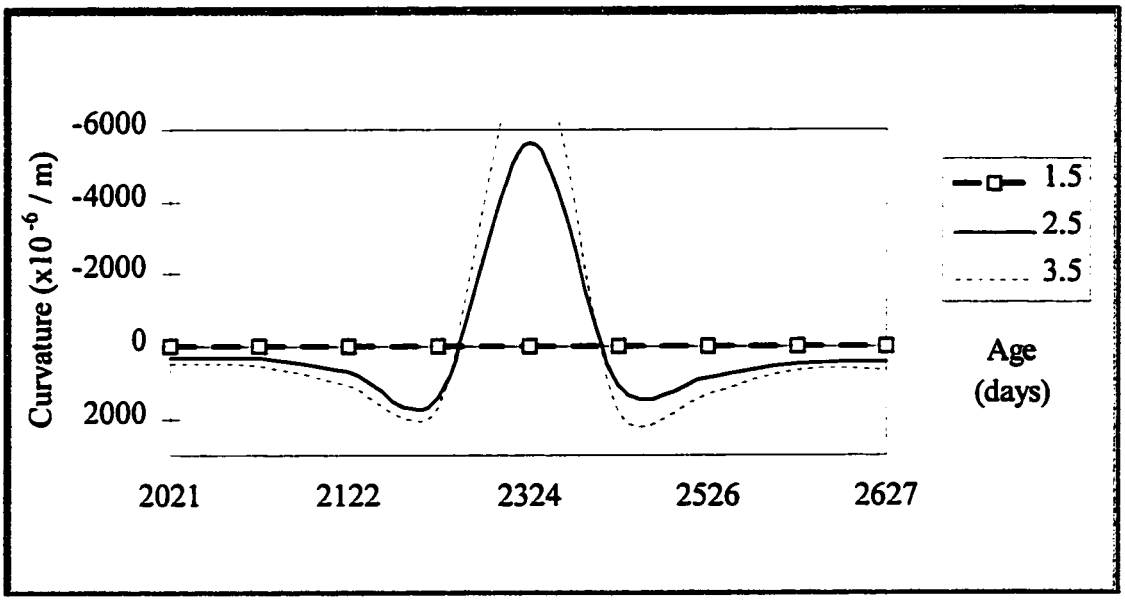

Figure 4.42 Curvature development along slab 100-8
(+ve curvature is concave upwards)

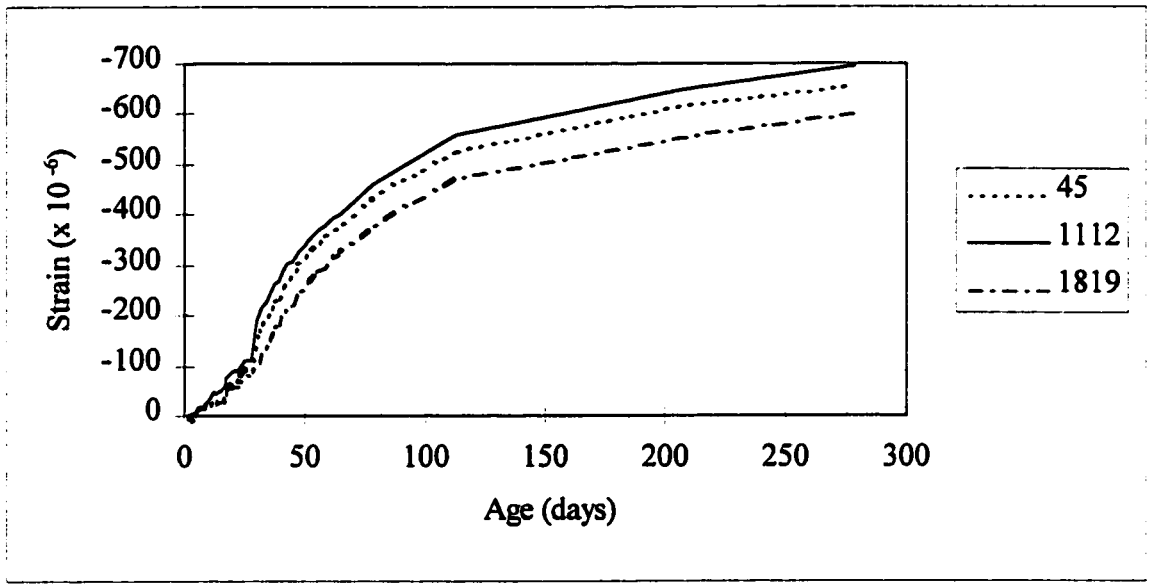

Figure 4.43 Shrinkage strain variation between centre and edge for slab 30-2

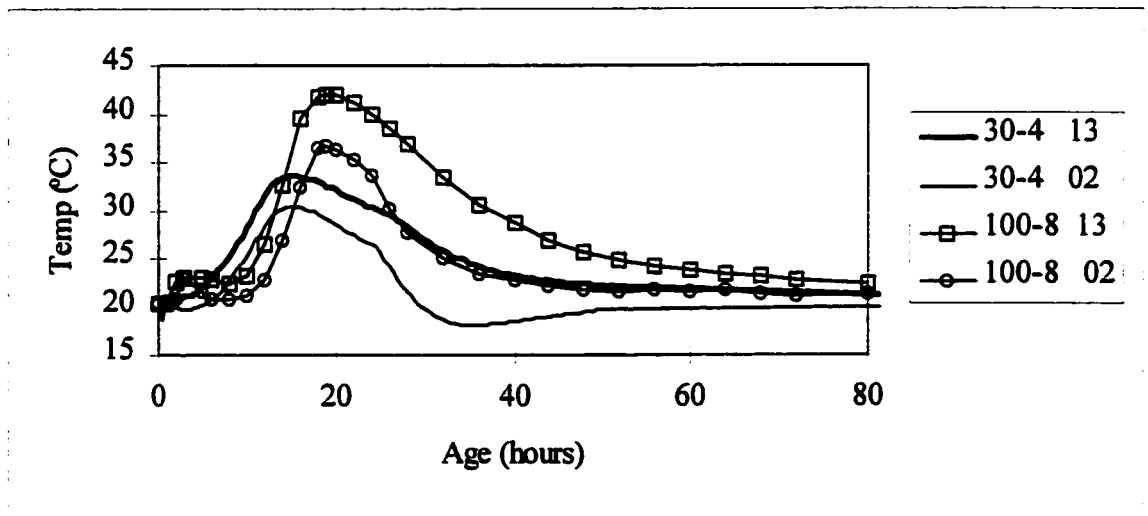

Figure 4.44 Temperature development during hydration and subsequent cooling (Legend: Slab, Thermocouple No.)

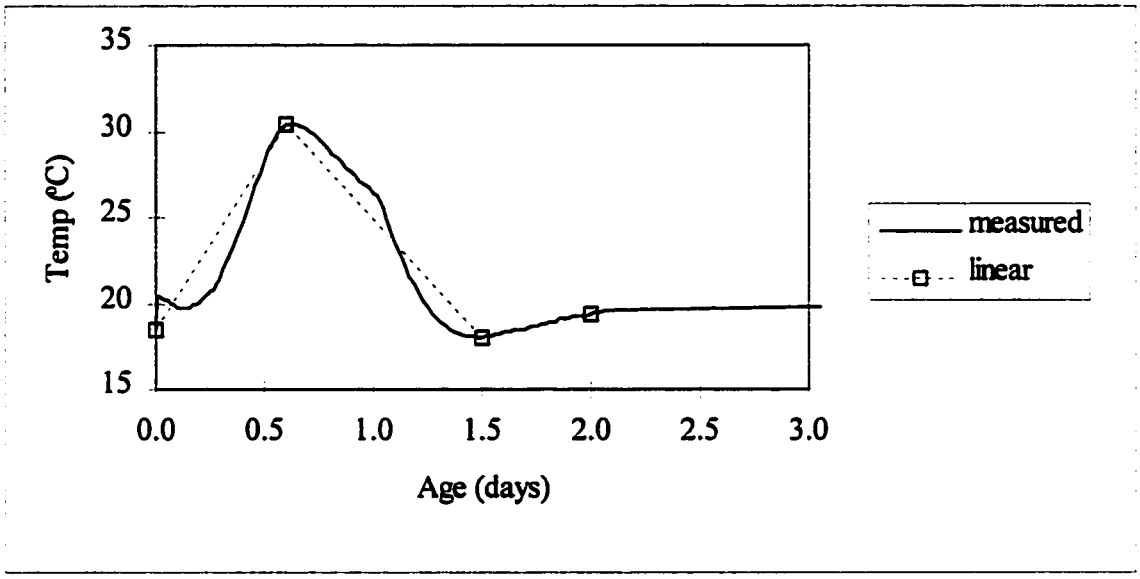

Figure 4.45 Slab 30-4: division of temperature development into linear intervals for time step analysis

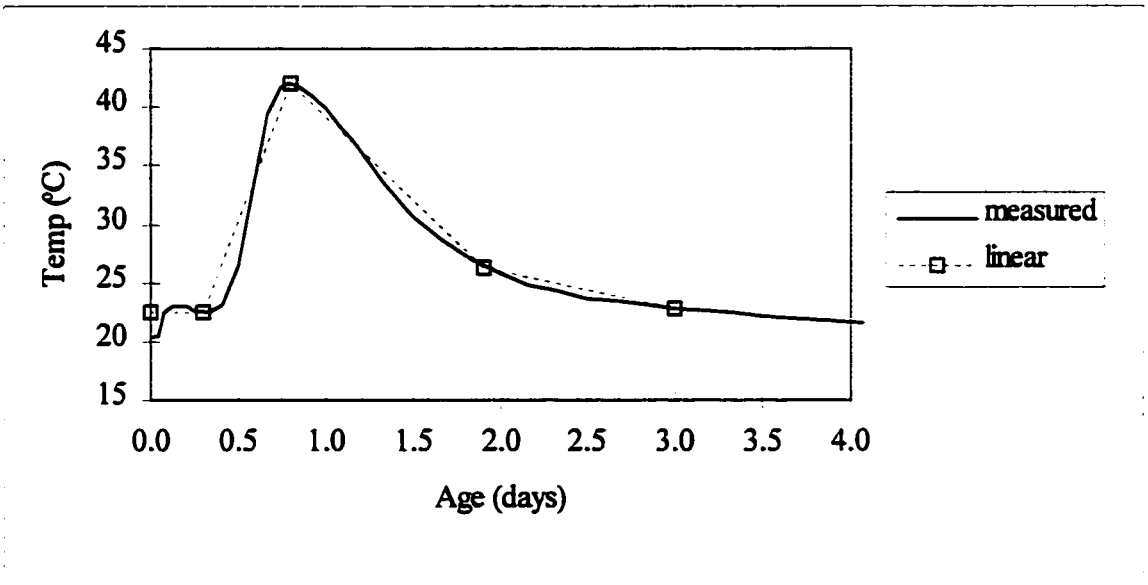

Figure 4.46 Slab 100-8: division of temperature development into linear intervals for time step analysis

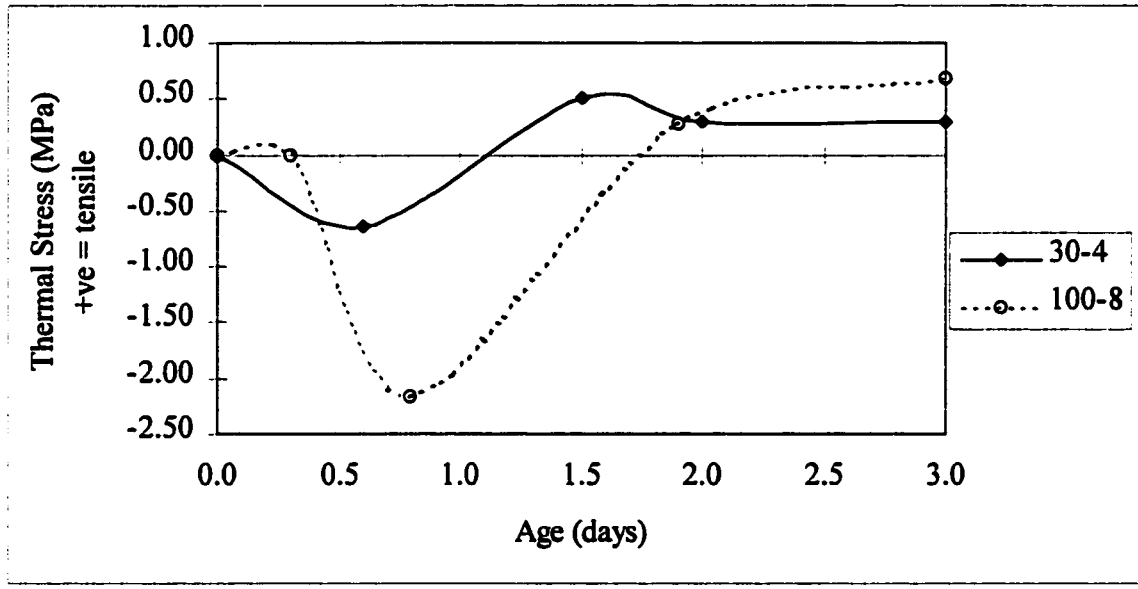

Figure 4.47 Predicted development of thermal stress in slabs 30-4 and 100-8 (using measured temperature development)

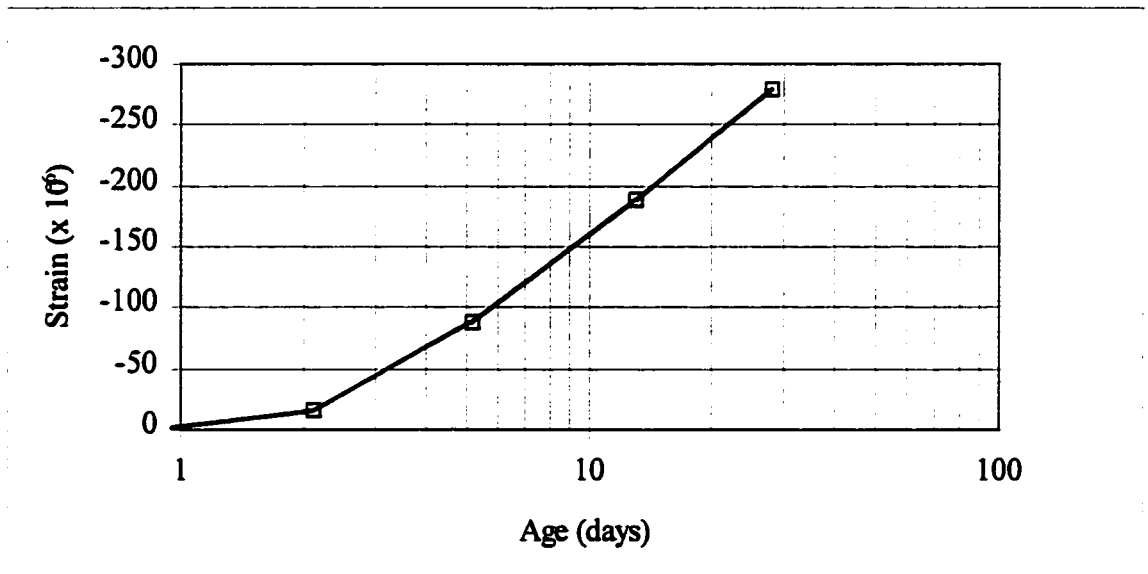

Figure 4.48 Slab 30-4: division of shrinkage development into linear intervals for time step analysis

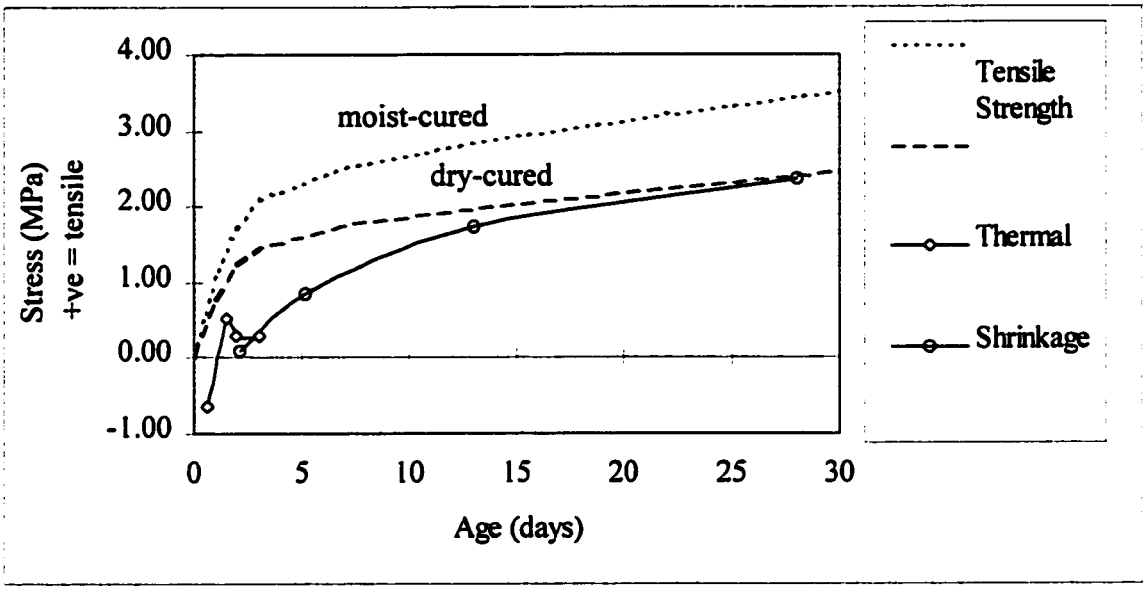

Figure 4.49 Predicted development of thermal and shrinkage stress, and tensile strength in NSC slabs 30-2, and 30-4

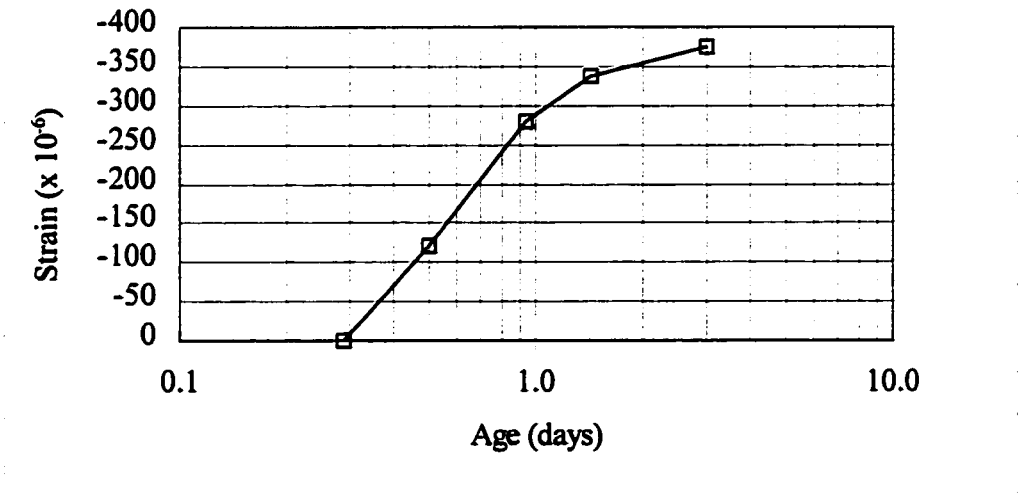

Figure 4.50 Slab 100-4: division of shrinkage development into linear intervals for time step analysis

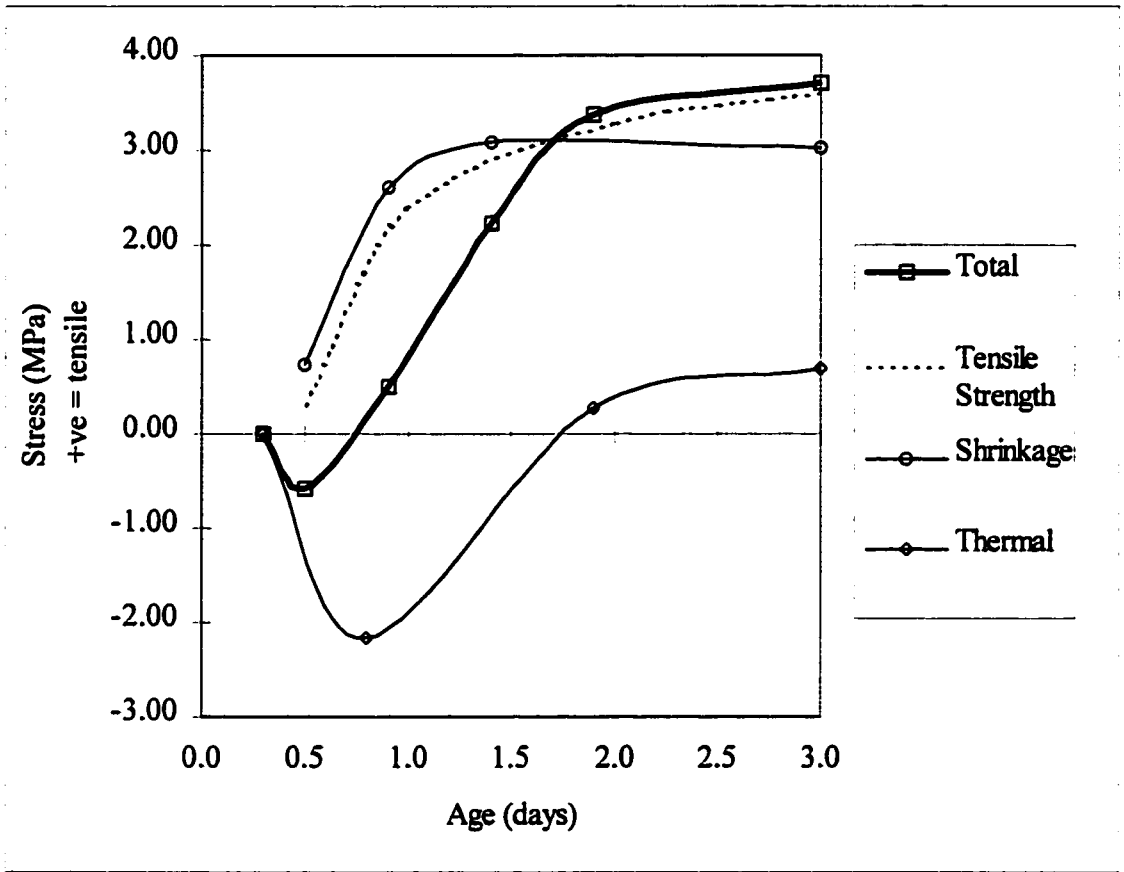

Figure 4.51 Predicted development of thermal, shrinkage, total stress, and tensile strength in HPC slabs 100-4, 100-8

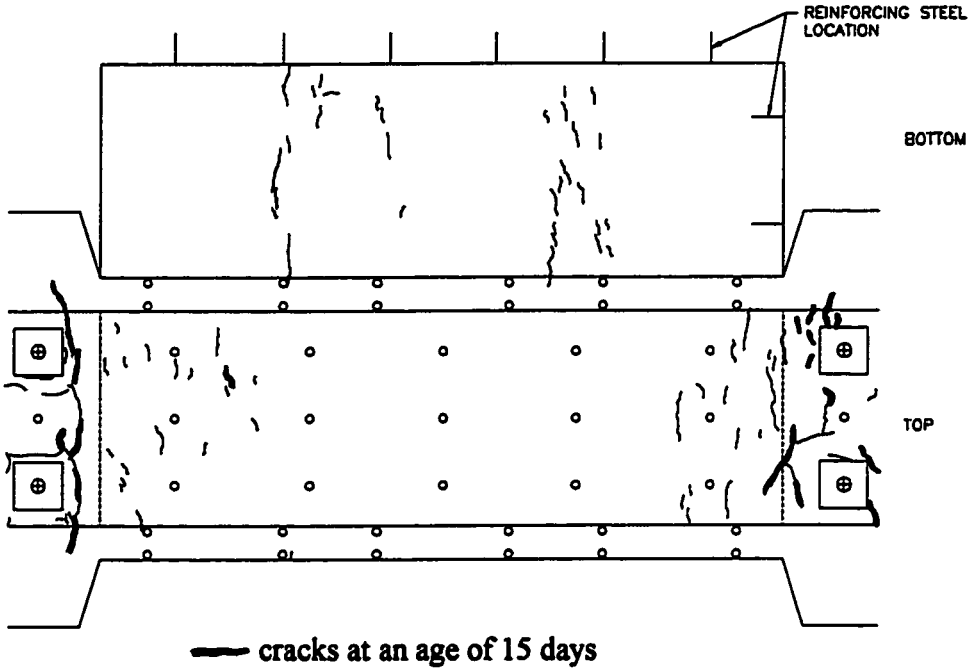

Figure 4.52 Crack pattern for slab 30-2 at an age of 25 days

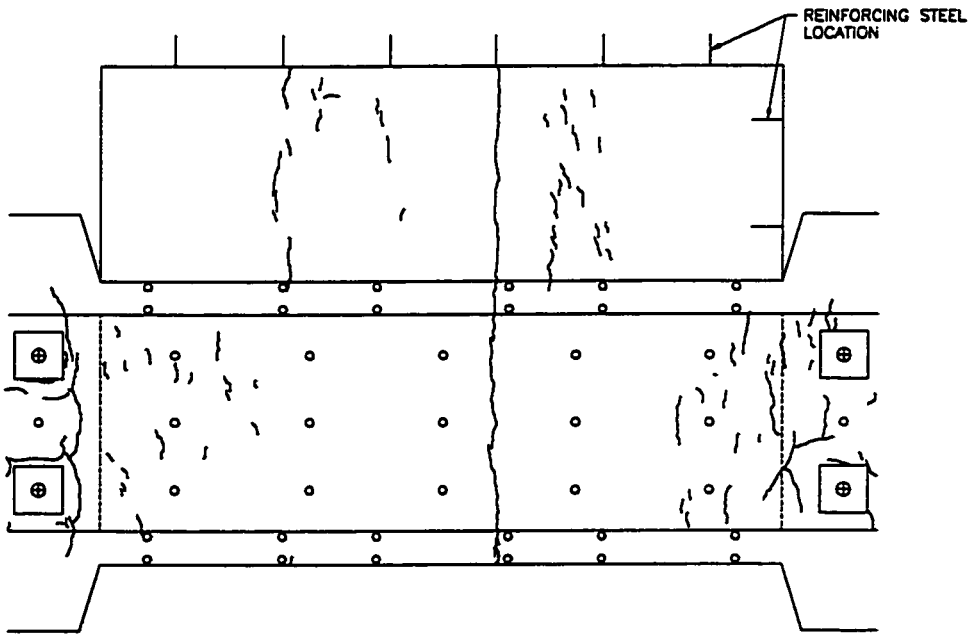

Figure 4.53 Crack pattern for slab 30-2 at an age of 30 days

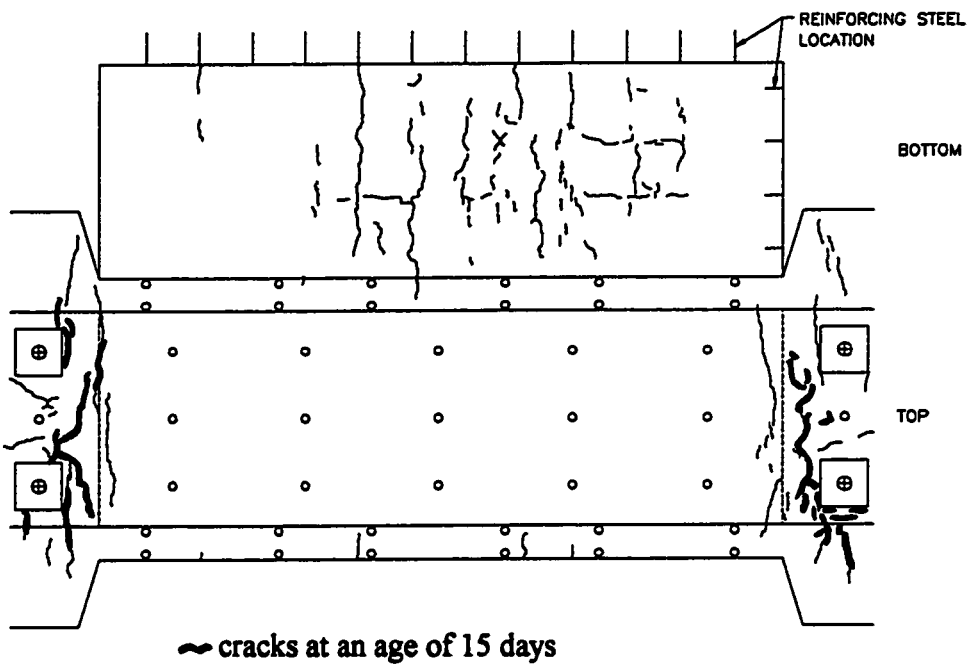

Figure 4.54 Crack pattern for slab 30-4 at an age of 35 days

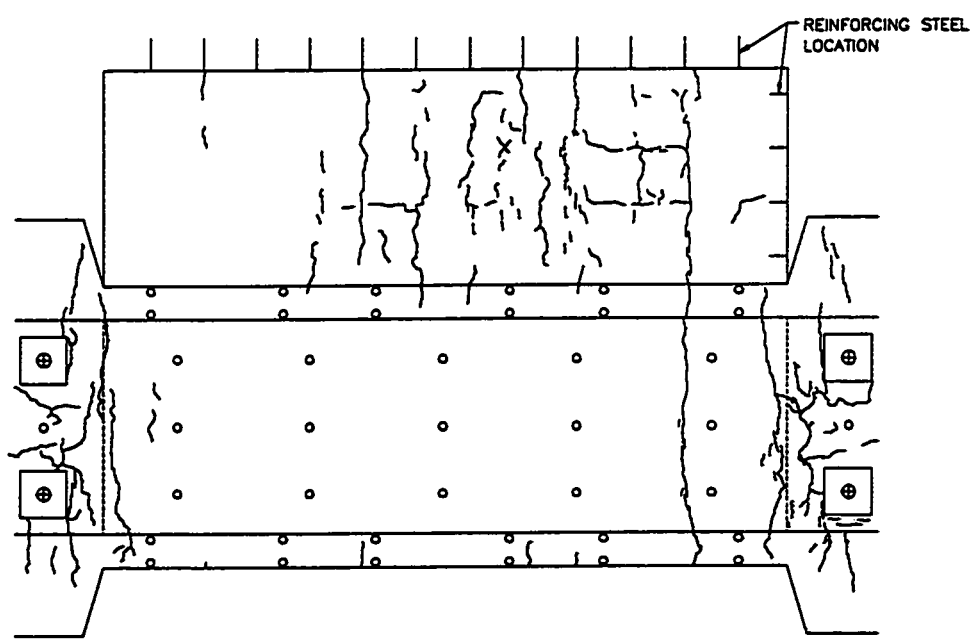

Figure 4.55 Crack pattern for slab 30-4 at an age of 300 days

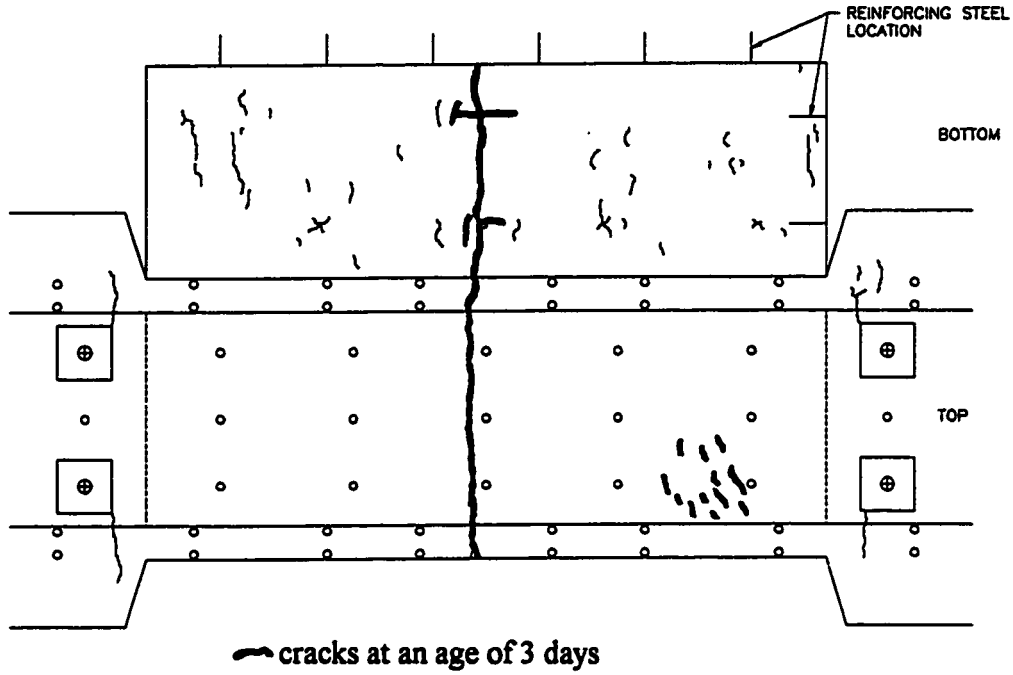

Figure 4.56 Crack pattern for slab 100-2 at an age of 5 days

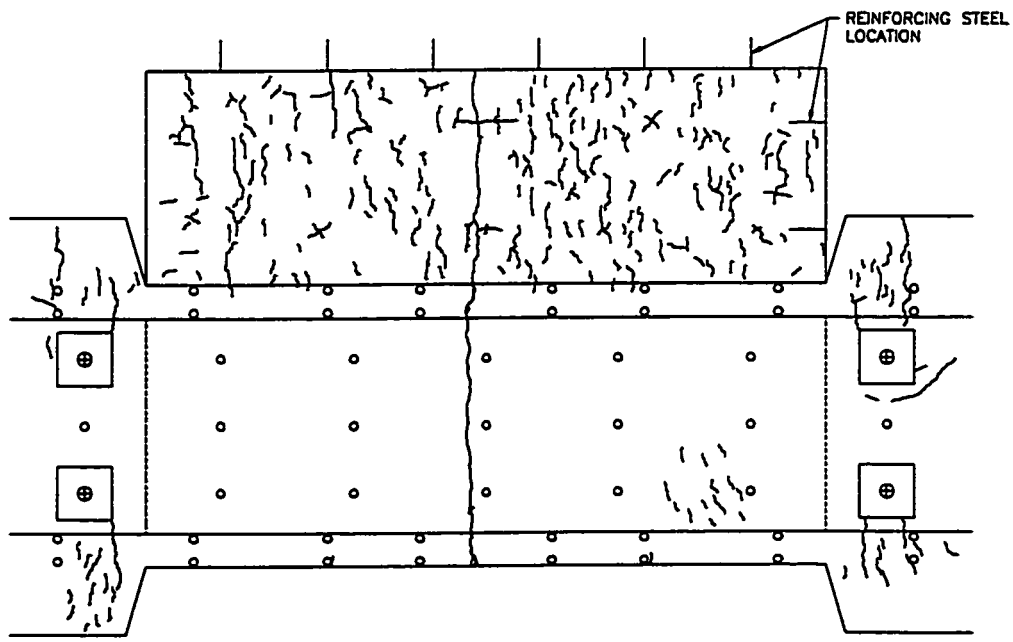

Figure 4.57 Crack pattern for slab 100-2 at an age of 500 days

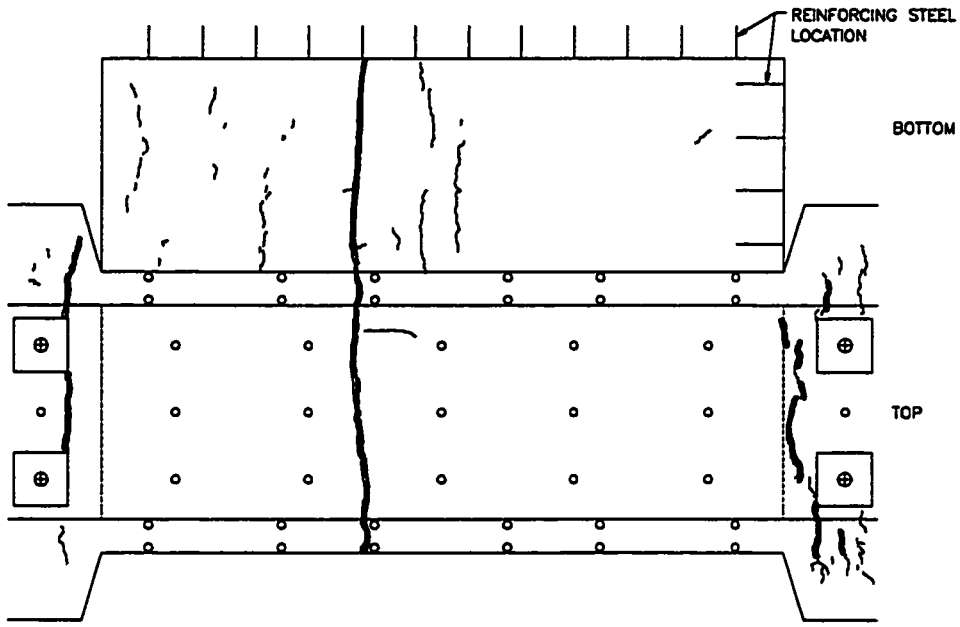

Figure 4.58 Crack pattern for slab 100-4 at an age of 5 days

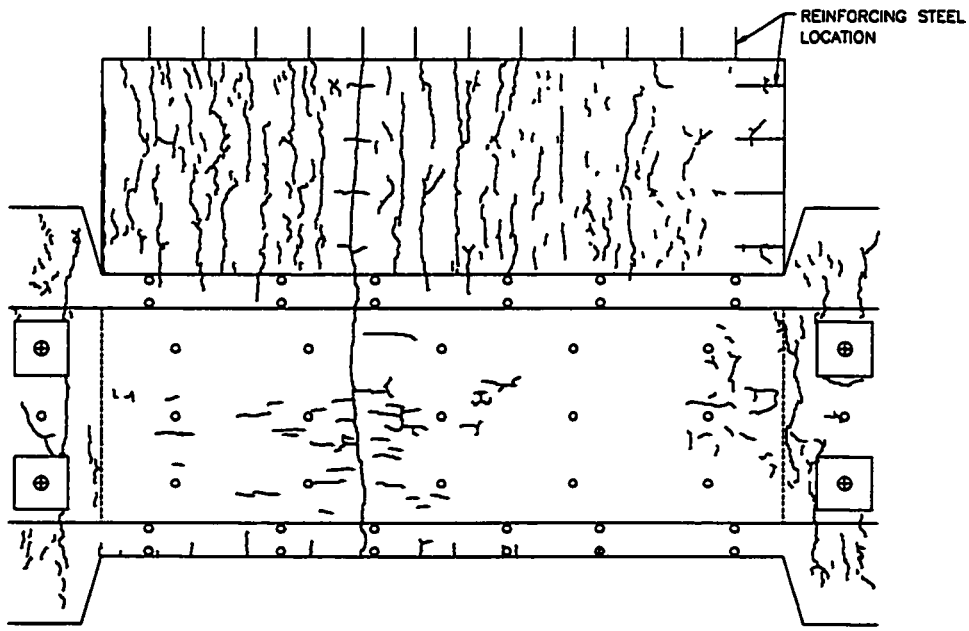

Figure 4.59 Crack pattern for slab 100-4 at an age of 450 days

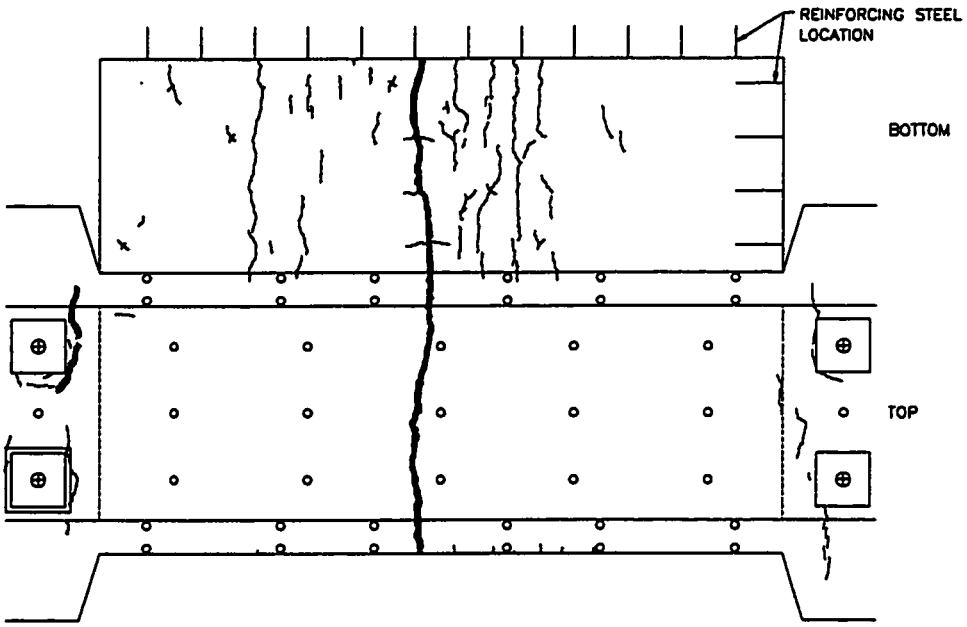

Figure 4.60 Crack pattern for slab 100-8 at an age of 9 days

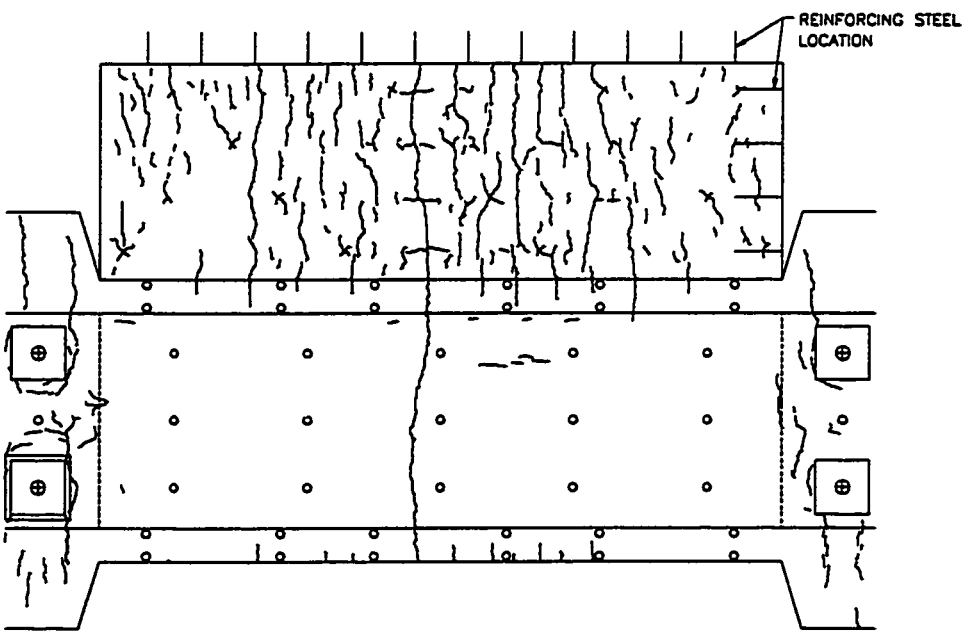

Figure 4.61 Crack pattern for slab 100-8 at an age of 450 days

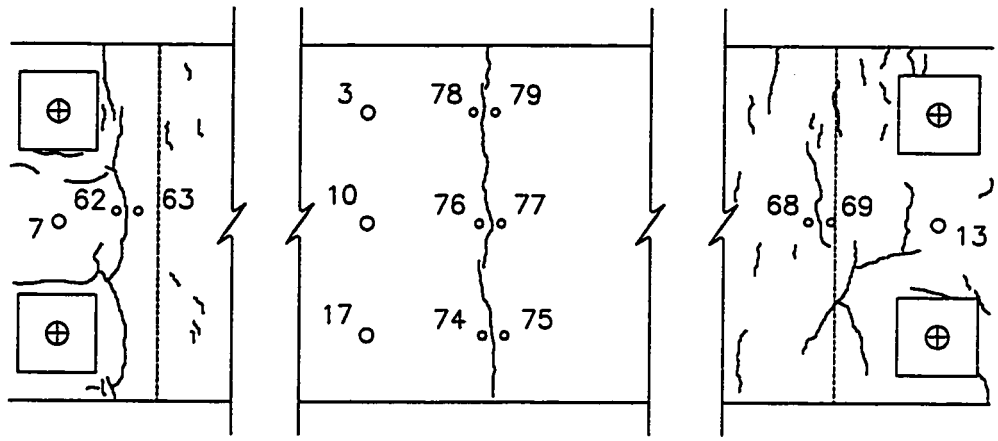

Figure 4.62 Locations of crack measurements: slab 30-2

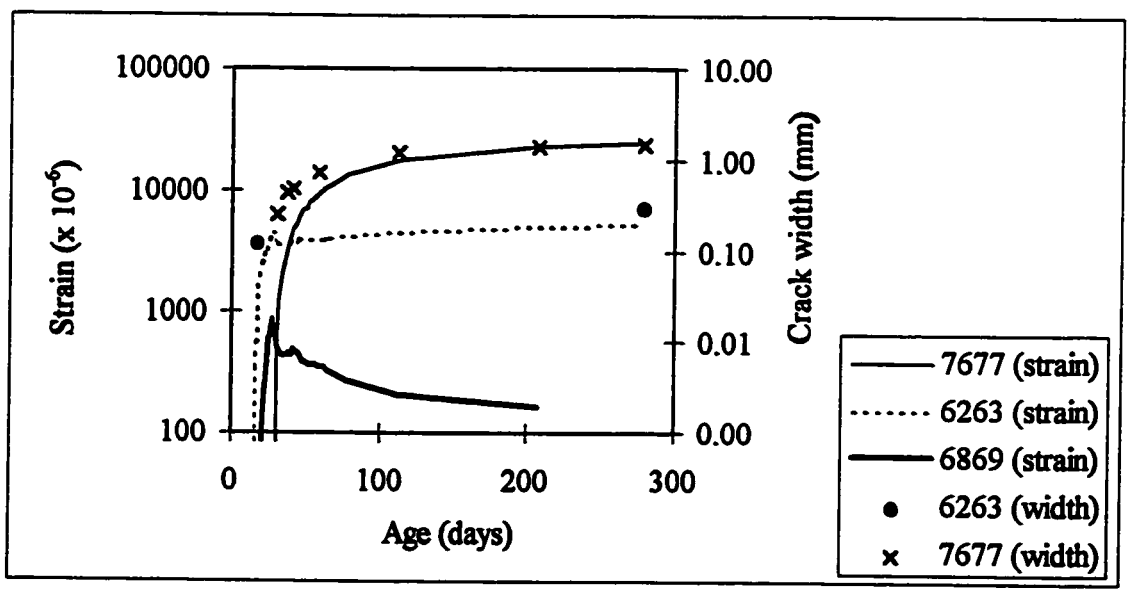

Figure 4.63 Crack development: slab 30-2

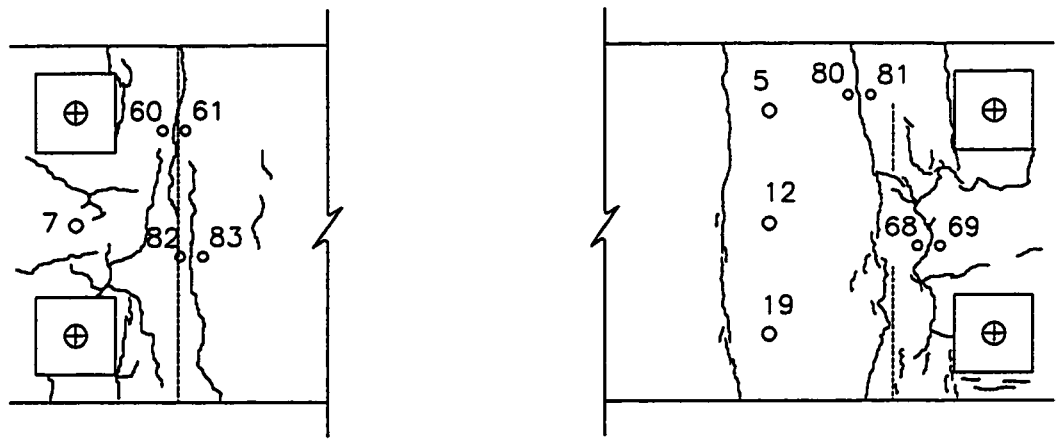

Figure 4.64 Locations of crack measurements: slab 30-4

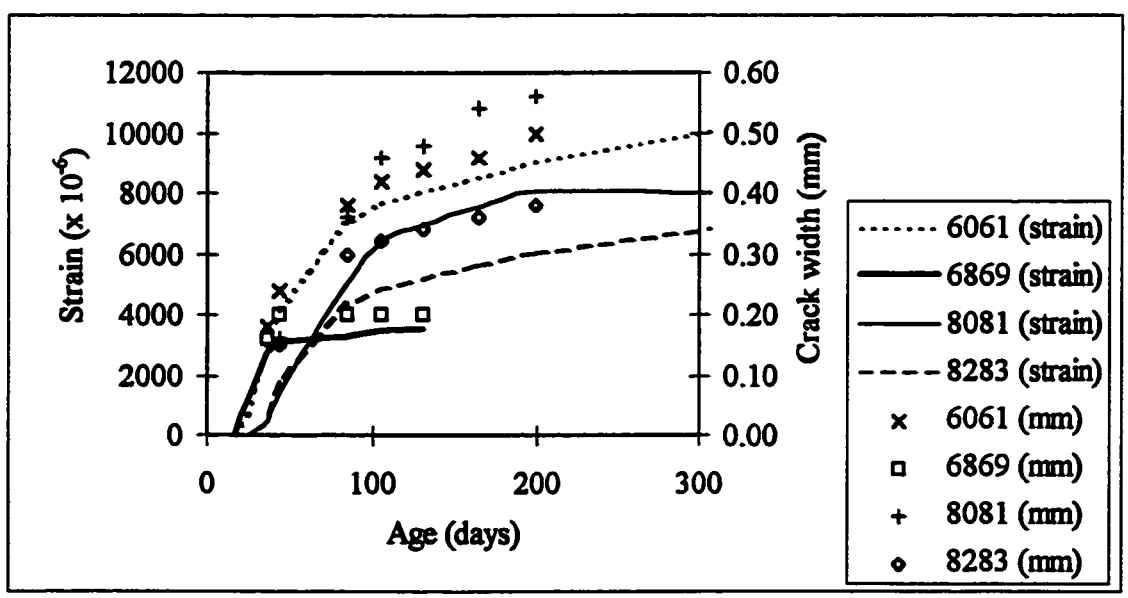

Figure 4.65 Crack development: slab 30-4

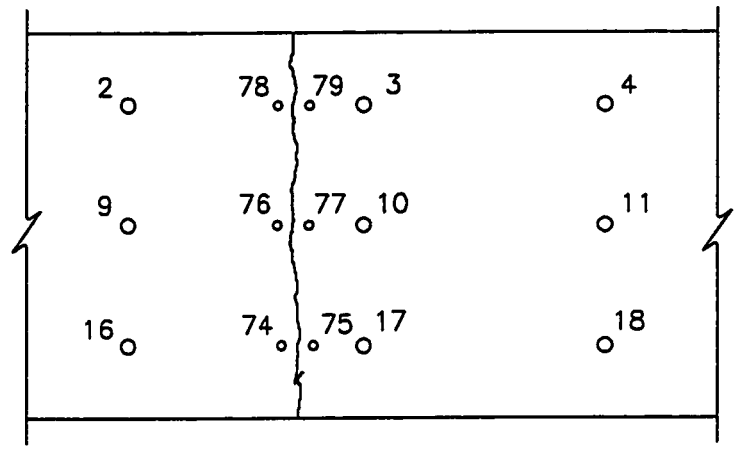

Figure 4.66 Locations of crack measurements: slabs 100-2, 100-4, 100-8

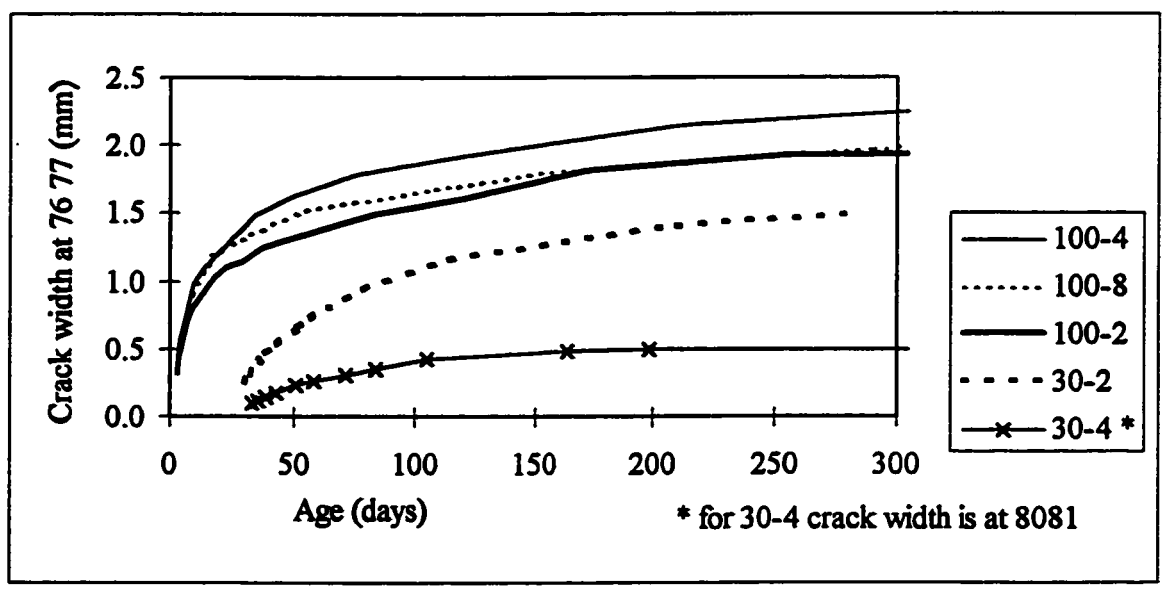

Figure 4.67 Crack development for all slabs

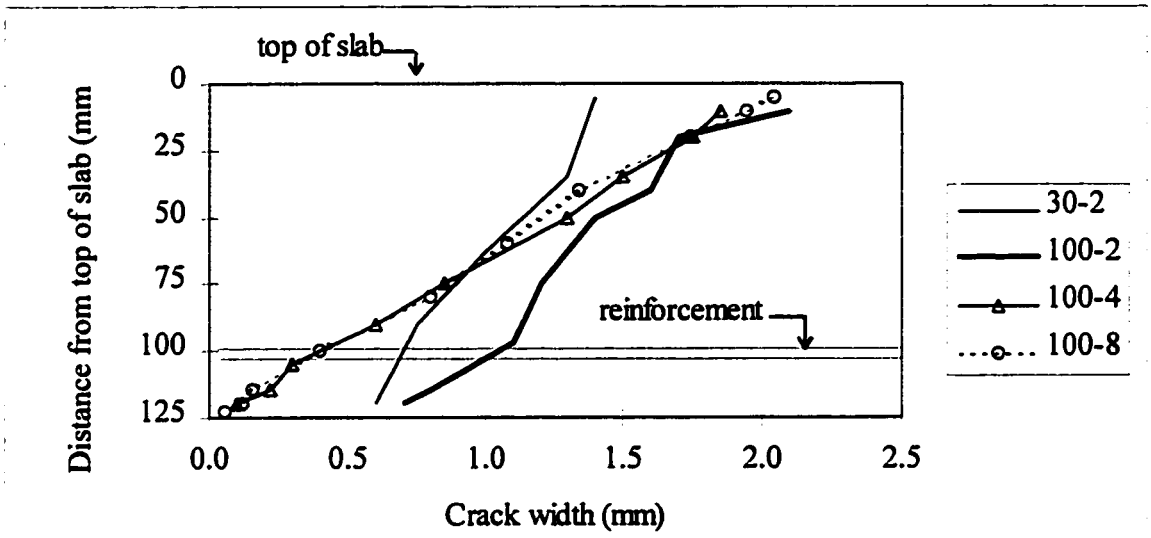

Figure 4.68 Final crack width profile along slab edge, for all slabs

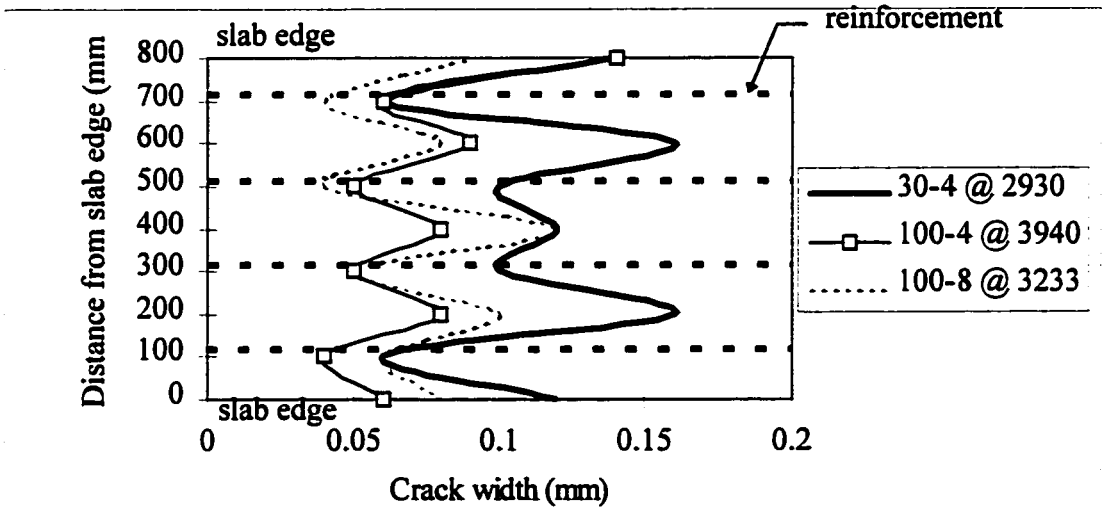

Figure 4.69 Final crack width on underside of slab: slab 30-4, 100-4, 100-8

CHAPTER 5

CONCLUSIONS AND RECOMMENDATIONS

5.1 Summary of principal observations

1. Predicted strength development for both the NSC and the HPC tested was quite accurate. The CEB MC90 model was within 10% for all compressive tests. For tensile tests, CEB results were about 20% low, while ACI 363R-84 methods were 10 to 15% high.

2. HPC developed strength much more rapidly than the NSC. Up to 50% of 28 day tensile strength was reached in 24 hours, compared with 30% for the NSC.

3. The HPC had a very high rate of early shrinkage: up to -200 x 10^{-6} strain within 30 hours after casting. The NSC reached -200 x 10^{-6} strain only after 15 days.

4. Long term free shrinkage, at an age of 400 days, was -800 x 10^{-6} for the HSC, and -700 x 10^{-6} for the NSC.

5. The HPC underwent significant basic shrinkage, as measured on the sealed surface of the free specimens: nearly -100 x 10^{-6} within 3 days.

6. Prediction of free shrinkage by the CEB MC90 and ACI 209 methods was unsatisfactory. The CEB method greatly underestimated and the ACI method greatly overestimated shrinkage. The extremely low humidity in the laboratory, outside the range of validity for both models, may explain the CEB's low predictions.

7. The level of restraint achieved by prestressing the end blocks of the test slabs to the load floor of the laboratory was very good. End to end shortening of the slabs was between 2 and 8% of the shortening due to free shrinkage.

8. Thermal stresses within the test slabs were estimated using a time step creep-adjusted analysis. A thermal tensile stress of 0.3 MPa was determined for the NSC slabs, and 1.4 MPa for the HPC slabs.

9. Principal cracks formed much earlier for the HPC slabs, at about 3 days, than for the NSC, at about 30 days. Crack width increased more rapidly for the HPC slabs.

10. Wide cracks formed in all of the test slabs except 30-4. The following table summarizes the final measurements:

Slab	Max. crack width at top of slab (mm)	Max. crack width at bottom of slab (mm)	Age (days)
30-2	1.5	0.5	280
30-4	0.6	0.2	570
100-2	2.2	0.6	460
100-4	2.4	0.2	420
100-8	2.1	0.2	360

Table 5.1 Summary of final crack width measurements

11. For the slabs which experienced a single large crack, the crack occurred when free shrinkage strain had reached about -250×10^{-6}. For slab 30-2 this was at an age of about 30 days, while for the HPC slabs the main crack formed at 3 days.

5.2 Conclusions

1. The use of 0.4% reinforcement (bottom-only) was found to adequately control cracking in highly restrained NSC slabs (slab 30-4). This value is twice that recommended by CSA A23.3.

2. No reasonable minimum amount of reinforcement (bottom-only) can be provided to properly control cracking in highly-restrained HPC slabs under conditions of extremely low humidity. Even with 0.8% reinforcement, four times the minimum prescribed by CSA A23.3, unacceptable cracking occurred (slab 100-8).

3. The amount of bottom reinforcement which was used in the HPC slabs had no effect on the crack widths at the top of the slabs.

4. The use of minimum top and bottom reinforcement may provide good crack control. The resulting crack widths on the underside of slab 100-2 (maximum of 0.5 mm) point towards this possibility. Although cracks on the top surface of a slab at midspan will not generally be noticeable since positive bending will close these cracks, magnified deflections would result. Thus, minimum top reinforcement to control deflections in thin HPC slabs may be necessary.

5. High shrinkage at a very early age, caused each HPC slab to develop a wide isolated crack through their midspan cross-sections.

6. The potential for early-age cracking in HPC slabs due to the addition of shrinkage and thermal stresses was noted. Maximum thermal stress was equal to about 25% of the tensile strength of the HPC.

5.3 Practical recommendations

1. Using reinforcement to control cracking in restrained HPC structures may not be practical because of the large quantities required. Methods to reduce shrinkage may be more effective. The use of shrinkage strips (portions of the slab left open until the majority of shrinkage has occurred) may also be better. These strips could be closed fairly soon because of the high-early shrinkage of HPC.

2. The production of HPC slabs must be given extra attention. Due to rapid slump loss and lack of bleed water, placement and finishing must be done quickly. The difficulty in finishing HPC slabs might be reduced by providing some entrained air (Aïtcin 1996; FIP-CEB 1990). Alternatively, a retarding admixture might be used (de Larrard, Malier 1992; ACI 363R-84). The placement of trial batches is recommended.

3. The industry-favored method of using a curing compound was not sufficient to control early age cracking in the HPC test slabs. To reduce the rapid early age shrinkage experienced by HPC slabs, water or fog curing is likely better (Aïtcin 1996, de Larrard et al. 1994, ACI 363R-84). Water curing may also be expected to help reduce long-term drying shrinkage (Dilger et al. 1996). However, because of the rapid development of a dense microstructure, free water may not be able to penetrate and replace that lost through self-desiccation (FIP-CEB 1990).

4. Thermal strains may be reduced by cooling the concrete mix. Substituting crushed ice for a portion of the mix water, or adding liquid nitrogen are methods that have been recommended by FIP-CEB 1990. Since thermal contraction can contribute to early age cracking in HPC slabs, temperature reduction would be beneficial.

5.4 Recommendations for future research

1. Shrinkage measurements should be started as early as possible for HPC because of rapid development.

2. The elastic modulus of the HPC used in future tests should be measured directly. The large variation in modulus due to the influence of aggregate stiffness has been identified (Mitchell 1996).

3. Tensile creep and elastic modulus tests at early ages would be beneficial in improving the accuracy of the stress-strain analyses which are needed to predict cracking. Cylinders which are cured under the same conditions as the large test specimens should be tested.

4. The use of expanding admixtures which produce shrinkage-compensating concrete might be tested as an alternative to higher amounts of reinforcement (Enyi and Huizhen, 1994).

5. Previous research has shown that highly distributed reinforcement, such as steel fibers can be used to eliminate early age cracking (Bloom, Bentur 1993). Results of the current research support this since even high amounts of concentrated reinforcement were found to be ineffective for HPC. Future slab tests might consider the use of fibers, or a combination of top and bottom reinforcing bars.

REFERENCES

Acker, P., (1995), "The Shrinkages of Concrete: Physical Origins, Parameters of Influence, Analysis by Type of Structure and by Mode of Placement", RILEM GMC Shrinkage, pp. 1-12, April 1995.

Ahmad, S.H., Khaloo, A.R., Poveda, A. (1986), "Shear Capacity of Reinforced High-Strength Concrete Beams", ACI Structural Journal , March-April 1986, pp. 297-305.

Aïtcin, P.C. (1996), "High-performance Concrete", Technology Transfer Day on High-Performance Concrete", The Network of Centres of Excellence on High-performance Concrete, Concrete Canada, 1996.

American Concrete Institute Committee 209, Draft Report (1995), "Creep and Shrinkage Prediction Model for Analysis and Design of Concrete Structures (Model B3)".

American Concrete Institute Committee 209, Report No. ACI 209R-82 (1982), "Prediction of Creep, Shrinkage, and Temperature Effects in Concrete Structures".

American Concrete Institute Committee 363, Report No. ACI 363R-84 (1984), "State-of-the-Art Report on High-Strength Concrete".

American Concrete Institute Committee 318, Building Code Requirements for Reinforced Concrete (ACI 318-89), 1989.

ASTM C 39-86, "Standard Test Method for Compressive Strength of Cylindrical Concrete Specimens", American Society for Testing and Materials, 1986.

ASTM C 192-88, "Standard Method of Making and Curing Concrete Test Specimens in the Laboratory", American Society for Testing and Materials, 1986.

ASTM C 496-86, "Standard Test Method for Splitting Tensile Strength of Cylindrical Concrete Specimens", American Society for Testing and Materials, 1986.

Battista, D.D., (1992) "Minimum Reinforcement Requirements of Reinforced High-Strength Concrete Slabs", MASc. Thesis, Department of Civil Engineering, University of Toronto, Canada.

Beer, F.P., and Johnston, E.R., (1985), Mechanics of Materials, McGraw-Hill Ryerson Ltd., Toronto, Canada.

Bergner, H. (1993), "Crack Width Control of High-Strength Concrete Members Under Centrical Restraint", Darmstadt Concrete Vol. 8, Technische Hochschule Darmstadt, Germany, 1993.

Bergner, H. (1994), "Minimum Reinforcement of High-Strength Concrete Members Under Centrical Restraint", Darmstadt Concrete Vol. 9, Technische Hochschule Darmstadt, Germany, 1994.

Bertero, V.V. (1979), "Inelastic Behavior of Structural Elements", in Proceedings of the Workshop on HSC, S.P. Shah, Editor, National Science Foundation, Chicago, Illinois.

Bissonette, B., and Pigeon, M. (1994), "Tensile Creep at Early Ages of Ordinary and Silica Fume Concretes", The Network of Centres of Excellence on High-performance Concrete, Concrete Canada, Universite Laval, Quebec.

Bloom, R., and Bentur, A. (1995), "Free and Restrained Shrinkage of Normal and High-Strength Concrete", ACI Materials Journal, March-April 1995, pp. 211-217.

Bloom, R., and Bentur, A. (1993), "Restrained Shrinkage in High Strength Concrete" in Third International Symposium on Utilization of High-Strength Concrete, Lillehammer, Norway pp. 1007 - 1014.

Bosco, C., Carpinteri, A., Debernardi, P. G. (1990), "Minimum Reinforcement in High-Strength Concrete", Journal of Structural Engineering, ASCE, Vol. 116, No. 2, Feb. 1990, pp. 427-437.

Canadian Standards Association, Standard A23.3-94, "Design of Concrete Structures", Rexdale, Ontario, 1994. (Cited in the text as CSA A23.3)

Carrasquillo, R.L., Nilson, A.H., and Slate, F.O. (1981), "Properties of High Strength Concrete Subject to Short-Term Loads", ACI Journal, V. 78, N.3, May-June, American Concrete Institute, Detroit, 1981.

Comite Euro-International du Beton and Federation Internationale de la Precontrainte, "CEB-FIP Model Code 1990", Thomas Telford, 1990. (Cited in text as CEB MC90)

De Larrard, F., and Malier Y., (1992) "Engineering properties of very high performance concretes", in High Performance Concrete: From material to structure, edited by Y. Malier, E&FN Spon, pp. 85 to 115, 1992.

Dilger, W.H., (1993), Course Notes for Reinforced Concrete Members, The University of Calgary.

Dilger, W.H., Wang, C., Niitani, K. (1996), "Experimental Study on Shrinkage and Creep of High-Performance Concrete," in 4th International Symposium on Utilization of High-Strength / High-Performance Concrete, Paris, France.

Dilger, W.H., Wang, C., Niitani, K. (1997), "A Creep and Shrinkage Prediction Model for High-Performance Concrete", International Conference on Engineering Materials, Canadian Society for Civil Engineering and Japanese Society for Civil Engineering, June 1997, Ottawa, Canada.

Dilger, W.H., Wang, C. (1998), "Time-Dependent Properties of High Performance Concrete", to be presented at the XIII FIP Congress, Amsterdam, May 23 - 29, 1998.

Elbadry, M., and Ghali, A. (1995), "Control of Thermal Cracking of Concrete Structures", ACI Structural Journal, July - August 1995, pp. 435-450.

Enyi, C., and Huizhen L. (1994), "Role of Expansive Admixtures in High-Performance Concrete", in High-Performance Concrete, Proceedings ACI International Conference , SP-149, Singapore, pp. 575 - 587.

FIP-CEB Working Group on High Strength Concrete (1990), "High Strength Concrete: State of the Art Report", FIP (Federation Internationale de la Precontrainte) SR 90/1, CEB (Comite Euro-International Du Beton) Bulletin No. 197. (Cited in text as FIP-CEB 1990)

Ghali, A., and Favre, R. (1986), Concrete Structures: Stresses and Deformations, Chapman and Hall, New York.

Gilbert, R.I. (1992), "Shrinkage Cracking in Fully Restrained Concrete Members", ACI Structural Journal, March-April 1992, pp. 141-149.

Guenot, I., Torrenti J.-M., and Laplante, P., (1996), "Stresses in Early-Age Concrete: Comparison of Different Creep Models", ACI Materials Journal, May-June 1996, pp. 254-259.

Han, N., Walraven, J.C. (1995), "Creep and Shrinkage of High-Strength Concrete at Early and Normal Ages", in Advances in Concrete Technology: Proceedings of the Second CANMET/ACI International Symposium, Las Vegas, American Concrete Institute SP-154, pp. 73-94.

Hanevy, P. (1996) "Reinforced High-Strength Concrete Columns ", Master of Science Thesis, Department of Civil Engineering, The University of Calgary, 1996.

Hwang, S.-J., Lee, Y.-Y., and Lee, C.-S. (1994), "Effect of Silica Fume on the Splice Strength of Deformed Bars of High-Performance Concrete", ACI Structural Journal, May-June 1994, pp. 294-301.

Imam, M., Vandewalle, L., Mortelmans, F., (1993) "Indirect Tensile Strength of Very High-Strength Concrete" in Third International Symposium on Utilization of High-Strength Concrete, Lillehammer, Norway pp. 1114 - 1121.

Iravani, S., (1996) "Mechanical Properties of High-Performance Concrete", ACI Materials Journal, September-October, 1996, pp. 416-425.

Jaccoud, J.P., Charif, H., Farra, B., (1993) "Cracking Behaviour of HSC Structures and Practical Consequences for Design" in Third International Symposium on Utilization of High-Strength Concrete, Lillehammer, Norway pp. 225 - 232.

Lambotte, H., and Taerwe, L.R., (1990) "Deflection and Cracking of High-Strength Concrete Beams and Slabs " in Second International Symposium on Utilization of High-Strength Concrete, American Concrete Institute, SP-121, pp. 109 - 128.

Leslie, K.E., Rajagopalan, K.S., Everard, N.J. (1976), "Flexural Behavior of High-Strength Concrete Beams", ACI Journal, April 1976, pp. 517-521.

Lessard, M., and Aïtcin, P-C., (1992) "Testing high performance concrete", in High Performance Concrete: From material to structure, edited by Y. Malier, E&FN Spon, pp. 197 to 213, 1992.

Mather, B. (1987), "Curing of Concrete", in Lewis H. Tuthill International Symposium, ACI SP-104.

Mindess, S. (1994), "Materials selection, proportioning and quality control", in High Performance Concrete: Properties and Applications, McGraw-Hill, New York.

Mitchell, D. (1996), "Special Requirements for High-strength Concrete in the 1994 CSA Standard A23.3", Technology Transfer Day on High-Performance Concrete, The Network of Centres of Excellence on High-Performance Concrete, Concrete Canada, 1996.

Muller, H.S. (1992), "New Prediction Models for Creep and Shrinkage of Concrete", in Creep and Shrinkage of Concrete: Effect of Materials and Environment, American Concrete Institute SP-135, pp. 1-18.

Naaman, A.E. (1992), "Unified Design Recommendations for Reinforced, Prestressed, and Partially Prestressed Concrete Bending and Compression Members", ACI Structural Journal, March - April 1992, pp. 200-210.

Nagataki, S., and Yonekura, A., (1982), "Drying Shrinkage and Creep of High-Strength Concrete with Superplasticizer", in Designing for Creep and Shrinkage in Concrete Structures , American Concrete Institute SP-76, Houston, pp. 403 - 420.

Nawy, E.G., (1972), "Crack Control Through Reinforcement Distribution in Two-Way Acting Slabs and Plates", ACI Journal, April 1972, pp. 217-219.

Neville, A.M., Dilger, W.H., and Brooks, J.J., (1983) Creep of Plain and Structural Concrete, Construction Press, Longman Group Ltd., New York.

Ngab, A.S., Nilson, A.H., and Slate, F.O., "Shrinkage and Creep of High Strength Concrete", ACI Journal, July-August 1981, pp. 255-260.

Nilson, A.H., (1994), "Structural Members", in High Performance Concrete: Properties and Applications, McGraw-Hill, New York, pp. 213 - 236.

Ouyang, C., and Shah, S.P., "Fracture Energy Approach for Predicting Cracking of Reinforced Concrete Tensile Members", ACI Structural Journal, January-February 1994, pp. 69-78.

Pendyala, R., Mendis, P., and Patnaikuni, I, (1996), "Full-Range Behavior of High-Strength Concrete Flexural Members: Comparison of Ductility Parameters of High and Normal-Strength Concrete Members", ACI Structural Journal, January-February 1996, pp. 30-35.

Punkki, J., Golaszewski, J., Gjorv, O.E., (1996) "Workability Loss of High-Strength Concrete", ACI Materials Journal, September-October 1996, pp. 427 - 431.

Ravindrarajah, R.S., Mercer, C.M., and Toth, J. (1994), "Moisture-Induced Volume Changes in High-Strength Concrete", in High-Performance Concrete, Proceedings ACI International Conference , SP-149, Singapore, pp. 475 - 490.

Russell, H. G., (1994), "Structural design considerations and applications", in High Performance Concrete: Properties and Applications , McGraw-Hill, New York, pp. 313-339.

Prestressed Concrete Institute, PCI (1994), "Guide to Using Silica Fume in Precast / Prestressed Concrete Products", Committee Report in the PCI Journal, Sept./Oct. 1994.

Rangan, B.V., (1992) "Serviceability Design in Current Australian Code " in Designing Concrete Structures for Serviceability and Safety, American Concrete Institute, SP-133, pp. 93 - 105.

Rüsch, H., Jungwirth, D., and Hilsdorf, H.K., (1983) Creep and Shrinkage: Their Effect on the Behavior of Concrete Structures , Springer-Verlag, New York.

Ryell, J., Bickley, A., (1987), "Scotia Plaza: High Strength Concrete for Tall Buildings", in Utilization of High Strength Concrete , Proceedings of the Symposium, Stavanger, Norway, pp. 641-654.

Sakata, K., (1995) "Prediction of Creep and Shrinkage According to the New Japanese Building Code", Seminar at the University of Calgary, Department of Civil Engineering, April 25, 1995.

Shah, S.P. (1994), Preface to High Performance Concrete: Properties and Applications, McGraw-Hill, New York,

Shin, S-W., Ghosh, S.K., Moreno, J. (1989), "Flexural Ductility of Ultra-High-Strength-Concrete Members", ACI Structural Journal, July-August 1989, pp. 394-400.

Smith, R. (1998), Department of Geography, The University of Calgary, Personal communication, data not published.

Standard Association of Australia, Standard AS 3600-1988, "Concrete Structures", North Sydney, N.S.W. (Cited in text as AS 3600)

Wang, C. (1997), Department of Civil Engineering, The University of Calgary, Personal communication, data not yet published.

Wiegrink, K., Marikunte, S., and Shah, S.P. (1996), "Shrinkage Cracking of High-Strength Concrete", ACI Materials Journal, September-October 1996, pp. 409-415.

Wittmann, F.H. (1979), "Micromechanics of Achieving HSC", in Proceedings of the Workshop on HSC, S.P. Shah, Editor, National Science Foundation, Chicago, Illinois.

Yokoyama, K., Hiraishi, S., Kasai, Y., Kishitani, K., (1994) "Shrinkage and Cracking of High-Strength Concrete and Flowing Concrete at Early Ages", in Fourth CANMET/ACI International Conference on Superplasticizers and Other Chemical Admixtures in Concrete, American Concrete Institute, SP-148, pp. 243 - 258.

APPENDIX A
CONCRETE MIX DESIGN DATA

Normal Strength Concrete: NSC (f'_c = 30 MPa approx.)

Quantities are per m^3 of fresh concrete

water	216 kg	w / c *	0.64
cement	309 kg	type	Portland 10
fine aggregate	862 kg	nominal size	concrete sand
coarse aggregate	1320 kg	nominal size	14 mm
fine / total agg.	40 %		
silica fume	0	type	n/a
superplasticizer	1.0 L	type	Master Builders' SPN

* Water / cement : calculated allowing for fine aggregate in dry condition.

High-Performance Concrete: HPC (f'_c = 85 MPa approx.)

water	150 kg	w / (c + sf) *	0.30
cement	419 kg	type	Portland 10
fine aggregate	765 kg	nominal size	concrete sand
coarse aggregate	1056 kg	nominal size	14 mm
fine / total agg.	42 %		
silica fume	47 kg	type	Hanna
superplasticizer	11.0 L	type	Master Builders' Rheobuild 1000

* Water / (cement + silica fume): calculated allowing for fine aggregate in dry condition; water in superplasticizer included

APPENDIX B
PETROGRAPHIC ANALYSIS OF AGGREGATE

Note: The same aggregate was used for both the NSC and the HPC mixes.

Coarse Aggregate, 10 mm Rock

ROCK TYPE	14 - 10 mm % in fraction	10 - 5 mm % in fraction	5 - 2.5 mm % in fraction
GOOD			
Quartzite	23.4	23.7	26.7
Limestone	60.6	70.0	66.1
Sandstone	5.0	1.9	1.3
Chert		2.9	2.8
FAIR			
Quartzite		0.4	2.2
Chert		0.1	
Sandstone	6.3		
Siltstone	4.7	0.7	1.0
POOR			
Siltstone		0.3	
% of fraction	21.7	70.5	7.8

Fine Aggregate, 5 mm Washed Sand

ROCK	5.0 - 2.5 mm	2.5 - 1.25 mm	1.25 mm - 630 µm	630 - 315 µm	315 - 160 µm	160 - 80 µm
Quartzite	35.2	25.1	44.9	39.4	21.4	4.3
Limestone	53.0	70.7	50.0	33.1	36.8	27.5
Sandstone	2.6	0.5	0.5	0.8		
Chert	9.1	3.7	3.7	4.8	4.5	1.4
Quartz			0.9	21.9	37.3	66.8
% of fraction	0.1	16.3	12.6	12.0	31.1	23.0

APPENDIX C

CALCULATIONS FOR TIME-STEP ANALYSIS OF SHRINKAGE STRESS-STRAIN IN TEST SLABS

NSC Slabs

The following calculations are derived based on the input from Table 4.7 for t_i and $\varepsilon_{sh}(t_i)$, which is the measured value of free shrinkage strain (points 5253). Prediction values for $E(t_i)$ and $\phi(t_{i+1}, t_i)$ are according to CEB MC90, with $E(t = 28) = 25750$ MPa (Section 4.4). Equation (4.4) is used to calculate summations of ε_j and $\sigma(t_{i+i})$.

First interval, $i = 1$, $t_i = 1.5$ days

$\sigma(t_{i-i})$ = 0.0 (shrinkage just beginning; no initial stress)

$E(t_i)$ = 0.660 E (28 days) = 0.660 x 25750 = 17000 MPa

$\phi(t_{i+1}, t_i)$ = ϕ (2.1 , 1.5) = 0.79

$$\sigma(t_{i+1}) = 0 + \frac{17000}{1+0.79}\left(+8\times10^{-6} - 0\right)$$

= +0.076 MPa (tension).

Second interval, $i = 2$, $t_i = 3.7$ days

$\sigma(t_{i-i})$ = +0.076 MPa

$E(t_i)$ = 0.803 E (28) = 0.803 x 25750 = 20680 MPa

$$\sum_{j=1}^{i} \Delta\varepsilon_j(t_{i+1}) = -[(-88-(-16))+(-8)] = +80\times10^{-6}$$

$\phi(t_{i+1}, t_i)$ = ϕ (5.2 , 3.7) = 0.88

For $j = 1$,

$\sigma(t_{j+i}) - \sigma(t_{j-1}) = +0.076$

$E(t_j)$ = 17000 MPa

and $i = 2$,

$$\phi\,(t_{i+1}, t_j) = \quad \phi\ (5.2\ ,\ 1.5) = 1.36$$

$$\therefore \sigma(t_{i+1}) = 0.076 + \frac{20680}{1+0.88}\left[+80\times10^{-6} - \frac{0.076}{17000}(1+1.36)\right]$$

$$= +0.076 + 0.88 - 0.121$$

$$= +0.84 \text{ MPa (tension).}$$

Third interval, $\quad i = 3,\ \ t_i = 9.1$ days

$\sigma\,(t_{i-i}) \ = \quad +0.84$ MPa

$E\,(t_i) \ = \quad 0.910\,E\,(28) = 0.910 \text{ x } 25750 = 23430$ MPa

$$\sum_{j=1}^{i} \Delta\varepsilon_j(t_{i+1}) = -[-188-(-8)] = +180\times10^{-6}$$

$$\phi\,(t_{i+1}, t_i) = \quad \phi\ (13.0\ ,\ 9.1) = 0.99$$

For $j = 1$,

$$\sigma\,(t_{j+i}) - \sigma\,(t_{j-1}) = +0.076$$

$$E\,(t_j) \qquad = 17000 \text{ MPa}$$

and $i = 3$,

$$\phi\,(t_{i+1}, t_j) = \quad \phi\ (13.0\ ,\ 1.5) = 1.90$$

For $j = 2$,

$$\sigma\,(t_{j+i}) - \sigma\,(t_{j-1}) = +0.764$$

$$E\,(t_j) \qquad = 20680 \text{ MPa}$$

and $i = 3$,

$$\phi\,(t_{i+1}, t_j) = \quad \phi\ (13.0\ ,\ 3.7) = 1.51$$

$$\therefore \sigma(t_{i+1}) = 0.84 + \frac{23430}{1+0.99}\left[+180\times10^{-6} - \frac{0.076}{17000}(1+1.90) - \frac{0.764}{20680}(1+1.51)\right]$$

$$= +0.84 + 2.12 - 0.153 - 1.09$$

$$= +1.72 \text{ MPa (tension).}$$

Fourth interval, $i = 4$, $t_i = 20.5$ days

$\sigma(t_{i-1})$ = +1.72 MPa

$E(t_i)$ = 0.979 $E(28)$ = 0.979 x 25750 = 25210 MPa

$$\sum_{j=1}^{i} \Delta\varepsilon_j(t_{i+1}) = -[-280-(-8)] = +272\times10^{-6}$$

$\phi(t_{i+1}, t_i)$ = ϕ (28.0 , 20.5) = 1.03

For $j = 1$,

$\sigma(t_{j+i}) - \sigma(t_{j-1})$ = +0.076

$E(t_j)$ = 17000 MPa

and $i = 4$,

$\phi(t_{i+1}, t_j)$ = ϕ (28.0 , 1.5) = 2.42

For $j = 2$,

$\sigma(t_{j+i}) - \sigma(t_{j-1})$ = +0.764

$E(t_j)$ = 20680 MPa

and $i = 4$,

$\phi(t_{i+1}, t_j)$ = ϕ (28.0 , 3.7) = 2.00

For $j = 3$,

$\sigma(t_{j+i}) - \sigma(t_{j-1})$ = +1.79

$E(t_j)$ = 23430 MPa

and $i = 4$,

$\phi(t_{i+1}, t_j)$ = ϕ (28.0 , 9.1) = 1.57

$$\therefore \sigma(t_{i+1}) = +1.72 + \frac{25210}{1+1.03}\left[+272\times10^{-6} - \frac{0.076}{17000}(1+2.42) - \frac{0.764}{20680}(1+2.00) - \frac{0.880}{23430}(1+1.57)\right]$$

= +1.72 + 3.37 - 0.19 - 1.38 - 1.19

= +2.35 MPa (tension).

HPC Slabs

The following calculations are derived based on the input from Table 4.8 for t_j and ε_{sh}. Prediction values for $E(t_i)$, $\phi(t_{i+1}, t_i)$ are according to Dilger, Niitani, and Wang (1997). Equation (4.4) is used to calculate summations of ε_j and $\sigma(t_{i+1})$.

First interval, $i = 1$, $t_i = 0.4$ days

$\sigma(t_{i-i})$ = 0.0 (shrinkage just beginning; no initial stress)

$E(t_i)$ = 0.624 E (28 days) = 0.624 x 32300 = 20200 MPa

$\phi(t_{i+1}, t_i)$ = ϕ (0.5,0.4) = 0.69

$$\sigma(t_{i+1}) = 0 + \frac{20200}{1+0.69}\left(+60\times10^{-6} - 0\right)$$

= +0.72 MPa (tension).

Second interval, $i = 2$, $t_i = 0.7$ days

$\sigma(t_{i-i})$ = +0.72 MPa

$E(t_i)$ = 0.681 E (28) = 0.681 x 32300 = 22000 MPa

$$\sum_{j=1}^{i} \Delta\varepsilon_j(t_{i+1}) = -[(-278-(-120))+(-60)] = +218\times10^{-6}$$

$\phi(t_{i+1}, t_i)$ = ϕ (0.9 , 0.7) = 0.67

For $j = 1$,

$\sigma(t_{j+i}) - \sigma(t_{j-1})$ = +0.72 MPa

$E(t_j)$ = 20200 MPa

and $i = 2$,

$\phi(t_{i+1}, t_j)$ = ϕ (0.9 , 0.4) = 1.09

$$\therefore \sigma(t_{i+1}) = 0.72 + \frac{22000}{1+0.67}\left[+218\times10^{-6} - \frac{0.72}{20200}(1+1.09)\right]$$

= +0.72 + 2.87 - 0.98 = +2.61 MPa (tension).

Third interval, $i = 3$, $t_i = 1.2$ days

$\sigma(t_{i-i})$ = +2.61 MPa

$E(t_i)$ = 0.736 E (28) = 0.736 x 32300 = 23800 MPa

$$\sum_{j=1}^{i} \Delta\varepsilon_j(t_{i+1}) = -[-338-(-60)] = +278\times10^{-6}$$

$\phi(t_{i+1}, t_i)$ = ϕ (1.4 , 1.2) = 0.52

For $j = 1$,

$\sigma(t_{j+i}) - \sigma(t_{j-1})$ = +0.72

$E(t_j)$ = 20200 MPa

and $i = 3$,

$\phi(t_{i+1}, t_j)$ = ϕ (1.4 , 0.4) = 1.27

For $j = 2$,

$\sigma(t_{j+i}) - \sigma(t_{j-1})$ = +2.61 - 0.72 = +1.89

$E(t_j)$ = 22000 MPa

and $i = 3$,

$\phi(t_{i+1}, t_j)$ = ϕ (1.4 , 0.7) = 0.94

$$\therefore \sigma(t_{i+1}) = 2.61 + \frac{23800}{1+0.52}\left[+278\times10^{-6} - \frac{0.72}{20200}(1+1.27) - \frac{1.89}{22000}(1+0.94)\right]$$

= +2.61 + 4.35 - 1.26 - 2.62

= +3.08 MPa (tension).

Fourth interval, $i = 4$, $t_i = 2.2$ days

$\sigma(t_{i-i})$ = +3.08 MPa

$E(t_i)$ = 0.798 E (28) = 0.798 x 32300 = 25800 MPa

$$\sum_{j=1}^{i} \Delta\varepsilon_j(t_{i+1}) = -[-374-(-60)] = +314\times10^{-6}$$

$\phi(t_{i+1}, t_i)$ = ϕ (3.0 , 2.2) = 0.59

For $j = 1$,

$\sigma(t_{j+1}) - \sigma(t_{j-1}) = +0.72$

$E(t_j) = 20200$ MPa

and $i = 4$,

$\phi(t_{i+1}, t_j) = \phi(3.0, 0.4) = 1.51$

For $j = 2$,

$\sigma(t_{j+1}) - \sigma(t_{j-1}) = +2.61 - 0.72 = +1.89$

$E(t_j) = 22000$ MPa

and $i = 4$,

$\phi(t_{i+1}, t_j) = \phi(3.0, 0.7) = 1.21$

For $j = 3$,

$\sigma(t_{j+1}) - \sigma(t_{j-1}) = +3.08 - 2.61 = +0.47$

$E(t_j) = 23800$ MPa

and $i = 4$,

$\phi(t_{i+1}, t_j) = \phi(3.0, 1.2) = 0.94$

$$\therefore \sigma(t_{i+1}) = +3.08 + \frac{25800}{1+0.59}\left[+314\times10^{-6} - \frac{0.72}{20200}(1+1.51) - \frac{1.89}{22000}(1+1.21) - \frac{0.47}{23800}(1+0.94)\right]$$

$= +3.08 + 5.10 - 1.45 - 3.08 - 0.62$

$= +3.03$ MPa (tension).

APPENDIX D
EQUIPMENT LIST

The following is a list of equipment used to gather data presented in this thesis.

Cylinder load testing frame:	Amsler #79/233 U of C ID # 016525
	with,
	Allied Industries digital load monitor U of C ID # 245080
500 mm Demec gauge:	Mitutoyo U of C ID # 130314
50 mm Demec gauge:	W.H. Mayes & Son (No. 3746) U of C ID # 183852

TEST TARGET (QA-3)

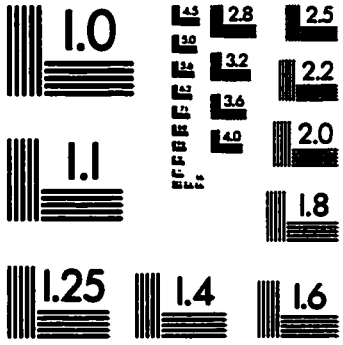

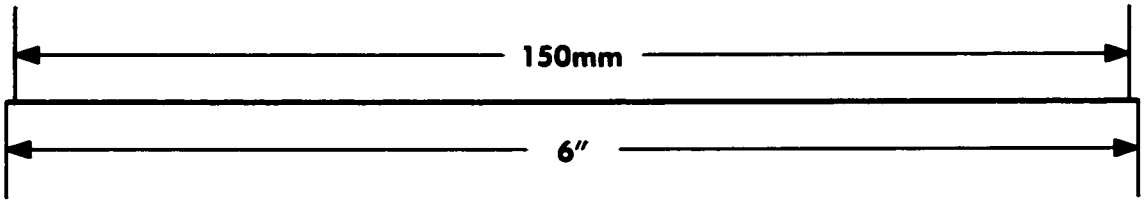

APPLIED IMAGE, Inc
1653 East Main Street
Rochester, NY 14609 USA
Phone: 716/482-0300
Fax: 716/288-5989